CFD MODELING OF A CENTRIFUGE FOR OIL - WATER SEPARATION

H.G.S.M.Thilakarathna

(149268 K)

Degree of Master of Science

Department of Chemical and Process Engineering

University of Moratuwa

Sri Lanka

April 2017

CFD MODELING OF A CENTRIFUGE FOR OIL - WATER SEPARATION

Hirimuthu Godage Sachini Manjula Thilakarathna

(149268 K)

Thesis submitted in partial fulfillment of the requirements for the degree Master of Science

Department of Chemical and Process Engineering

University of Moratuwa

Sri Lanka

April 2017

DECLARATION

I declare that this is my own work and this thesis does not incorporate without acknowledgement any material previously submitted for a Degree or Diploma in any other University or institute of higher learning and to the best of my knowledge and belief it does not contain any material previously published or written by another person except where the acknowledgement is made in the text.

Also, I hereby grant to University of Moratuwa the non-exclusive right to reproduce and distribute my thesis, in whole or in part in print, electronic or other medium. I retain the right to use this content in whole or part in future works (such as articles or books).

Signature: Date:

The above candidate has carried out research for the Masters under my supervision.

Name of the supervisor: Dr. Mahinsasa Narayana

Signature of the supervisor: Date:

ABSTRACT

Centrifugation is an efficient, economical and environmentally friendly method to remove undesirable water content from oil and water mixtures and separate out the desired oil content. Moreover, the disc stack centrifuges are widely used for separating liquids of different densities and applied in industrial coconut oil clarification as well.

The main focus of this research work is to model the fluid flow inside the Westfalia disc stack centrifuge using Ansys Fluent and identify the flow behavior. With the availability of the limited computer hardware facility, the model has been run without the discs to avoid complexities. In the developed 3 dimensional model, the fluid dynamic behavior of the multiphase flow has been considered and modeled using the VOF multiphase model available in fluent.

The step by step procedure of the model development has been discussed such as the very first stage of geometry selection, drawing and importing to the fluent, mesh generation, all solution set ups and even the two stage simulation procedure.

The simulation results of this research work provides an out line of the resulted flow parameters of velocity and pressure profiles, turbulent effects such as turbulence intensity, turbulent kinetic energy, and specific dissipation rate and also the phase volume fractions which have been saved in every critical stage of the simulation process. Despite the phase volume fraction which has been experimentally validated, all other results were theoretically validated.

CFD modeling of flow behavior inside the centrifuges is not a popular topic among the researchers due to the complex flow patterns and the requirement of advanced computer hardware facility. However this research work provides a platform to model the similar flow behaviors and even to model the same case including the discs.

KEY WORDS:

CFD, centrifuge, VOF, multiphase

DEDICATION

I dedicate this thesis to my courageous father, gracious mother and supportive husband for their unconditional love and affection.

ACKNOWLEDGMENTS

This research work would not be a success without the guidance and support of several inspiring personalities whom I am greatly in debt.

First and foremost I would like to express my sincere gratitude to my outstanding research supervisor Dr.Mahinsasa Narayana for his continuous guidance, support, motivation and valuable knowledge sharing sessions throughout the whole period of master program of Sustainable Process Development. Thank you very much sir for being a role model to me.

I extend my immense gratitude to Dr.Sanja Gunawardena and Dr.P.G. Rathnasiri who are the current and former Heads of the Department of Chemical and Process Engineering, University of Moratuwa.

I wish to express my sincere thanks to non-academic staff of the department for their valuable assistance that has been given throughout the research work. My special appreciation goes to Mr.Shantha Peris, Mr.Nihal Perera, Mr.Senarath Epa and Mr.Sunil Dayananda for spending their precious time in facilitating me.

I am profoundly in debt to my friends, Ms. Thamali Jayawickrama, Ms. Bhagya Herath, Ms. Imesha Samarathunga, Ms.Sureshini Warnasooriya and Ms.Gayani Jayathunga for the valuable comments and sharing their research experience.

I would like to express my immense gratitude to my parents, for giving me life in the first place and for educating me with all arts of life and also my two loving brothers for being my life's strength.

Last but not least, I wish to express my sincere thanks to my loving husband for his silent motivation and sustained patience during the many long hours I spent working on this research and thesis at the university.

TABLE OF CONTENTS

LIST OF FIGURES

LIST OF TABLES

LIST OF ABBREVIATIONS

CFD	Compoutational Fluid Dynamics
DPM	Discrete Phase Model
FVM	Finite Volume Method
LES	Large Eddy Simulations
MRF	Moving Reference Frame
PISO	Pressure Implicit with Splitting of Operator
RANS	Reynolds Average Navier Stokes Equation
RNG	Re-Normalization Group
RSM	Reynolds Stress Model
SST	Shear Stress Transport
VOF	Volume Of Fluid
Fr	Froude Number

LIST OF APPENDICES

CHAPTER 1 : INTRODUCTION

The chapter 1, initiates by providing an introductory explanation on research background in section 1.1 which summarizes the importance of centrifugation as an industrial separation process as well as it's wide range of applicability to process different sizes of material. Yet, it also offers synopsis of an impact of technological advancement during 20^{th} century to CFD modeling of fluid flows. The section 1.2 includes a brief history of the disc stack centrifuge whereas section 1.3 has an outline of industrial applications of disc stack centrifuge. Status of earlier performed researches for CFD modeling of swirling effect has been illustrated in section 1.4 which also describes the swirl effect inside cyclones and centrifuges in section 1.4.1. The subsection 1.4.2 contains a summary of the descriptive 1.4.1 subsection. The chapter concludes with section 1.5 which contains research objectives and scope.

1.1 Background

Separation processes are one of the key procedures in any industry, as almost all natural or synthetic raw materials and generated waste are mixtures of two or more substances. On the other hand, the techniques of separation are of great economic importance and process optimization would significantly affect the final profit as well. However, centrifugation is a mechanical separation process which separates substances from homogeneous or heterogeneous mixtures, using the density difference of constituents and applied centrifugal force.

The centrifuges can be used to separate wide range of materials, micro scale algae to macro scale solid effluents. Type, size and rotational speed of the centrifuge depend on the application, capacities and condition of in and out flows. Furthermore, lab scale centrifuges are used to collect micro organisms, cellular debris and proteins in clinical practices whereas solid bowl centrifuges and decanters to remove solid effluents from industrial waste water and disc stack centrifuges to separate liquids of different densities such as oil and water mixtures.

Disc stack centrifuges are widely applied in oil processing industries to remove undesirable water content and separate out virgin oil product. One such industry is production of virgin coconut oil with the use of coconut milk. Primarily, there are three methods available in virgin coconut oil production such as fermentation, cold process or expeller press method and centrifugation. Out of these three, centrifugation is known to be the least intrusive of all. In centrifugation process, the virgin coconut oil is separated out from coconut milk which is said to be a natural emulsion of oil suspended in water. Moreover, the virgin coconut oil which is prepared by centrifugation is more expensive compared to the oil produced by other methods, since not only it smells and taste like fresh coconut, but also the product retains the valuable nutrients like vitamins and minerals. However, the separation efficiency of the production can be enhanced by increasing the temperature, rotational time and speed.Further, analysis of complex fluid flow patterns inside the centrifuge using modern techniques will significantly improve and optimize the process of separation while broadening the understanding about the fluid flow field.

Emerging technological advancements during 20^{th} century, have brought up more efficient and sophisticated methods to analyze complex fluid flow patterns. These fluid flow modeling and simulation techniques are more easier to carry out in comparison to real time empirical methods that have been practiced by earlier researchers. Progression of Computational Fluid Dynamics (CFD) has facilitated to solve fluid flow equations numerically which is more convenient than analytical solution approach. However the experimental analysis of a particular approach can never be replaced by CFD analysis, but can be used as a supportive tool to avoid costly, complicated repetitive experimental procedures and ultimately save huge amount of materials and precious research time. Nevertheless, experimental results of a similar set up should be aligned with the CFD results of the same approach to confirm the model accuracy and get validated.

1.2 History of Disc Stack Centrifuge

The revolutionary invention of a Swidish inventor, Dr. Gustaf de Laval in June 1878, is considered as the first patented centrifuge. It marked a prominent mile stone in dairy industry by improving the efficiency of cream separation from raw milk. It didn't contain any discs, yet the efficiency improved by means of 20% or more.

During 1890, Clemens Von Bechtolsheim who was a German, modified the machinery by introducing so-called Alpha discs which has shown a significant improvement in separation efficiency as well as the capacity.

Application of the centrifugal separator has widened immensely, during and post war era as it was used to purify lube oil for turbines. The growth of engineering processes during 1920 has broadened again the applicability of centrifuges for processes such as, to purify cutting oils, hardening oils and many more workshop liquids [1, p. 23].

A complete study on efficiency, hydrodynamics and monitoring techniques for oil-water separation, inside a disc stack centrifuge has been done by Lindon during 1987. The centrifugal geometry and the liquid flow path of the respective centrifuge has been clearly captured and discussed in his thesis as well as highlights the centrifuges performance with the liquid interface position [1].

1.3 Industrial applications of disc stack centrifuge

Disc stack centrifuge is a quite common equipment which is being used at the clarification stage in oil processing industries. On the other hand, it is used to treat oil containing waste water before discharge back to sea. However newly built disc stack centrifuges contain more advanced and sophisticated options such as self cleaning facility.

Disc stack separators performs a key role in processing fuel oil for gas turbines, in order to remove unwanted heavy phases such as water and fine solids. The gas turbine fuel requires high degree of purity, otherwise the turbine would get damaged. Further, disc stack centrifuges are used in several steps of bio diesel production to remove

(a) Industrial centrifuge

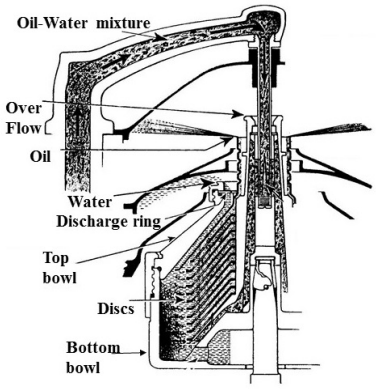

(b) Cross section

Figure 1.1: The disc stack centrifuge

undesirable methanol and water[2].

Other than in coconut oil processing, disc stack separator is used in processing of several other vegetable and animal oils such as avocado oil, palm oil, olive oil and several fish oils. In addition to oil processing, disc stack separators are applied in beverage and brewing industry to process fruit and vegetable juices, pectin, beer, wine, portable alcohol and etc. Further, industrial/mineral oils are clarified with the use of disc stack centrifuges and the applications include processing of slop oil and oil residues after being processed via tricanter[3].

The industrial disc stack centrifuge and it's cross section are depicted by figures 1.1a and 1.1b respectively.

1.4 CFD modeling of swirling effect

1.4.1 Swirling flows inside cyclones and centrifuges

CFD modeling of 3D, swirling flows was unrevealed among earlier researchers due to the unavailability of intensive computer hardware power. Swirling flows typically encounter inside cyclones and centrifugal separators. Since, both cases involve more than one phase ultimately demands additional computer facility as well. However, it can be seen that lack of research work has been carried out for modeling centrifugal separators specially for liquid-liquid separations, comparable to flow modeling inside

cyclones and solid-liquid separations inside decanter type centrifuges.

A prominent research work has been carried out by Boysan during early 80's in developing 2D, fundamental mathematical model for two phase flow inside a cyclone. Boysans states that his approach could be applied for similar kind of swirling flows comprises two phases which has ultimately widen up the research platform [4] - [5]. However, simulating the swirl effect has complexities of its own which do not perfectly captured by the k-ϵ model and later the technological advancements facilitate the hybrid renormalization group theory (RNG) to model swirling flows with much better accuracy [5] - [6].

Conversely, during late 90's a study carried out by Hoekstra, revealed unrealistic axial and tangential velocities in 2D flow simulation using k-ϵ and RNG models. The revolutionary evaluation of computer hardware technology just before the millennium provided opportunity for the researchers to use Reynolds Stress Models (RSM) and Large Eddy Simulation (LES) which together improved the accuracy of 2D swirling flow simulations [5] - [6]. Yet, these 2D research studies do not supportive enough to disclose the complicated 3D nature of swirling flows.

The research work carried out by Nowakowski and his team in 2004, has been revealed several issues and improvements that have to be dealt with when CFD modeling of 2D or 3D hydro cyclones. Few of them includes, challenges in geometry representing, selecting boundary conditions and suitable turbulence model. Besides, he also states many functional similarities between centrifuges and hydro cyclones [7].

Erik Dick along with his research colleagues predicted the performance of centrifugal pumps with the available CFD tools in fluent. Three calculation methods which are of Multiple Reference Frame, Mixing plane method and Sliding mesh method were the considered since they can be used to analyze flow inside turbo machinery. However the main focus of the research was the steady nature of first two methods and the unsteady nature of the third method. Further, the rotor and stator domains were calculated with the use of rotating reference frame and absolute reference frame respectively. However Erik concludes the uselessness of steady methods in general performance prediction of turbo machinery[8].

Fluid flow inside an annular centrifugal contactor was studied by Wardle during 2006 with simplifying assumptions and widely available CFD models to obtain qualitatively accurate results. There, steady state, full liquid without any air core has been assumed and Discrete Phase Model (DPM) model was used to track particles.Further, Wardle discuss the challenges in CFD modeling of unsteady, turbulent, multiphase flow behavior [9].

Later, during 2011 Wardle again simulated the 3D liquid flow inside the annular centrifugal contactor using Volume Of Fluid (VOF) model for multiphase flow modeling with widely used Open FOAM software. Besides, Large Eddy Simulation (LES) technique has been used for turbulence modeling. Moreover, he emphasis the requirement for more advanced multiphase models which accurately capture complicated flows[10].

A complete 3D CFD model of Evodos centrifuge to de-water micro algae has been developed by Bowen Yu during 2012. DPM model in Fluent was used to track particles and conservation equations have been solved using finite volume method.On the other hand, Shear Stress Transport (SST) k-ω model which is not commonly used, but the most recommended turbulence model for fluid flow modeling inside the centrifuge has been selected and Pressure Implicit with Splitting of Operator (PISO) is chosen as the pressure velocity coupling algorithm. Moreover,The model has been validated through visual result from algae separation test runs, theoretical equations and starch test run measurements. Bowen states the importance of optimizing the geometry of the parallel plates and impeller chamber to improve the separation efficiency and also the requirement of modification to the multi-phase model to track the air core [11].

Fernández obtained sharp gas-liquid interface for the results of numerical of solid bowl centrifuge which used for waste management. VOF multiphase model and DPM have been used for modeling multi-phase flow and tracking the particles respectively. Further, he first simulated 2D rotation, symmetrically avoiding the radial walls. Later, one fourth of centrifuge has been three dimensionally developed to confirm the obtained patterns and circumferential gradients [12].

In work of Dong-Liang Sun, numerical (CFD) and semi-analytical techniques were

used in the simulation of an eccentric tube centrifugal oil pumping system for hermetic compressors. The computational mesh consisted of 400,000 tetrahedral cells and VOF model has been used to model the gas-liquid interface. The turbulent behavior of flow inside the pumping system has been modeled using k-ϵ model with default constants[13].

During 2014,Dong Liandong numerically simulated the pressure field inside a decanter type centrifuge using Moving Reference Frame (MRF) method and k-ε turbulent model in Fluent. Besides, his simulation results revealed the differences between simulated and theoretical hydraulic pressure caused by the lag of liquid rotation increased with increase in rotational speed[14].

1.4.2 Summary of CFD modeling of swirling flows

Few decades ago, the requirement of much advanced computer power for modeling the swirl effect as well as the multi-phase nature inside cyclones and centrifuges immensely limit the popularity of it's CFD modeling. However, with the availability of sophisticated computer facility after the millennium has considerably enhanced CFD modeling of swirling flows, as it is more economically viable and trouble-free rather than performing experiments dealing with high volumes of materials and large machinery. Besides, CFD modeling allows the researcher to view the nature of the flow inside which is not still disclose through repetitive experiments. It is very advantageous, as the researcher can focus even on very minor adjustment required to optimize the performance.

Even though the swirl effect inside cyclones and centrifuges have been examined and modeled in multiple view points, CFD modeling of disc stack centrifuges for oil-water separation has infrequently been studied. Hence, a lot more to be disclosed through continuous research works of different aspects, in order to fill this knowledge gap and improve existing modeling techniques.

However, Open FOAM and ANSYS Fluent software packages allow the user for CFD modeling of multi-phase flow inside cyclones and centrifuges with much better accuracy. In summary, the elaborate flow field out put provided by simulation results

can be used to optimize the performance of equipment and direct impact can be made to gain economic benefits of the organization.

1.5 Research Objectives and Scope

1.5.1 Objectives

1. The key objective of this research work is to develop a CFD model for Westfalia disc stack centrifuge with the use of ANSYS Fluent software package.

2. Another important objective is to validate the model theoretically and experimentally. The experimental validation can be done by performing real time experiments with the Westfalia disc stack centrifuge only equipping the parts that has been used to draw the geometry.

3. Identification and analysis of flow characteristics and parameters such as velocity, pressure, turbulent properties and phase volume fractions.

Other than these primary and significantly important objectives, this research attempt would achieve subsidiary tasks inline with the major ones.The considered flow is quite complex since it is a rotating and multiphase flow. Since the modeling of these kind of flows are not much popular among researchers, this attempt will contribute an initial guidance for the next move of modeling the similar flow types.

1.5.2 Scope

The research scope has been outlined by considering the compatibility to the available resources. Therefore, the research goals have been sub divided, in order to easier identification of completed tasks.

1. Literature survey on oily water separation technologies and similar swirl flow simulation cases in computational fluid dynamics with the use of different simulation software packages.

2. Identify and shrink the real disc stack centrifuge geometry, to keep the compatibility to the available computer hardware facility.

3. Generate the three dimensional drawing of the fluid volume inside the centrifugal separator using SOLIDWORKS 2013.

4. Create a quality mesh and run 3D model using ANSYS Fluent 2015, inline with the accessible computer power.

5. Validate the simulation results by performing real time experiments with the use of centrifuge that contains only the selected geometric features(without discs).

CHAPTER 2 : MODELING THEORY AND TECHNIQUE

This chapter includes an illustrative explanation on theory behind centrifugation and it's modeling methods in ANSYS Fluent. The chapter initiates with the theoretical background of liquid mixture centrifugation inside a disc centrifuge which describes in section 2.1. The section 2.2 summarizes the basic fluid flow equations of mass and momentum conservations. In section 2.3 which elaborates moving zone modeling, further describes the mass and momentum conservation of frame and mesh motion in relative and absolute velocity formulations respectively. Section 2.4 covers the turbulence modeling including the model selection whereas the section 2.5 illustrates the solver selection for the considered application in ANSYS Fluent. Multiphase flow modeling technique is represented in section 2.6, including brief descriptions of all available multiphase flow model approaches and appropriate model selection with justification. Finally, the chapter ends up with an explanation on available discretization schemes in ANSYS Fluent as well as the finite volume method and the selected schemes which covers in section 2.7, 2.7.1 and 2.7.2 respectively.

2.1 Theory behind centrifugation of liquid mixtures in a disc centrifuge

Disc type centrifuges are commonly used to separate two mutually immiscible liquids and the separation depends on their density and viscosity difference. It has been verified that unlike the pressure gradient of a liquid column which is constant in all heights, the centrifugal pressure gradient depends on height and function of radius, 'r'. Even at its usual operating speed, the centrifugal force is significantly larger than the gravitational force. Also at higher rotational speeds, the liquid layers become straighten vertically and the gravitational force is negligible. Hence, function of centrifuge is independent of orientation of axis of rotation. Therefore, pressure gradient at a radius 'r'is given as equation 2.1.[15, p. 477]

$$\frac{\partial P}{\partial r} = \rho w^2 r \tag{2.1}$$

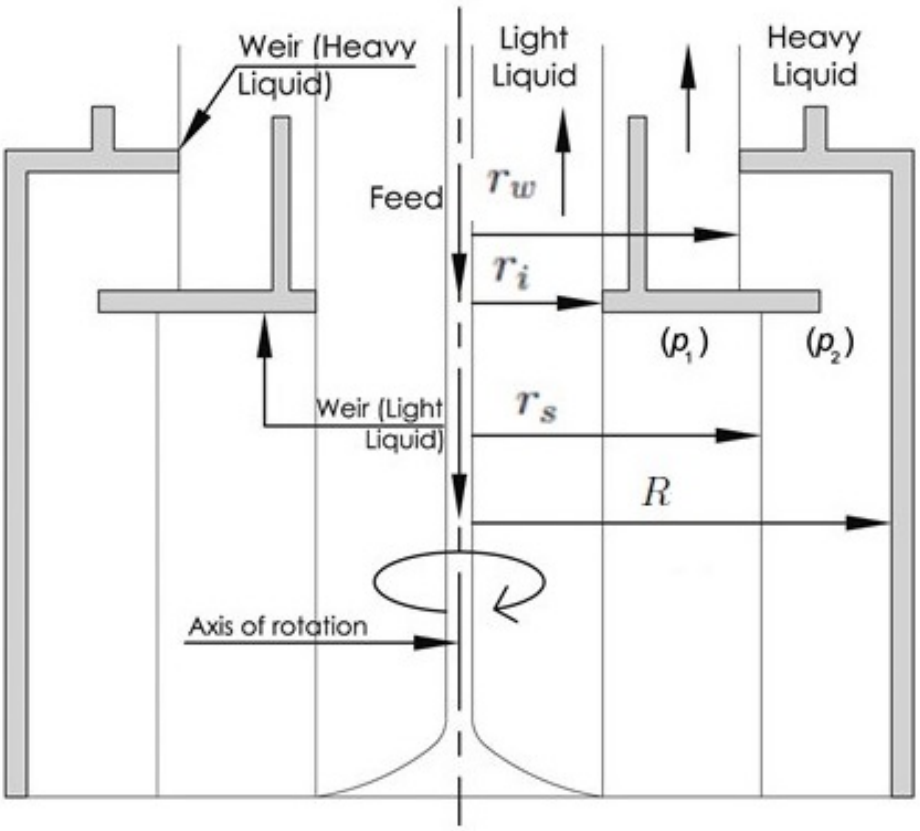

Figure 2.1: Two immiscible liquid separation using disc centrifuge

The integration of equation 2.1 can be simplified to find the pressure P, exerted on walls of centrifuge.

$$P = \frac{1}{2}\rho w^2(R^2 - r_i^2) \tag{2.2}$$

where:

R is radius of bowl

r_i is inner surface of the liquid

Since the pressure exerted on wall by heavy liquid alone at radius of R is equal to the summation of liquid pressure created by two liquids within the bowl, by using equation 2.2 the following relationships can be obtained referring to figure 2.1.

$$\frac{1}{2}\rho_2 w^2(R^2 - r_w^2) = \frac{1}{2}\rho_2 w^2(R^2 - r_s^2) + \frac{1}{2}\rho_1 w^2(r_s^2 - r_i^2) \tag{2.3}$$

$$\frac{(r_s^2 - r_i^2)}{(r_s^2 - r_w^2)} = \frac{\rho_2}{\rho_1} \tag{2.4}$$

where:

r_s is radius of the interface between two liquids

r_w is radius of the outer weir (heavy liquid outlet)

It can be assumed, no slip condition between phases. Since the equal residence time needed for both phases, the following relationship can be derived.

$$\frac{Q_1}{Q_2} = \frac{(r_s^2 - r_i^2)}{(R^2 - r_s^2)} \tag{2.5}$$

where:

Q_1 is heavy liquid flow rate

Q_2 is light liquid flow rate

[15, p. 479]

2.2 Basic fluid flow equations for simulation

2.2.1 Mass Conservation

The general three dimensional form of mass conservation equation for an unsteady, compressible fluid flow can be expressed as,

$$\frac{\partial \rho}{\partial t} + \nabla.(\rho \vec{v}) = S_m \tag{2.6}$$

where:

ρ is liquid density

t is time

$\vec{v}$ is velocity vector

S_m is the source term for mass source or sink

Since it was assumed liquid flow with no liquid droplet evaporation inside the centrifuge, the equation 2.6 can be simplified to,

$$\frac{\partial \rho}{\partial t} + \nabla.(\rho \vec{v}) = 0 \tag{2.7}$$

2.2.2 Momentum Conservation

Conservation of momentum in non accelerating/inertial frame is given as,

$$\frac{\partial \rho \vec{v}}{\partial t} + \nabla.(\rho \vec{v}\vec{v}) = -\nabla P + \nabla.\tau_s + \rho \vec{g} + \vec{F} \tag{2.8}$$

where:

P is static pressure

τ_s is the stress tensor

$\rho \vec{g}$ is gravitational body force

$\vec{F}$ is external body force

According to the Newton's second law, the rate of change of momentum of a fluid particle equals to the sum of forces acting on the fluid particle. Further, the momentum conservation equation which is represented by equation 2.8, is an illustrative version of the Newton's second law and it is based on unit volume.

Basically, momentum is transported by random motion of molecules(molecular momentum transport) and flow of bulk fluid(convective transport). The first term ($\frac{\partial \rho \vec{v}}{\partial t}$) in equation 2.8 denotes the rate of increase of momentum whereas the second term ($\nabla.(\rho \vec{v}\vec{v})$) represents the rate of momentum addition due to convection. Moreover, the summation of third and fourth terms ($-\nabla P + \nabla.\tau_s$) calculates the rate of momentum addition by molecular transport due to molecular stresses. Obviously, pressure forces and viscous forces contribute for molecular stresses since they are acting on the surface of the fluid particle of interest. However, the stress tensor is due to the viscous forces of the fluid and the governing equation for stress tensor represent in equation 2.9.

$$\tau_s = \mu[(\nabla\vec{v} + \nabla\vec{v}^T) - \frac{2}{3}\nabla.\vec{v}I] \tag{2.9}$$

where:

μ is molecular viscosity

I is the unit tensor

$\frac{2}{3}\nabla.\vec{v}I$ is effect of volume dilation

The final two terms ($\rho\vec{g}$ and $\vec{F}$) of equation 2.8 represent the body forces which act within the fluid such as gravitational body force and body forces that can be acted externally. For instance forces like centrifugal force and coriolis force which act on fluid particles when the fluid is rotating.

[16, p. 2,3]

2.3 Modeling the moving zone

Fluent solves wide variety of problems that involve moving zones. However the problem setup may differ according to the behavior of the concerned CFD domain.

In order to find the better initial conditions, the first stage of the simulation was performed as a steady state case with frame motion in relative velocity formulation. However the two liquid components of interest (water and oil) get separated inside the centrifuge due to the transient nature of the flow field. Since the transient, mesh motion set up and coupled solvers only supports the absolute velocity formulation, mass and momentum equations which adjusted to absolute velocities have been considered in transient flow modeling.

2.3.1 Equations for frame motion with relative velocity formulation

The velocity relation

$$\vec{v_r} = \vec{v} - (\vec{\omega} \times \vec{r}) \tag{2.10}$$

where:

v_r is the relative velocity

$\vec{v}$ is the absolute velocity

$\vec{r}$ is the position vector in rotating frame

Mass conservation

$$\frac{\partial \rho}{\partial t} + \nabla.(\rho \vec{v_r}) = S_m \tag{2.11}$$

Momentum conservation

$$\frac{\partial \rho \vec{v_r}}{\partial t} + \nabla.(\rho \vec{v_r} \vec{v_r}) + \rho(2\vec{\omega} \times \vec{v_r} + \vec{\omega} \times \vec{\omega} \times \vec{r}) + \rho \frac{\partial \vec{\omega}}{\partial t} \times \vec{r} = \nabla.\bar{\tau_r} + \rho\vec{g} + \vec{F} \tag{2.12}$$

where:

$\rho \frac{\partial \vec{\omega}}{\partial t} \times \vec{r}$ is variable rotational speed part which has been neglected in fluent modeling

$\rho(2\vec{\omega} \times \vec{v_r} + \vec{\omega} \times \vec{\omega} \times \vec{r})$ represents the Coriolis Effect

[16, p. 20]

2.3.2 Equations for mesh motion with absolute velocity formulation

Mass Conservation

$$\frac{\partial \rho}{\partial t} + \nabla.(\rho \vec{v_r}) = 0 \tag{2.13}$$

Momentum Conservation

$$\frac{\partial \rho \vec{v}}{\partial t} + \nabla.(\rho \vec{v_r} \vec{v}) + \rho[\omega \times (\vec{v} - \vec{v_t})] = -\nabla P + \nabla.\bar{\tau} + \rho\vec{g} + \vec{F} \tag{2.14}$$

[16, p. 21]

2.4 Turbulence Modeling

The centrifugal separator feed contains a mixture of water and coconut oil with 0.5 volume fraction of each, which can be considered as an incompressible, Newtonian

viscous fluid. Depending on the dimensionless flow Reynolds number value the flow regime could be classified as laminar, turbulent or transition. The Reynolds number points out the ratio of inertial forces to the viscous forces and ultimately quantifies the relative effect of these two forces for a given flow condition.

However in literature, it says that the turbulence effect inside a mixing vessel type flow regimes can be assumed with the use of modified Reynolds number. Therefore by assuming the flow pattern inside the Westfalia centrifuge without discs, was somewhat similar to the flow pattern inside the mixing vessel, and the modified Reynolds number has been calculated as follows. [1, p. 44]

$$ModifiedReynoldsNumber(R_D) = \frac{ND^2}{\nu} \tag{2.15}$$

where:

N is the rotational speed (revolutions per second)

D is the diameter (m)

ν is the the kinematic viscosity ($m^2 s^{-1}$)

By using the related values for the centrifuge, where N as $163.67 revs^{-1}$, approximate mean diameter as 0.095 m and ν of the mixture as 8.120601×10^{-6} (by Gambill method [17]) the modified Reynolds number has been estimated as 1.8189×10^7. The detail calculation of kinematic viscosity and modified Reynolds number is in Appendix A.

It has been deduced that, fully developed turbulence exist when the value of modified Reynolds number exceeds 10^4. Therefore, a fair conclusion can be obtained as the flow inside the centrifuge is a fully developed turbulent flow.

The Reynolds number could be found during the entire flow simulation stage as well. In comply with the modified Reynolds number calculations, strong turbulence has also been observed in certain locations inside the centrifuge in simulation results. Since the literature findings also supported the turbulence behavior in similar cases, it is essential to select a suitable turbulent model for CFD flow simulation inside the centrifuge.

2.4.1 Model selection for turbulence modeling

The turbulence flow behavior is intrinsically random and chaotic. Therefore velocity and all other properties vary in a chaotic way, despite the constant imposed boundary conditions. Due to the nature of Navier Stokes equation, three dimensional turbulence models are complex, as it is inherently non linear, time dependent and comprises of three dimensional partial differential equations.

Selection of a suitable viscous model for a specific application is one of the crucial decisions of any researcher, since various facts should have to be considered other than the model suitability. One such essential aspect is available computational cost in terms of memory and CPU time. Moreover, relevancy of the applied viscous model for the particular application would definitely end up with accurate and reliable simulation results. Figure 2.2 represents the selected viscous model options and corresponding parameters supported in ANSYS Fluent.

Three basic viscous models have been considered when selecting an appropriate turbulence model for the considered centrifugal separator's fluid motion modeling stage. However, key features of the considered viscous models have been briefly illustrated below, in order to identify the capabilities and limitations of each. For the model simulation, $k-\varepsilon$ (2 equation), $k-\omega$ (2 equation) and Reynolds Stress (7 equation) models were basically taken in to account. The selected model functionality is inline with the literature findings and theoretical background of the centrifuge performance.

The standard $k-\varepsilon$ model (Launder and Spalding, 1974) has two model equations, one for the turbulent kinetic energy(k) which determines the energy of turbulence and one for the turbulent dissipation rate ε which indicates the scale of turbulence. This technique is less computationally demanding compared to others, but the ε equation has been suspected as one of the main sources of accuracy limitations. Besides, it's assumption of isotropic eddy viscosity is not accurate enough as well. The RNG (renormalization group) version of $k-\varepsilon$ model has strain-dependent correction constant for ε equation that leads to more accurate swirl simulation results than the standard $k-\varepsilon$ approach.[18, p. 77]

Another most widely use empirical turbulence model is, $k-\omega$ model which has two

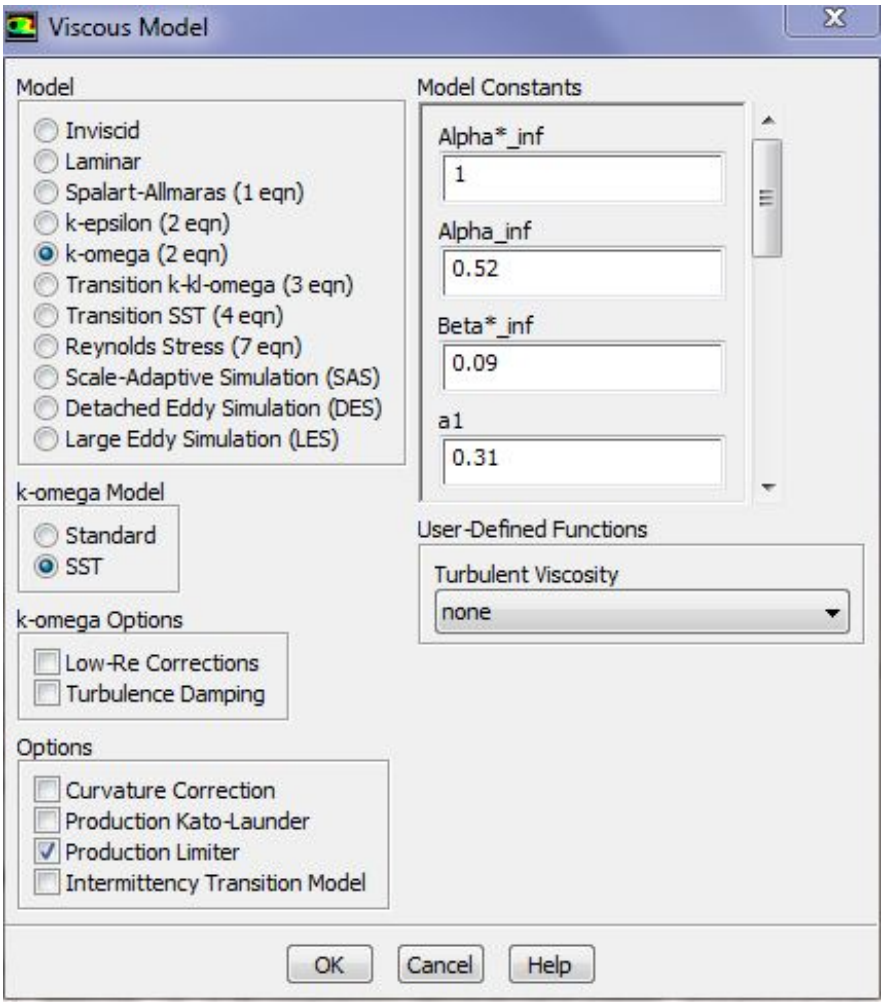

Figure 2.2: Selected viscous model options in Fluent

forms as standard and SST (Shear Stress transport) $k-\omega$ model. $k-\omega$ model predicts near wall while $k-\varepsilon$ model predicts far from the boundary. It includes two extra transport equations for turbulent kinetic energy (k) and specific dissipation rate(ω) which equals to ε/k. It does not require wall damping functions in low Reynolds number applications which is a great advantage in simulations. SST $k-\omega$ model is a variant of standard $k-\varepsilon$ model which also compatible for the flows with adverse pressure gradients. It combines standard $k-\omega$ model and $k-\varepsilon$ model which simulates the inner region with standard $k-\omega$ and the free shear flow with $k-\varepsilon$ model.

In Reynolds Stress model, the Reynolds stresses are directly figured out, discarding the eddy viscosity approach. It is a second order or second moment closure model with better accuracy than any other two equation models. Since seven additional transport

equations, including number of partial differential equations have to be solved during 3D simulation stage of Reynolds Stress model, it is more computationally intensive, compared to other viscous models. However it is one of the complete turbulent model options available which works well for most engineering flows.

When considering the flow behavior, Reynolds Stress (7 equation) model shows reasonable fidelity. But since it requires high CPU time and memory, it is not economically viable to use with the available computer facility. Even though $k-\omega$ models are considered as modification of $k-\varepsilon$, as they are empirical models it is decided to choose a $k-\omega$ model for turbulence modeling. Therefore SST $k-\omega$ model which is said to be more preferable for separating flows has been selected for the turbulence modeling of the centrifugal separator.[18, p. 78]

Transport equations for SST $k-\omega$ model

In SST $k-\omega$ model, the turbulent kinetic energy(k) and specific dissipation rate(ω) are obtained from the following transport equations[19].

$$\frac{\partial(\rho k)}{\partial t}+\frac{\partial(\rho k u_i)}{\partial x_i}=\frac{\partial(\Gamma_k \frac{\partial k}{\partial x_j})}{\partial x_j}+G_k-Y_k+S_k \tag{2.16}$$

where:

Γ_k is the effective diffusivity of k

G_k is the generation of turbulent kinetic energy due to mean velocity gradient

Y_k is the dissipation of k

S_k is the user defined source term

$$\frac{\partial(\rho \omega)}{\partial t}+\frac{\partial(\rho \omega u_i)}{\partial x_i}=\frac{\partial(\Gamma_\omega \frac{\partial \omega}{\partial x_j})}{\partial x_j}+G_\omega-Y_\omega+D_\omega+S_\omega \tag{2.17}$$

where:

Γ_ω is the effective diffusivity of ω

G_ω is the generation of ω

Y_ω is the dissipation of ω

D_ω is the cross diffusion term

S_ω is the user defined source term

2.5 Solver Selection

There are two basic solver types available in fluent, called as 'Density Based Solver'and 'Pressure Based Solver'. Therefore the appropriate solver for a particular application should be chosen by considering the nature of the flow field and compatibility of the selected solver with other solvers.

Pressure based solver is applicable for wide range of flow regimes from low speed in-compressible to high speed compressible flows whereas density based solver can be applied when strong coupling or interdependence exists between density, energy, momentum and/or species. Pressure based solver can be categorized as segregated solver which sequentially solves the pressure correction and momentum and coupled solver which solves pressure and momentum simultaneously. Further, the solution procedure for pressure based solver is represented in figure 2.3 [20, p. 40].The density based solver is a coupled solver that uses vector form to solve continuity, momentum, energy and species equations. Pressure is computed through equation of state and other scalar equations are solved in a segregated fashion.

Flow inside the centrifuge is regarded as high speed, in-compressible, multi-phase flow. Since the Volume of Fluid which is the only multi-phase model that is appropriate for coconut oil – water mixture separation, compatible only with the pressure based solver it is chosen for the 3 D modeling of the centrifuge [16, p. 474].Moreover, Pressure Implicit with Splitting of Operators (PISO) which is said to an extension of Semi-Implicit Method for Pressure-Linked Equations(SIMPLE) algorithm has been selected for pressure-velocity coupling which also used to simulate the similar cases in literature [11, p. 24]. PISO algorithm includes one predictor step and two corrector steps which improve the performance of transient flows under complex geometry conditions including grid cells with higher skewness.

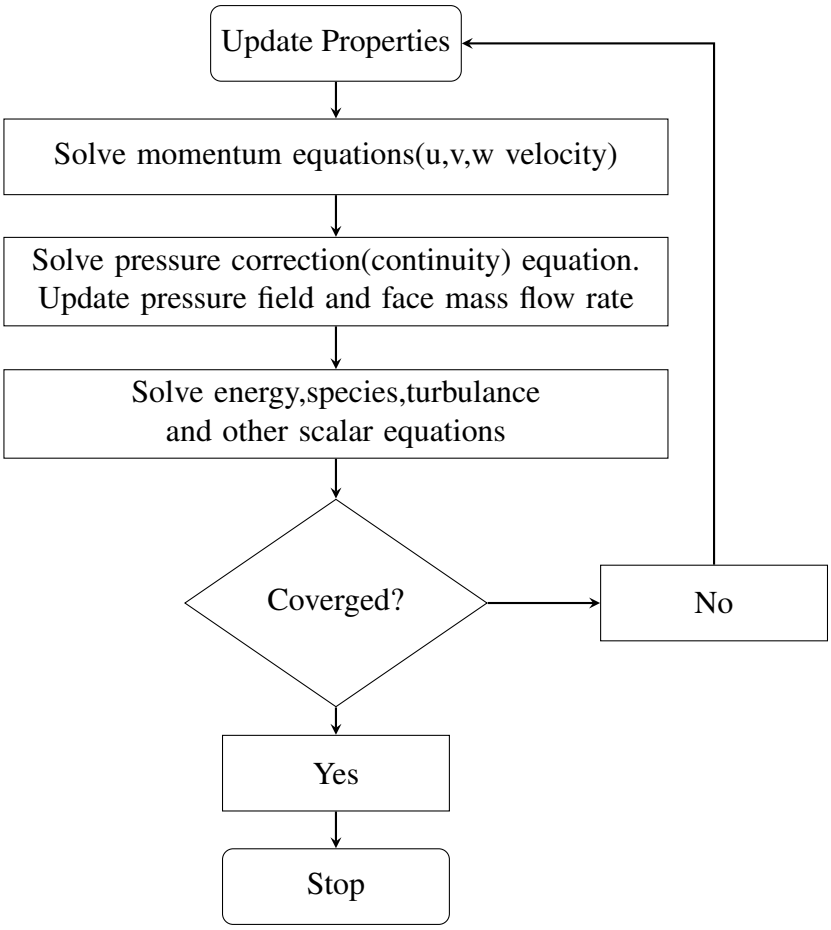

Figure 2.3: Solution procedure of pressure based solver

2.6 Multi-phase Flow Modeling

In general, three physical phases: solid, liquid and gas encounter in natural systems and the flow regimes are mixtures of two or more phases which can be identified as multi-phase flows. However, the ANSYS Fluent has a far broader understanding about the concept of phases and multi-phase systems,rather than the idea of mixtures of two or three basic physical phases. In a multi-phase flow, a phase could be defined as an identifiable class of material that has particular inertial response and interaction with the flow and the potential field in which it is immersed. Therefore, a mixture of liquids of different densities can also be considered as a multi-phase flow which has been used in flow modeling of the centrifuge.

The advancement of computational fluid mechanics have provided more sophisticated techniques to model the multi-phase flow regimes which includes two basic ap-

proaches: Euler-Lagrange approach and Euler-Euler approach. Euler-Lagrange model is based on an assumption of low dispersed phase volume fraction which leads the model inappropriate for the liquid-liquid mixtures. However, in this approach time averaged Navier Stokes equation is used to solve the fluid phase considering it as a continuum whereas the dispersed phase is solved by tracking large number of particles through the calculated flow field.

In Euler-Euler approach, the different phases are assumed to be as interpenetrating continua. It introduces the phase volume fractions which are continuous functions of space and time. Moreover, sum of all the volume fractions must be equal to one and the approach is also compatible with the liquid-liquid mixtures. Since there are three modeling techniques: Mixture Model, VOF Model and Eulerian Model also available in this approach, a suitable multi-phase Euler-Euler model which represents the respective flow can be selected considering the individual characteristic of each [16, p. 468].

Mixture model is the simplest of all which solves one momentum equation for the n-phases being transported. So that, less computational effort is required. Further, it has been identified that, the model works well for the particle-laden flow with low loading. Therefore it doesn't match with the modeling requirements of the liquid phases inside the centrifuge.

Eulerian multi-phase model is computationally demanding, but more accurate modeling option. It solves momentum equation for each and every phase separately and they are coupled through inter phase interaction forces which are addressed by interpolating source terms. With the availability of limited computer facility, it is difficult to apply this technique for multi-phase flow modeling inside the centrifuge.

VOF model is better applicable for free surface flows or separated flows with two or more immiscible fluids only with a pressure based solver. It solves a single set of momentum equations and tracks the volume fraction of each domain. VOF model works well for liquid-liquid inter phase modeling like a mixture of oil and water. Concerning the aspect of the fluid flow field of interest, VOF is considered as the appropriate modeling option for multi-phase flow modeling inside the centrifuge. However, from the

available Implicit and Explicit schemes, Implicit scheme has been chosen as it doesn't have any Courant number limitation and compatible even with the low quality mesh. Even though Explicit scheme provides an accurate solution with sharper interface, it requires high quality mesh, which again a barrier with available limited computer facility. Further, in body force formulation of Implicit VOF, the implicit body forces have been allowed. According to the literature findings, this option has been designed for the flows with large body forces such as in centrifugal separators and rotating machinery which has larger rotational accelerations.

2.7 Selection of Discretization schemes

2.7.1 Finite Volume Method

Finite Volume Method (FVM) or control volume method is the technique that uses in ANSYS Fluent solvers. This approach divides the desired domain in to a finite set of control volumes and the general conservation equations for mass, momentum, species and etc are solved based on this set of control volumes. In FVM, the partial differential equations of general transport equations are discretized in to algebraic equations which can be ultimately solved numerically to yield the solution. The general form of a scalar transport equation comprises of an unsteady term plus convection term which equal to the diffusion term plus the source term of the respective scalar and can be expressed as Equation 2.18.

$$\frac{\partial \int_v \rho \Phi dv}{\partial t} + \oint_A \rho \Phi \vec{v}.d\vec{A} = \oint_A \Gamma_\Phi \nabla_\Phi .d\vec{A} + \int_v S_\Phi dv \tag{2.18}$$

where:

Φ is a scalar quantity

$\vec{A}$ is surface area vector

Γ_Φ is diffusion coefficient for scalar Φ

∇_Φ is gradient of scalar Φ

S_Φ is source of scalar Φ per unit control volume

The equation 2.18 can be discretized on a control volume to obtain the equation 2.19.

$$\frac{\partial \rho \Phi}{\partial t} V + \sum_{f}^{N_{face}} \rho_f \vec{V_f} \Phi_f . \vec{A_f} = \sum_{f}^{N_{face}} \Gamma_\Phi \nabla \Phi_f . \vec{A_f} + S_\Phi V \tag{2.19}$$

where:

N_{face} is number of faces in a cell

V is the volume of a cell

Φ is a scalar quantity

Φ_f is the value of scalar Φ convectted through face f

$\rho_f \vec{V_f} \Phi_f . \vec{A_f}$ is mass flux through face f

Γ_Φ is diffusion coefficient of scalar Φ

$\nabla \Phi_f$ is gradient of scalar Φ at face f

S_Φ is source of scalar per unit volume

[21]

2.7.2 Selected Discretization Schemes in Modeling

It is very important to choose suitable spatial discretization schemes from the available different options in ANSYS Fluent. Therefore, by considering the behavior of the flow inside the centrifuge and compatibility to the available computer power, spatial discretization schemes for 'Gradient', 'Pressure', 'Momentum', 'Volume Fraction'and 'Turbulent Kinetic Energy'were selected.

Gradients of solution variables are required to evaluate diffusive fluxes which is represented by the first term after the equal sign in equation 2.18. Further, the gradients of solution variables at faces are computed using multidimensional Taylor series

expansion. In ANSYS Fluent, there are three options available for gradient formulation of solution variables such as 'Green Gauss Cell Based', 'Green Gauss Node Based'and 'Least Square Cell Based'. The 'Green Gauss Cell Based'method is the default one and the solution can have false diffusion. The 'Green Gauss Node Based'and 'Least Square Cell Based'methods which minimize the false diffusion have same level of accuracy, but the first is recommended for tri/tet meshes whereas the latter is for polyhedral meshes. Therefore considering the mesh type and accuracy level, 'Green Gauss Node Based'option has been selected for gradient formulation of the fluid flow inside the centrifuge.

In ANSYS Fluent there are five interpolation schemes available for face pressure formulation. The 'Standard'is the default option which has reduced level of accuracy when steep pressure changes are exhibited by the flow. In contrast to 'Standard'option, 'PRESTO!'shows a better level of accuracy for highly swirling flows in curved domains with steep pressure gradients. The next 'Linear'option is generally applicable when convergent difficulties are encountered for highly unphysical flows where as the 'Second Order'option which cannot be applied with VOF multi-phase model, but can be applied for compressible flows. As the name implies the last option, 'Body Force Weighted'is for flows with high body forces. However, by considering the characteristics and applicability of each, 'PRESTO!'has been chosen for calculating the face pressure.

Among several spatial discretization techniques such as, first order upwind, second order upwind, QUICK and etc available in ANSYS Fluent to dicretise the convective term, the second order upwind scheme has been used to dicretise momentum, turbulent kinetic energy and turbulent dissipation rate. Even though its convergence is slow, it has second order accuracy. Also it has reasonable level of accuracy over other schemes for the complex geometries where the flow is not aligned with the grid [20].

The VOF model which has been selected for multi-phase flow modeling has two options such as Implicit and Explicit schemes for volume fraction formulation. Since Implicit scheme was selected for the volume fraction modeling inside the centrifuge with a clear justification mentioned in section 2.6, the discretization method for the

volume fraction has been selected by considering the information in table 2.1. By considering the accuracy, speed and compatibility with Implicit scheme, compressive interface scheme has been chosen to model the interface of water and coconut oil.

Table 2.1: Interface scheme comparison for VOF scheme

Interface Scheme	Implicit	Explicit	Accuracy	Speed
First Order	✓	X	Not recommended	Not recommended
Second Order	✓	X	Not recommended	Not recommended
QUICK	✓	✓	Low	High
Modified HRIC	✓	✓	Medium	High
CICSAM	X	✓	High	Medium
Compressive	✓	✓	High	Medium to high
Georeconstruct	X	✓	Very high	Low to medium
BGM	✓	X	Very high	Low to medium

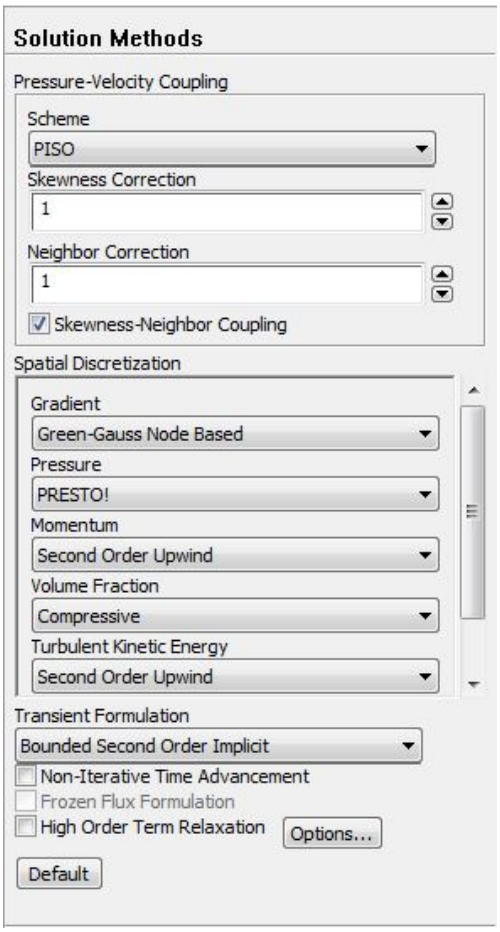

(a) Solution methods

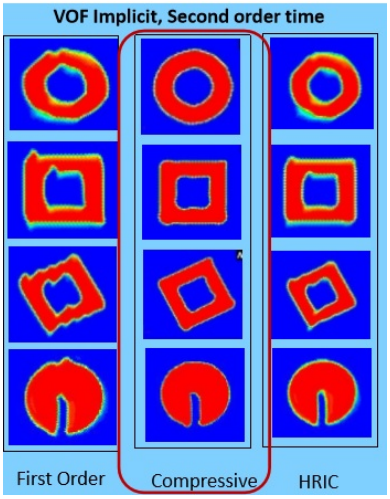

(b) Second order time discretization for implicit VOF

Figure 2.4: Selected solution methods and second order time discretization for implicit VOF

For transient formulation, Bounded Second Order Implicit scheme is appropriate to obtain a sharp interface comparable to most accurate Geo-Reconstruct, as recommended in literature. The selected solution methods and interface comparison for VOF Implicit scheme with Second Order time discretization is represented by figures 2.4a and 2.4b respectively.

CHAPTER 3 : METHODOLOGY

The purpose of this chapter is to elaborate the complete methodology in modeling the intended centrifuge geometry. The first and foremost 3.1 section summarizes the modeling approach which includes descriptions on the original Westfalia separator, the geometry selection in modeling with justifications and an overview on CFD modeling technique in 3.1.1, 3.1.2 and 3.1.3 sub sections respectively. The section 3.2 expounds the mesh interface, whereas 3.2.1 and 3.2.2 subsections comprise the features that have been applied in meshing the geometry and detailed clarification on quality of the generated mesh respectively. In order to avoid any duplication, a very brief description on solution set up is summarized in section 3.3 since; despite the boundary conditions, materials and phases almost all the sectors have been clearly illustrated in chapter 2. However this particular section includes five sub divisions from 3.3.1 to 3.3.5 as models, materials and phases, boundary conditions, 'solution methods and controls' and 'solution controls and initialization' in order to keep the flow of modeling methodology. The section 3.4 clarifies the step by step procedure that has been practiced during modeling and simulation. Finally the chapter 3 concludes with section 3.5 which covers the method of empirical validation of simulation results.

3.1 Geometry and CFD modeling

3.1.1 The Geometry Selection

The Westfalia Separator

The Westfalia separator is a disc type, motor driven centrifuge which is designed to separate two immiscible liquids. The centrifugation process is continuous which the feed and two effluents are supplied and collected continuously. The processing time depends on the properties of the liquids.

The equipment can be mounted or stand along the floor. The Westfalia separator with all it's parts and a cross section of the equipment and illustration of flow path inside a cross section are given in sub figures 3.1a and 3.1b respectively. It contains

(a) Centrifuge with all accessories

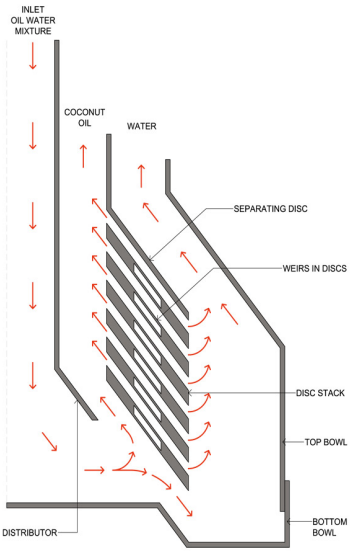

(b) Cross Section and Liquid Flow Path

Figure 3.1: The Westfalia Centrifugal Separator

intake vessel, top bowl, separating disc, 20 discs, distributor, bottom bowl and three collecting covers named as overflow, upper and lower. The feed mixture is supplied by a tap which allows controlling the mixture flow rate, to the intake vessel. Then it flows through a rotating passage and fills inside after flowing through the distributor.

Since the bowl rotates at the speed of 9820rpm (approximately 1028rad/s), mixture get separated and low density liquid (coconut oil) and high density liquid (water) can be collected at upper and lower collecting covers respectively. If there's any overflow present, it can be collected via overflow collecting cover. The discs inside the centrifuge improve the efficiency of separation while the separating disc separates the flow paths of heavier and lighter liquids.

3.1.2 Intended Centrifuge Geometry

The geometry of Westfalia separator has been simplified by removing 20 discs, in order to avoid model complexity. Resulting centrifuge geometry was modeled 3 dimensionally. At the stage of geometry drawing, it has only been considered the fluid region,

to avoid complexities in meshing as it allows to mesh the geometry as it is. If not, the cavity region of the intended centrifuge should be carefully extracted to ANSYS at the meshing stage. However, the simplified 3D geometry mesh has less number of mesh cells compared to the original which improves computational speed, reduce computational power and ultimately save time and money. On the other hand, VOF (Volume of Fluid) model which models the multiphase flow also computationally intensive. Therefore, unavailability of high speed, powerful computer facility ultimately leads to shrink the geometry to this selected state. The complete proposed geometry is given in figure 3.2. Since it doesn't contain any discs, the separation efficiency has significantly lowered. However, the proposed geometry includes inlet, two outlets for heavy and light liquids (outlet1 and 2), separating disc, distributor, top bowl and bottom bowls.

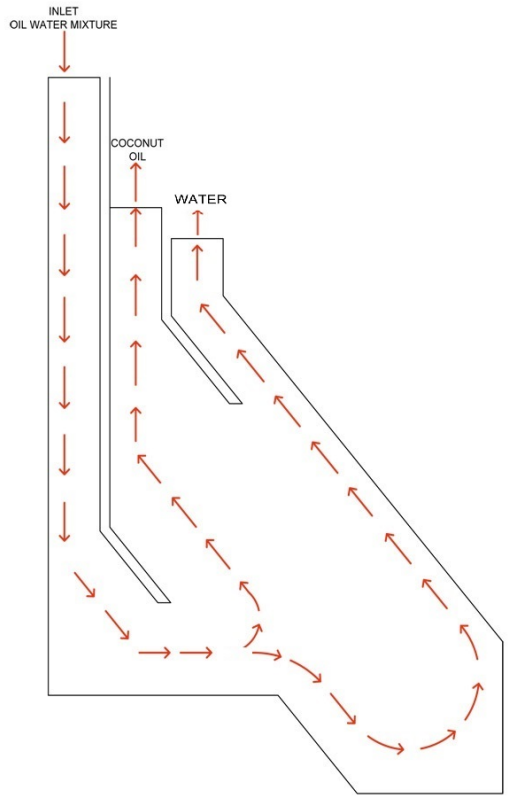

Figure 3.2: Liquid Flow region of the selected centrifuge geometry

3.1.3 Overview of CFD modeling approach

The intended 3D geometry has been sketched with accurate dimensions using Solid Works 2013 and the fluid flow field has been modeled using Ansys Fluent 15 commercial software package. Key steps in 3 dimensional fluid flow analysis inside centrifuge represents in figure 3.3.

The intended centrifuge geometry with reasonably precise dimensions has been imported to Workbench design modeler, by saving it in the file format of IGES (.igs). In Solid Works, the surface representation/system preferences have been changed from standard to ANSYS in order to attain the compatibility. The mixture inlet, oil and water outlet boundaries have been specified as inlet, outlet1 and outlet 2 by using the Named Selection tool available in Workbench.

Generation of 3D mesh is one of the crucial tasks when there's no powerful computer facility available. However, ANSYS Workbench provides robust, easy to use meshing tool that simplifies the mesh generation. With the available resources, a realistically better quality 3D mesh has been generated for intended centrifuge geometry and further details about mesh interface is given in section 3.2.

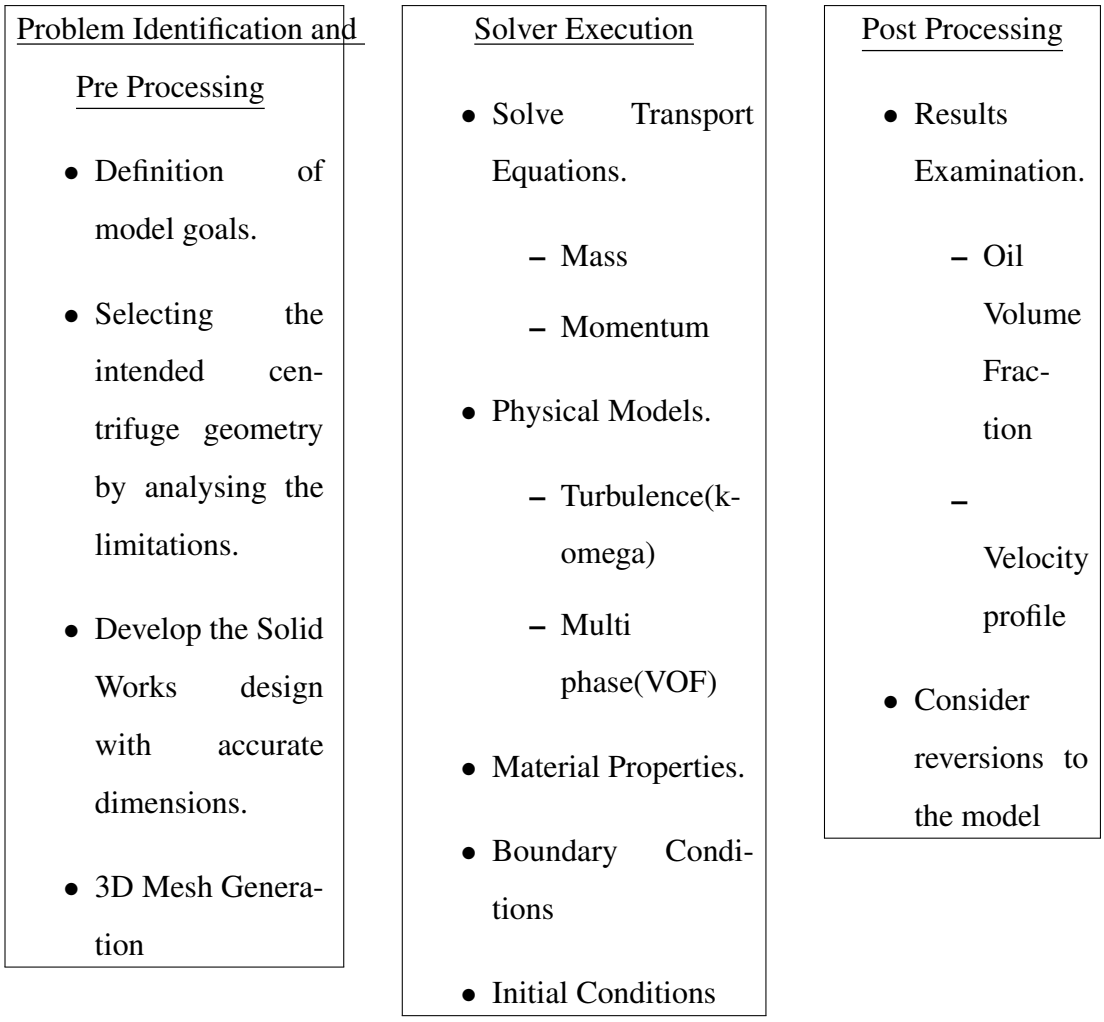

Figure 3.3: Basic steps of problem analysis in Fluent-CFD

At the stage of simulation the mass and momentum conservation equations are solved iteratively across the divided cells, considering the provided initial and boundary conditions. The Volume of Fluid multi-phase model tracks the interface between two liquids and solves single momentum equation and the velocity field is shared by the two phases. The $k-\omega$ viscous model determines the scale and energy of turbulence. Further, elaboration on theoretical background of conservation equations, viscous and multi-phase models, discretization techniques is given chapter 2.

The simulation results of required parameters like velocity profile, pressure profile or coconut oil volume fraction at any given location can be visualized via ANSYS Workbench post processing tool. The incompatibility of the obtained simulation results

with the empirical results would lead reversions to the model parameters or set ups.

3.2 Mesh Interface

Generating the most appropriate mesh for a particular geometry is one of the key tasks in CFD flow simulations. Ansys meshing is an automated, accurate, high performance tool which provides good quality mesh according to the user requirements. Availability of parallel meshing facility is one of the greatest advantages in Ansys meshing as it is efficient and ultimately saves time. Since the quality of mesh can be assessed with several quality checking parameters like element quality, orthogonal quality, skewness and etc, the user can re-mesh it, if the required quality limit does not attain. However with the limited on hand computer resources, a much better mesh has been generated for the selected centrifuge geometry, using the facilitated mesh featuring options in ANSYS Workbench. Quality of the generated mesh represents in table 3.1.

3.2.1 Applied features in ANSYS Fluent Meshing

In mesh sizing, advanced size function feature allows the user to create smooth and quality mesh with defaults that best suited to CFD solvers. On the other hand, it adaptively refines the mesh according to the geometric aspects like surface curvature and proximity. Proximity and curvature advanced size function which adequately captures all geometric features is the most appropriate from all, could not be used, due to the insufficient hardware availability. However, the curvature advanced size function has been selected for intended centrifuge geometry meshing which is reasonably better and automatically refines all regions of higher curvature.

In order to enhance the level of mesh accuracy, the element size has been refined by selecting 'Fine'Relevance Centre. Quality of the mesh elements can be further improved and smoothen by setting the smoothing and transition features to 'High'and 'Slow'respectively. The curvature based local refinements can be adjusted by selecting a 'Fine'span angle center ($36^0 - 12^0$) which sub divides the curvature regions of the meshing geometry until the individual element span this angle. The curvature normal angle has been set to 10^0 which is said to be finer the angle finer the mesh element

size, ultimately improves the level of accuracy,[22]. Moreover, the growth rate option which is the ratio of size of an element with size of previous element controls the rate of element, has been set to 1.10. Lesser the growth rate, finer and accurate the mesh, though the number of elements is higher. The below figure 3.4 depicts the applied features in meshing.

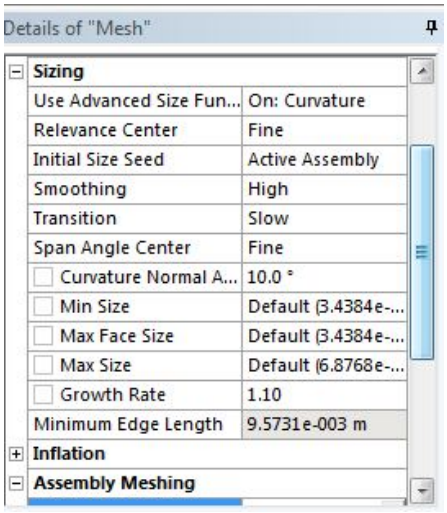

Figure 3.4: Applied mesh features

The generated mesh for the centrifuge and it's cross section are illustrated by the following 3.5 and 3.6 figures.

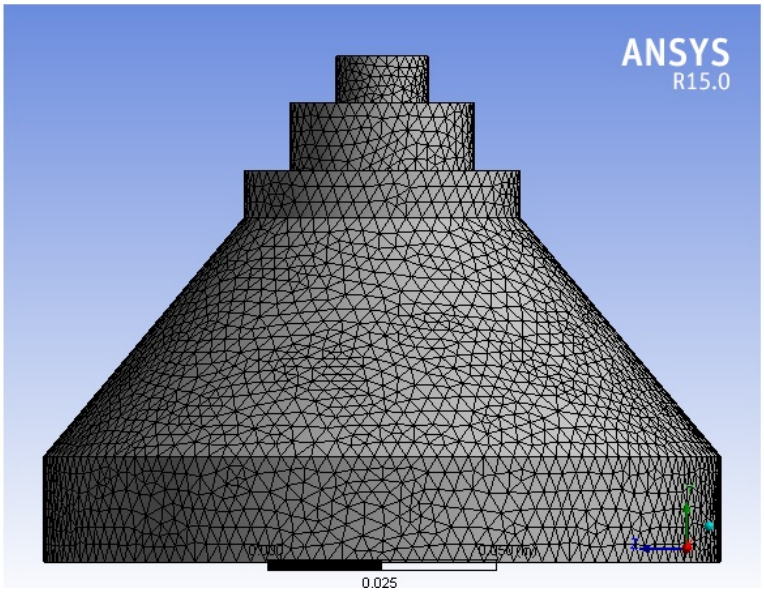

Figure 3.5: The generated tri/tet mesh for centrifuge

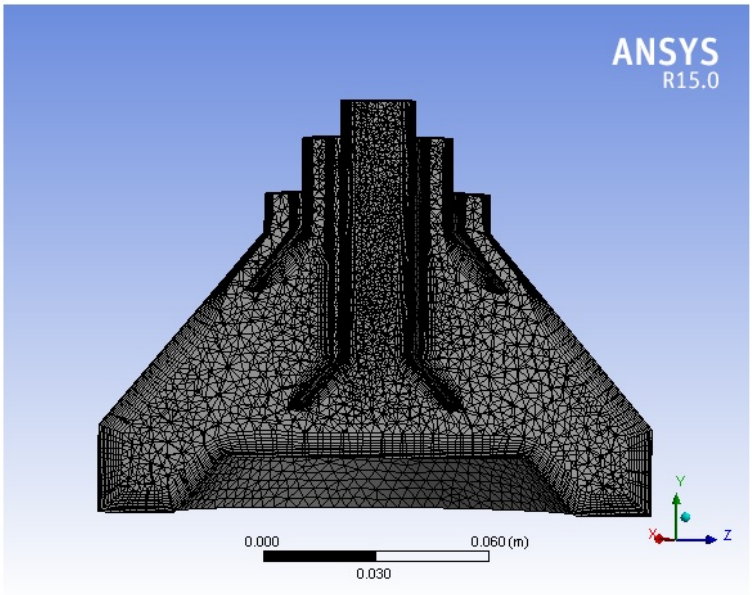

Figure 3.6: Cross section of the generated mesh

3.2.2 Quality of the generated mesh

With all these settings, the mesh of the intended centrifuge geometry consists of 53,192 nodes and 286,977 elements and the mesh is compatible with the hardware availability as well.

In ANSYS meshing, it is recommended to keep maximum cell skewness less than 0.95 as high skewed cells lead to inaccurate solution and slow convergence. Further, maximum skewness in between 0.5 and 0.8 is considered as a good quality mesh which has been achieved in this geometry meshing[23].

Table 3.1: Quality parameters of the generated mesh

	Element Quality	Aspect Ratio	Jacobian Ratio	Warping Factor and Parallel Deviation	Maximum Corner Angle	Skewness	Orthogonal Quality
Min	0.2185	1.1663	1	0	71.0180	3.4734	0.2314
Max	0.9998	10.137	1	0	159.030	0.7968	0.9959
Average	0.8396	1.8380	1	0	95.8060	0.2232	0.8611

3.3 The solution setup

3.3.1 Models

An illustrative justification for selecting of $k-\omega$ model as viscous model and VOF as multiphase model is given in 2.4.1 and 2.6 sections in chapter 2.

3.3.2 Materials and phases

The inlet fluid of the centrifuge contains coconut oil and water mixture which are the two materials or phases considered in the flow simulation. Though the approximate room temperature in university premises is around 25^0C, most of all the values are published in literature are at 15^0C-20^0C. Therefore it has been assumed a negligible variation of density and viscosity within this 10^0C-5^0C range and the respective values has been used, as it was in literature. However, the density and viscosity values for water which are of 998.2 kgm^{-3} and 0.001003 $kgm^{-1}s^{-1}$ respectively have been retrieved from the fluent database. Since the coconut oil is not a defined material in fluent database, it has been added with relevant values. Therefore, density and viscosity of coconut oil have been considered as 924 kgm^{-3} and 0.06 $kgm^{-1}s^{-1}$ respectively[24].

3.3.3 Boundary Conditions

Selection of different boundary types is another critical task, since the selected boundary types should align with the conservation of fluxes. However, the centrifuge geometry of interest comprises of four defined boundaries such as Inlet, Outlet 1 for coconut oil out flow, Outlet 2 for water out flow and the centrifuge wall.

The inlet liquid mixture flow has been adjusted to supply a constant mass flow rate of 0.05kg/s as it can be controlled with the use of a controlling valve. Therefore by computing the inlet circular surface area, the inlet mixture flow velocity has been estimated and specified the boundary region as Velocity Inlet by assuming negligible level of inlet flow turbulence. Even though ANSYS fluent allows the mass flow inlet boundary condition, generally the velocity inlet boundary condition can be considered as more precise option since it has the facility to specify the flow direction.

With the Velocity Inlet upstream boundary condition, Pressure Outlet downstream boundary condition can be coupled. Therefore, the outlet 1 has been selected as a pressure outlet. In pressure outlet boundaries, for subcritical outlet flows (Fr<1), if there are only two phases, then the pressure is taken from the pressure profile specified over the boundary, otherwise the pressure is taken from the neighboring cell [16].

When the two outlet boundaries are closer, it is not recommended in ANSYS Fluent to select both as Pressure Outlets. Hence, the Outlet 2 has been selected as an Outlet Vent boundary condition which is also compatible with the inlet, Velocity Inlet boundary condition. Moreover, the super sonic gauge pressure at the inlet has been specified as $190,000Pa$ and as recommended, the gauge pressures at two outlets has been set $8psi$ ($55158.1Pa$) less in comparison with the inlet [25].

The wall of the centrifuge has been specified as a non-slip, rotational moving wall which is of the same rotational velocity as the mesh. The table 3.2 represents the boundary values used for the simulation.

Table 3.2: Boundary Conditions

Boundary	Boundary Type	Velocity/Rotational speed	Gauge Pressure (Pa)
Inlet	Velocity Inlet	0.1655967ms^{-1}	190,000
Outlet 1 (Oil Outlet)	Pressure Outlet	-	134,842
Outlet 2(Water Outlet)	Outlet Vent	-	134,842
Wall	Wall	1028 $rads^{-1}$	-

3.3.4 Solution methods and controls

An illustrative explanation on selection of PISO scheme for pressure velocity coupling is in section 2.5 solver selection section. Further, selected spatial discretization schemes for pressure, momentum, volume fraction, turbulent kinetic energy and etc has been elaborated with reasonable validations under section 2.7 selection of discretization schemes.

3.3.5 Solution controls and initialization

Under Relaxation factors for pressure, density and body forces have been set to 0.3,1,1 respectively whereas the under relaxation factors of momentum, volume fraction, turbulent kinetic energy, specific dissipation rate and turbulent kinetic energy set to 0.5. With the selected values, the simulation solution has converged without errors.

It is generally considered that the method of initialization is not important as long as the solution get converged. However in order to achieve faster convergence, an appropriate selection of initialization method is an advantage.For rotational, multiphase flow simulations, it is a common practice to use standard initialization [26].Therefore it has been selected as the initialization technique for simulation of flow inside the intended centrifuge.

3.4 The Simulation Procedure

The process of simulation has been divided in to two basic stages in order to obtain better final results. In the first stage of the simulation the case has been run in steady state to acquire better initial conditions[27].During this steady state stage, the model has been simulated using SIMPLE algorithm for 4000 iterations at one tenth ($102.8 rads^{-1}$) of the actual rotational speed of the centrifuge.

At the second stage of simulation, the exact transient flow behavior inside the centrifuge has been considered and the same case of steady state solution has been continued for this transient flow simulation. In addition PISO transient pressure velocity coupling scheme has been used with the time step size of 0.005s (5 mili seconds) with 40 maximum iterations for each time step. Even though smaller the time step and higher the number of iterations per time step, more accurate the solution is, with the available limited hardware resources no best time step size could be expected. Moreover, it is assumed that the Westfalia separator takes at least 16 seconds to attain its actual rotational speed. Therefore, the rotational speed of the centrifuge model has been fractionally increased in a way such that 0.1, 0.3, 0.5, 0.75 and finally 1, whereas to attain the rotational speeds of 102.8, 308.4, 514, 771 and 1028 $rads^{-1}$ respectively.

On the other hand, this rotational speed gradual increment method suggested in literature for rotational flow simulation for more accurate final results as well.[28]

The most intended simulation result is the coconut oil volume fraction in outlet 1 and the phase separation of two liquids inside the centrifuge. When the simulation is in progress, images of flow inside the centrifuge have been saved to capture the separation intensity in a cross section of the centrifuge.

3.5 Model Validation

In order to empirically validate the developed model, a series of experiments have been carried out using the Westfalia centrifugal separator in the laboratory. Since the considered geometry of the centrifugal separator does not comprise the disc stack, it has also been removed from the equipment at the experimenting stage. Therefore, the liquid separation efficiency has considerably reduced.

An inlet liquid mixture sample which contains 0.5 volume fraction of coconut oil has been prepared by mixing 1 liter of each of the liquids inside the mixing chamber. The mixture has been continuously agitated to keep homogeneous properties. The feed mixture flow rate has been kept constant by controlling the inlet valve and the equipment has operated at its constant rotational speed of 1028 rad/s. The out flows of oil and water has been collected to monitor the water and oil volume fractions. Further, the operating time has been measured using a stop watch.

The oil and water volume fractions of outflows have been measured by inserting them to a separating funnel and allowing the separation for 36 hours.

CHAPTER 4 : RESULTS AND DISCUSSION

This chapter contains the results and discussion of simulation and experiment. The section 4.1 basically covers the simulation results of velocity profile, pressure profile and measures of turbulence such as turbulence intensity, turbulent kinetic energy, specific dissipation rate and phase volume fraction with graphical representations and comparison with the theoretical approach. The section 4.2 includes an elaborate description of experiment procedure, experiment results and their relation to the simulation results.

4.1 Simulation Results and Discussion

4.1.1 Velocity Profile

The simulation results of velocity comprise the XY plot to depict the relative velocity magnitude in 'Z' direction and smoothly fitted relative velocity curve which are represented by figures 4.1 and 4.2 respectively. Since the graph is symmetric with respect to y axis, the positive z direction has only been considered for the fitted curve.

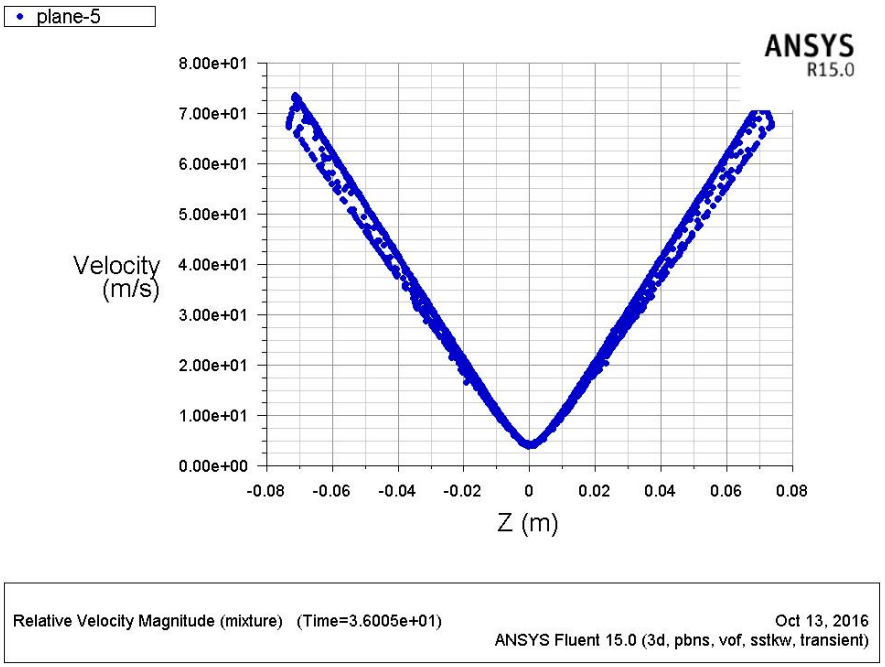

Figure 4.1: Graph of relative velocity magnitude vs 'z' direction in the mid plane

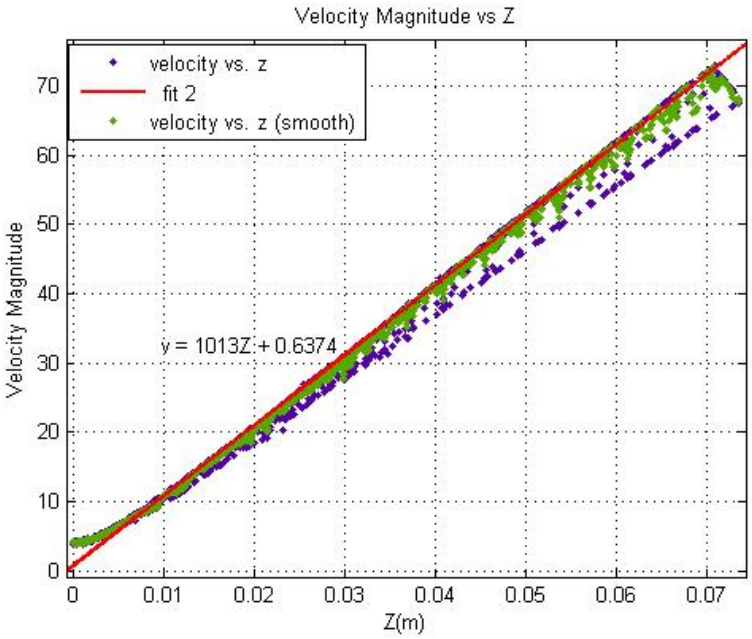

Figure 4.2: The fitted curve for relative velocity magnitude in positive z direction in the mid plane

The mesh motion of the three dimensional model has been observed relative to to the coordinate frame rotation at constant rate of ω and the velocity vector is measured with respect to the rotating axis 'Y'. Therefore, in comply with equation 2.10, it can be obtained that relative velocity magnitude should satisfy the following equation 4.1.

$$\vec{v} = \vec{r}.\vec{\omega} \tag{4.1}$$

Since the Westfalia centrifugal separator is running under constant speed of rotation, theoretically the velocity should be linearly increased from axis of rotation to wall of the centrifuge as elaborates in equation 4.1. The maximum radius of the bottom bowl is $7.2cm$ and the rotational speed of the centrifuge is approximately of $1028rads^{-1}$ and therefore the maximum velocity must be $74.016ms^{-1}$.

The XY 2D scatter plot (Figure 4.1) which can be generated out from the ANSYS Fluent post processor, delineates the maximum velocity magnitude closer to $75ms^{-1}$ which is much closely align with the theoretical result.

The linear trend line which has been fitted with the obtained simulation results of relative velocity magnitude using MATLAB curve fitting tool (Figure 4.2), also more

closely conform with equation 4.1, as the trend line equation can be resembled to equation 4.2.

$$v_r = 1013Z + 0.6374 \tag{4.2}$$

Therefore it is clear that, the simulation results are considerably compatible with the theoretical approach as the gradient of the trend line(1013) approximately equal to the rotational speed(1028) of the centrifuge.

The contour diagram which is a simplified version for simulation results representation, also confirms this incrementing nature of velocity magnitude in the mid plane of the centrifuge as shown in figure 4.3. There the velocity magnitude variation is in the range of 18.07 ms^{-1} to 74.45 ms^{-1} from axis of rotation to centrifuge wall and this range is divided to ten equal sub ranges which makes it much uncomplicated to understand.

The velocity vector in the wall of the centrifuge also confirms the increase of velocity magnitude as depicts in figure 4.4.

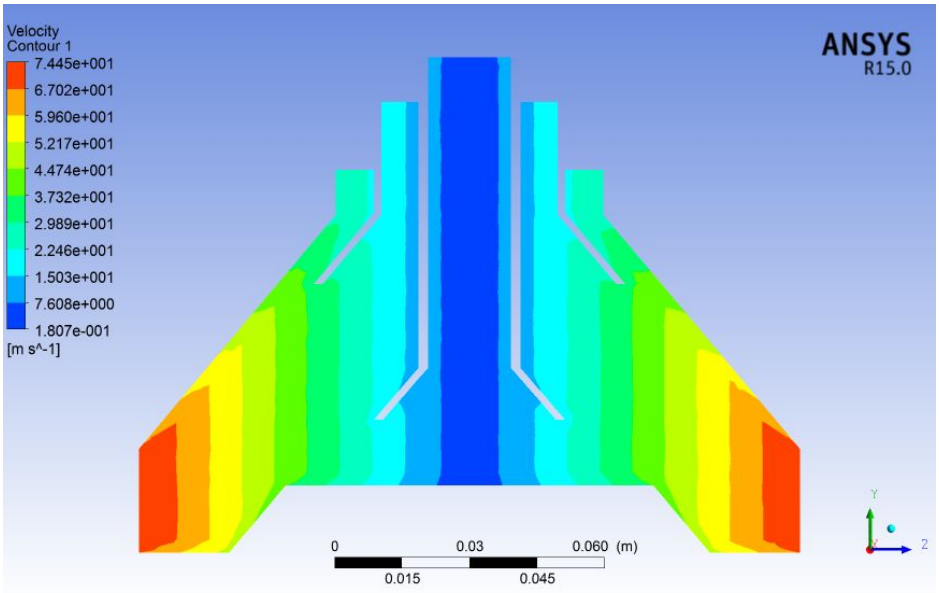

Figure 4.3: Contour diagram of velocity

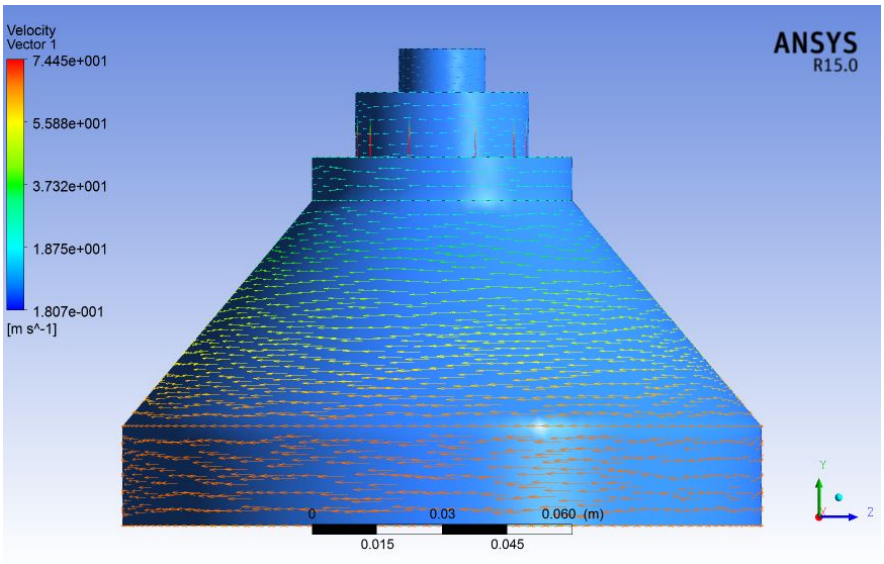

Figure 4.4: Vector diagram of velocity

4.1.2 Pressure Profile

Static Pressure

The theoretical, radial static pressure variation of a rotating fluid is illustrated in equation 2.1 in chapter 2. However, in the three dimensional centrifuge fluid model the direction of radius lies along in directions of 'X'and 'Z'whereas the axis of rotation coincides in 'Y'direction. Therefore, the static gauge and absolute pressure variations are considered at a constant height in 'Z'direction as represented in figure 4.5 and 4.6 respectively.

According to equation 2.2 ($P = \frac{1}{2}\rho\omega^2(R^2 - r^2)$) it is revealed that, the magnitude of static pressure should decrease with the distance from axis of rotation, thereby in the direction of 'Z' since at constant height, the bowl radius and speed of rotation are constant and the density variation is insignificant (924-998 kgm^{-3}).

On the other hand, the super sonic gauge pressure at the inlet has been specified as $190,000Pa$ and the gauge pressures at two outlets have been estimated as $134841Pa$ as elaborated in section 3.3.3. Withal, the figure 4.7 delineates the simulation results of gauge pressures at inlet and two outlets. Yet, in agreement with the set pressure boundary conditions the gauge pressure in outlet 1 and 2 in the ranges of 1.34×10^5–$1.36 \times 10^5 Pa$ and 1.33×10^5–$1.37 \times 10^5 Pa$ respectively. Besides, in con-

trast to prior set inlet gauge pressure boundary condition of $1.9 \times 10^5 Pa$, the simulation results of the respective value in the range of 1.38×10^5–$1.39 \times 10^5 Pa$.

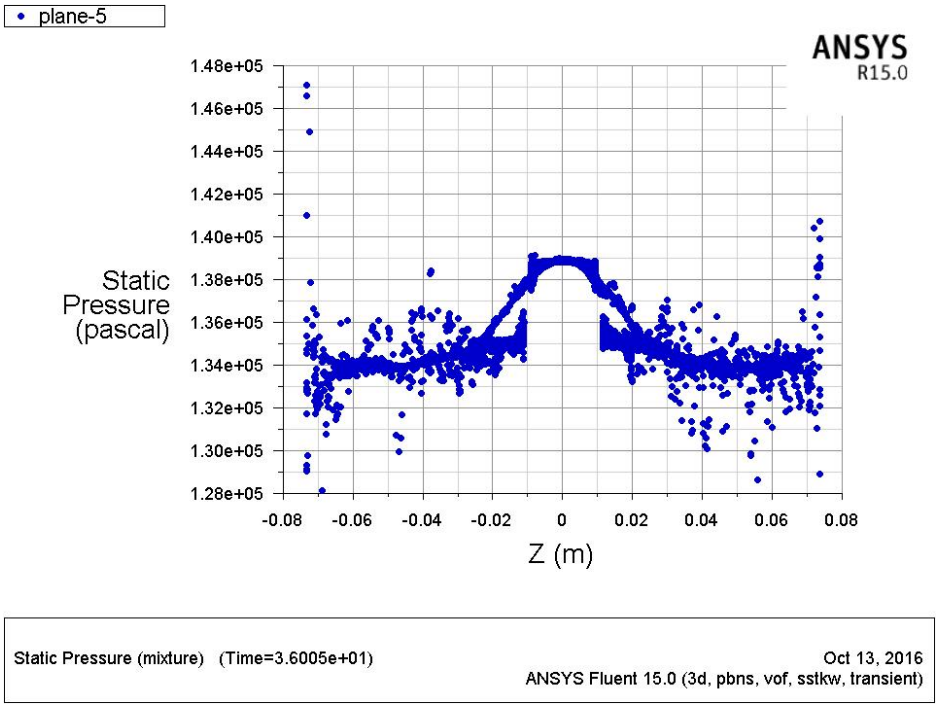

Figure 4.5: Graph of static pressure(gauge) vs Z in the mid plane of the centrifuge

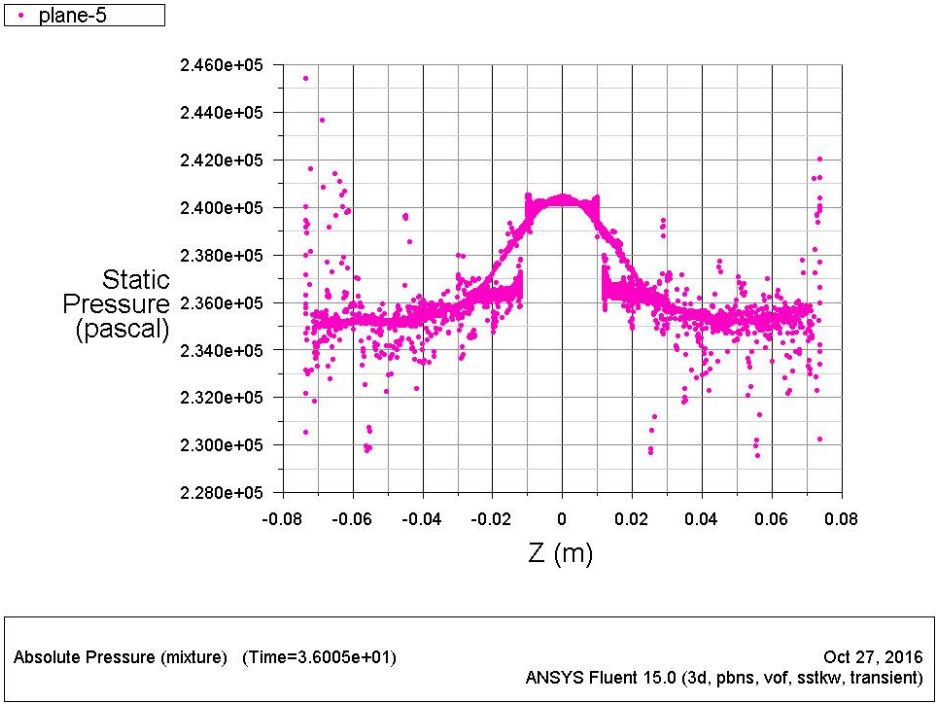

Figure 4.6: Graph of static pressure(absolute) vs Z in the mid plane of the centrifuge

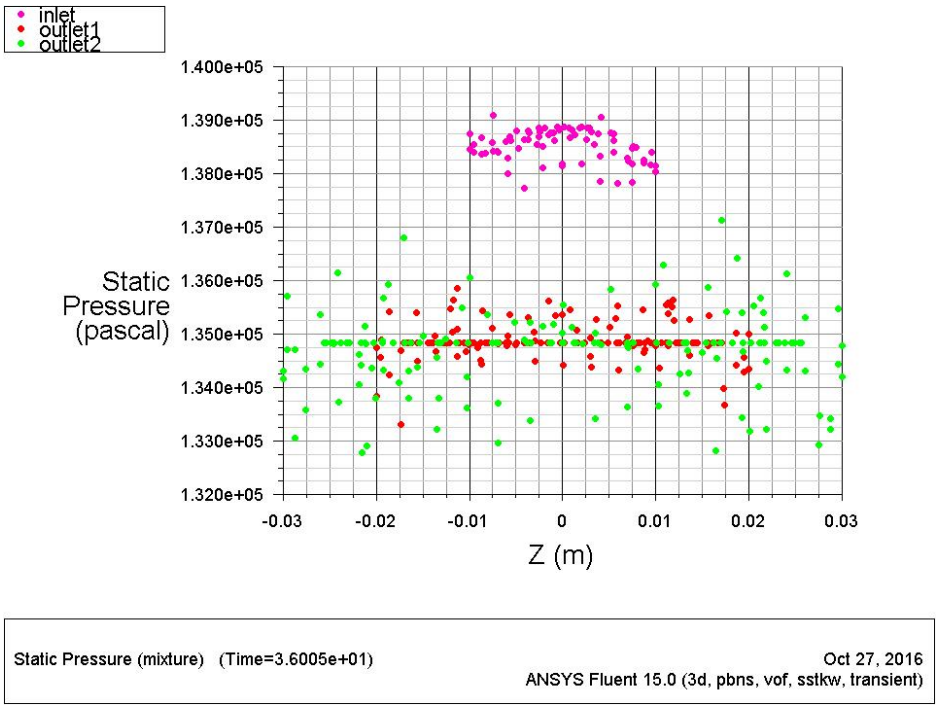

Figure 4.7: Graph of static pressure(guage) vs Z at inlet and two outlets

4.1.3 Measures of Turbulence

Turbulence Intensity (I)

Turbulence intensity(I) is an important measure of turbulence scale and defined as the ratio between root mean square of the velocity fluctuation ($u^{'}$) and Reynolds average mean velocity(U), as expressed in equation 4.3 [28]. In general, the value is declared as a percentage.

$$I = \frac{u^{'}}{U} \tag{4.3}$$

According to the common estimations in literature, turbulence intensity between 5% - 20% is regarded as a high turbulent case which is often found inside the complex geometries like heat exchanges and rotating machinery. In addition turbulence intensity between 1% - 5% is considered as medium turbulent case whereas below 1% falls under low turbulent case [29] .

In three dimensional model of the centrifuge, turbulence intensity at inlet and two outlets have been considered for better representation of simulation results as depicts

in figure 4.8. The turbulence intensity boundary condition at inlet and two outlets have been chosen as 5% according to the recommendations in the literature as it is mentioned that for internal flows the turbulence intensity can be fairly high values as ranging from 1% - 10% [30].

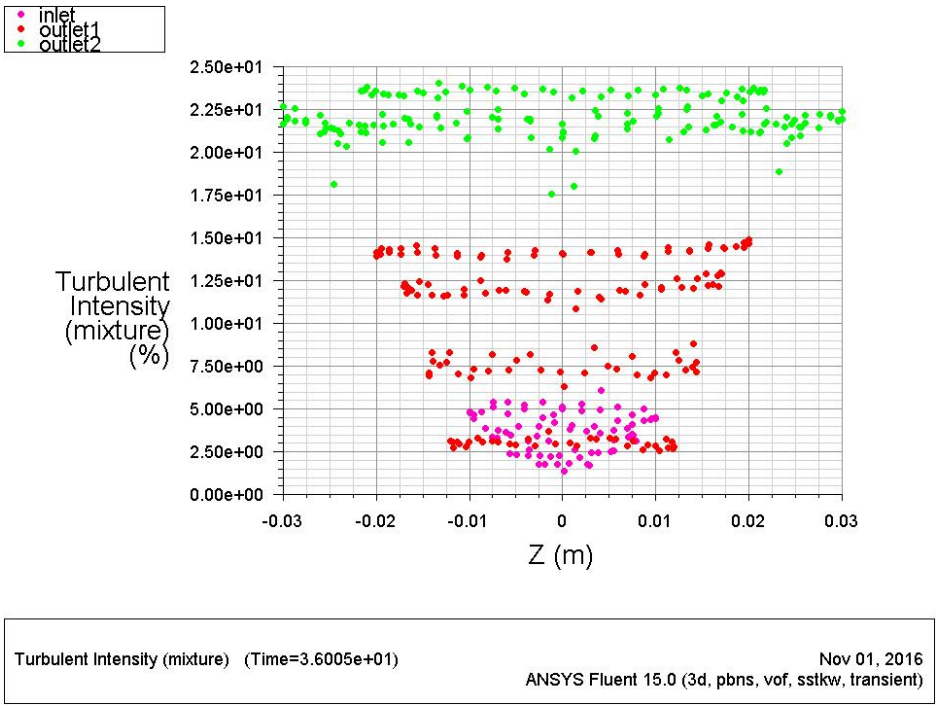

Figure 4.8: Graph of Turbulence Intensity vs Z at inlet and two outlets

By observing figure 4.8 it can be noticed that turbulent intensities at inlet, outlet 1 and outlet 2 is in the ranges of 1.25% - 5 %, 2.5% - 15% and 17.5% - 24.5% respectively. Despite the inlet having medium turbulence, two outlet flows are in the ranges of high turbulence.

The turbulent fluctuations have a three dimensional spatial character which even results rotational flow structures, so-called turbulent eddies. Moreover, it is the reason to consider the root mean square of the velocity fluctuation, in order to calculate the turbulence intensity as given in equation 4.4.

$$u^{'} = \sqrt{\frac{1}{3}(u_x'^2 + (u_y'^2 + (u_z'^2)} \tag{4.4}$$

However according to equation 4.4, it is clear that high fluctuating component in the velocity results high turbulence intensity. Since the centrifuge is running under very

high rotational speed of $1028 rads^{-1}$, the inlet and outlet flows become more turbulent with rotational eddies which ultimately results higher turbulence intensity.

Turbulent Kinetic Energy (k)

Turbulent kinetic energy is one of the transport variables in SST $k-\omega$ model which has been chosen to model turbulence inside the centrifuge. Equation 2.16 in chapter 2 denotes the transport equation for turbulent kinetic energy. However, turbulent kinetic energy, is the kinetic energy per unit mass of the turbulent fluctuations($u^{'}$) at a given point in the turbulent flow and is defined as equation 4.5.

$$k = \frac{1}{2}(\bar{u_x^{'2}} + \bar{u_y^{'2}} + \bar{u_z^{'2}}) \tag{4.5}$$

On the other hand, production and dissipation of turbulent kinetic energy in equation 2.16 can be found according to the following 4.6 and 4.7 equations respectively [19].

$$G_k = -\rho(\bar{u_i^{'}u_j^{'}})\frac{\partial u_j}{\partial x_i} \tag{4.6}$$

$$Y_k = \rho\beta^* k\omega \tag{4.7}$$

β^* is a piece wise function equals to 1

Moreover, the relationship between turbulence intensity and turbulent kinetic energy is represented by equation 4.8 [18]. Therefore, the turbulent kinetic energy variation in inlet and two outlets has also been considered other than the simulation results of the mid plane and the simulation results of the corresponding positions (inlet, outlet 1, outlet 2 and mid plane) are shown in figure 4.9 and 4.10 respectively.

$$k = \frac{3}{2}(I\bar{U})^2 \tag{4.8}$$

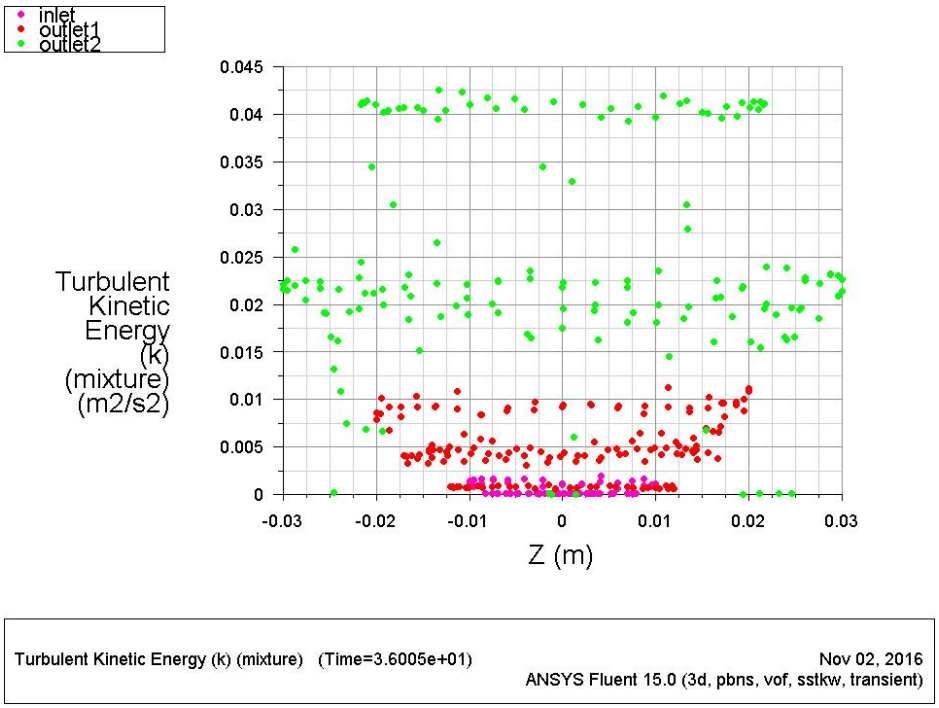

Figure 4.9: Graph of Turbulent kinetic energy vs Z at inlet and two outlets

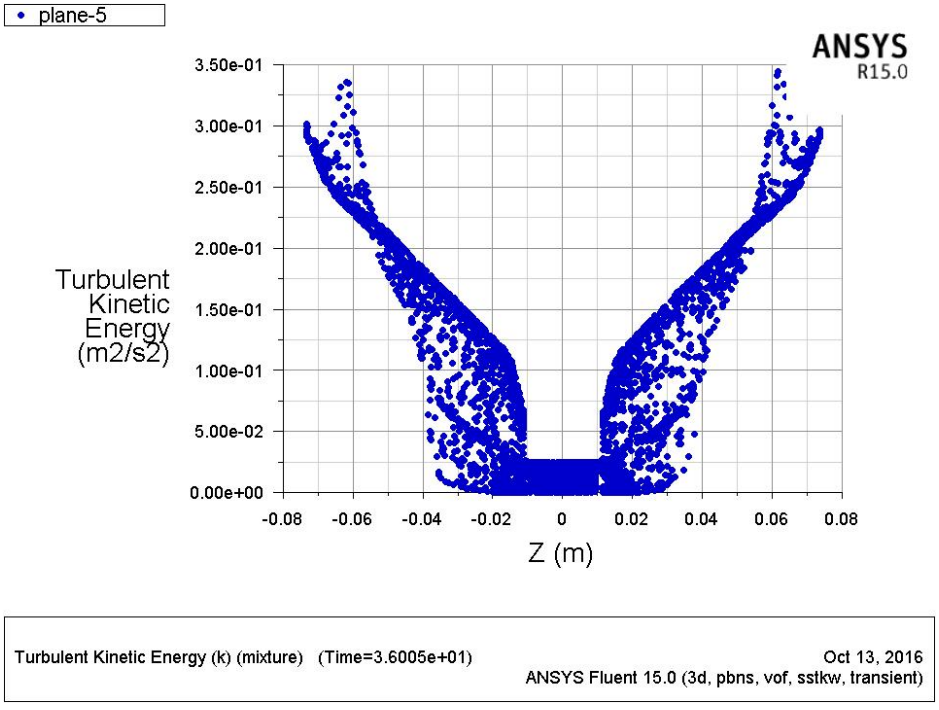

Figure 4.10: Graph of Turbulent kinetic energy vs Z at the mid plane

By observing figure 4.9 it can be summarized that the turbulent kinetic energy at the inlet is in the range of 0-0.0025 m^2s^{-2} whereas turbulent kinetic energies at outlet

1 and 2 are in the ranges of 0.00125-0.01 m^2s^{-2} and 0.015-0.0425 m^2s^{-2} respectively. According to equation 4.8, turbulent kinetic energy and turbulence intensity have a proportional relationship since average mean velocity ($\bar{U}$) is constant. In comply with figure 4.9 and simulation results of turbulent intensities at inlet and outlets, figure 4.9 also depicts highest turbulent kinetic energy at outlet 2 and lowest at the inlet.

The figure 4.10 which represents the turbulent kinetic energy variation in z direction at the mid plane, shows highest turbulent kinetic energy of 0.35 m^2s^{-2} near the wall region (at highest z values) and the lowest of 0 near the axis of rotation. Therefore it can be concluded that the flow becomes more turbulent in radial direction.

Moreover, as highlighted before the turbulent kinetic energy and turbulence intensity relate in the form of equation 4.9. Therefore when the simulation results of these two variables are plotted and fitted using MATLAB curve fitting tool, the resulted fit is considerably corresponding to the above equation 4.8. The figure 4.11 depicts the fitted curve of the simulation results for positive z direction and the equation of the fit is given in equation 4.9.

$$k = 0.02438I^2 + 0.07468I + 0.05722 \tag{4.9}$$

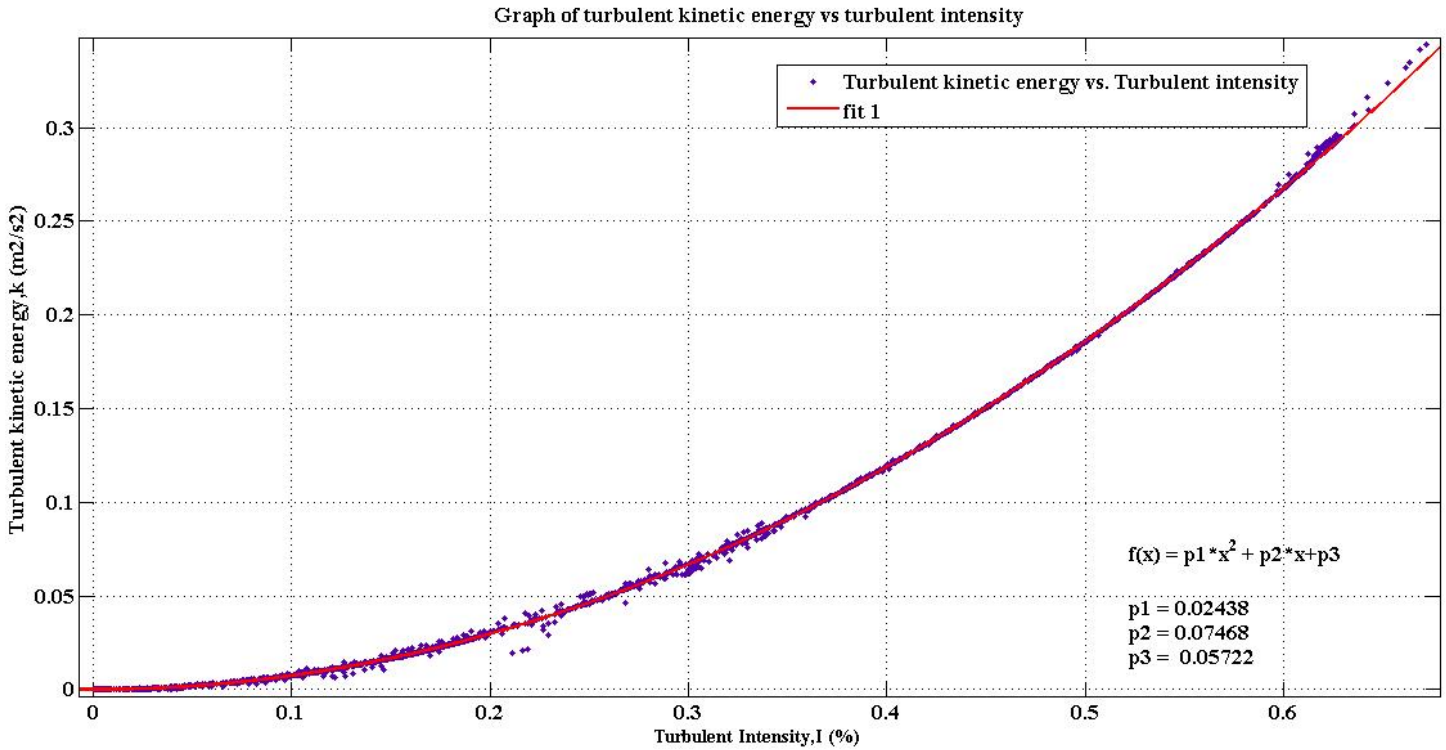

Figure 4.11: Graph of Turbulent kinetic energy vs Turbulence Intensity at the mid plane

In comparison of equation 4.8 and 4.9, it can be identified that equation 4.9 has first and zeroth order terms which raises a conflict with the theory as elaborated in equation 4.8. However, since both of them are polynomials of second order, it can be concluded that even though the fit is not the perfect match to the theory, it does not mean they are not in line.

Specific dissipation rate (ω)

Specific dissipation rate is the next transport variables in SST k-ω model other than turbulent kinetic energy(k). The corresponding transport equation is mentioned as equation 2.17 in chapter 2.

Specific dissipation rate is the rate at which the turbulent kinetic energy(k) is converted in to thermal internal energy per unit volume and time. Further it is determined by the ratio of turbulent dissipation rate to turbulent kinetic energy as given in equation 4.10[29].

$$\omega = \frac{\epsilon}{k\beta^*} \tag{4.10}$$

ϵ turbulent dissipation rate

β^* is a constant equals to 0.09

The simulation results of variation of turbulent dissipation rate and specific dissipation rate in z direction at the mid plane of the centrifuge are represented in figure 4.12 and 4.13 respectively.

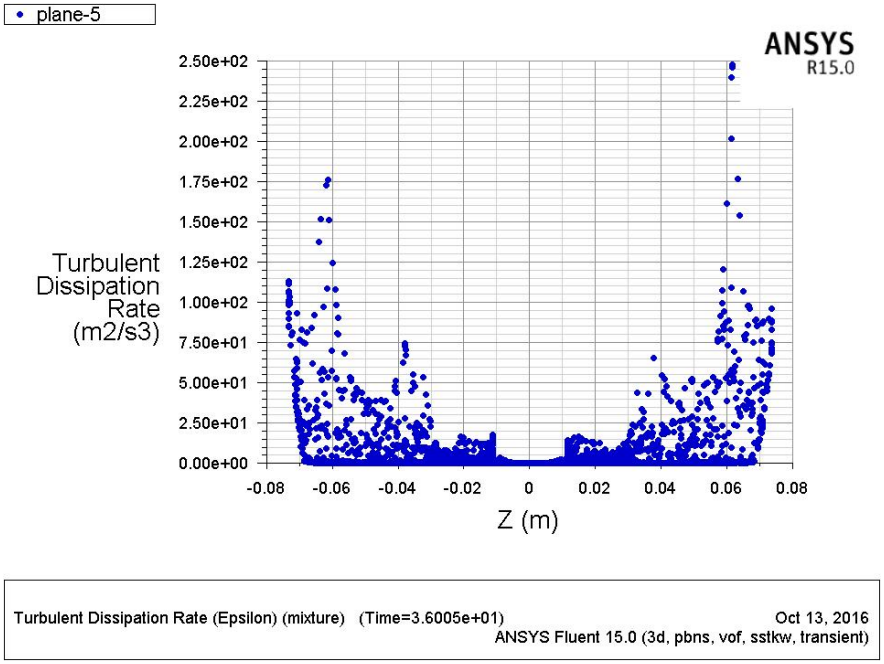

Figure 4.12: Graph of Turbulent dissipation rate vs Z at the mid plane

According to figure 4.12, the turbulent dissipation rate varies from 0-250m^2s^{-2} and the value is almost zero at the axis of rotation and gradually increasing up to the wall.

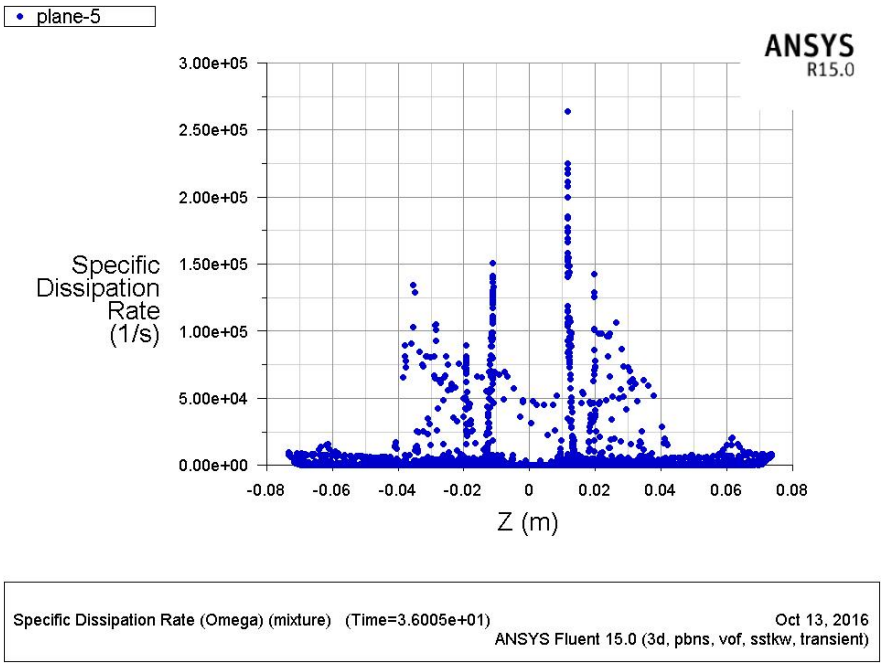

Figure 4.13: Graph of Specific dissipation rate vs Z at the mid plane

The specific dissipation rate in the mid plane of the centrifuge is in the range of 0-2.5x$10^5 s^{-1}$ as shown in figure 4.13. Even though turbulent dissipation rate(ϵ) and turbulent kinetic energy(k) tend to increase towards the wall from axis of rotation, the specific dissipation rate is maximized near the axis of rotation, to be perfect just after the inlet passage.

Since the simulation results do not reveal the turbulent kinetic energy value corresponds to maximum turbulent dissipation rate, it cannot be found whether the results satisfy equation 4.10. However for clarification, when the maximum turbulent dissipation rate of $250 m^2 s^{-3}$ and maximum turbulent kinetic energy of $0.35 m^2 s^{-2}$ are substituted in equation 4.10, the specific dissipation rate(ω) can be obtained as $0.79365 \times 10^5 s^{-1}$ or can be approximated to $0.8 \times 10^5 s^{-1}$ which is in the range of simulation results of specific dissipation rate.

4.1.4 Phase volume fraction

As mentioned in section 3.4 the simulation procedure has two stages. In the first stage of the simulation 4000 iterations have been run in steady state with one tenth of the rotational speed, to obtain better initial conditions. Subsequently, the second stage which continued with the simulation results of the first stage has been considered under transient flow condition with gradual increment of the rotational speed.

Figure 4.14 and figure 4.15 depict the oil volume fraction contour in the mid plane of the centrifuge after 1000 and 4000 steady iterations respectively. There, the water and oil phases are represented by blue and red colors respectively. Moreover, the color scheme and it's the corresponding volume fractions are depicted by the color spectrum in top left corner of each and every contour curve.

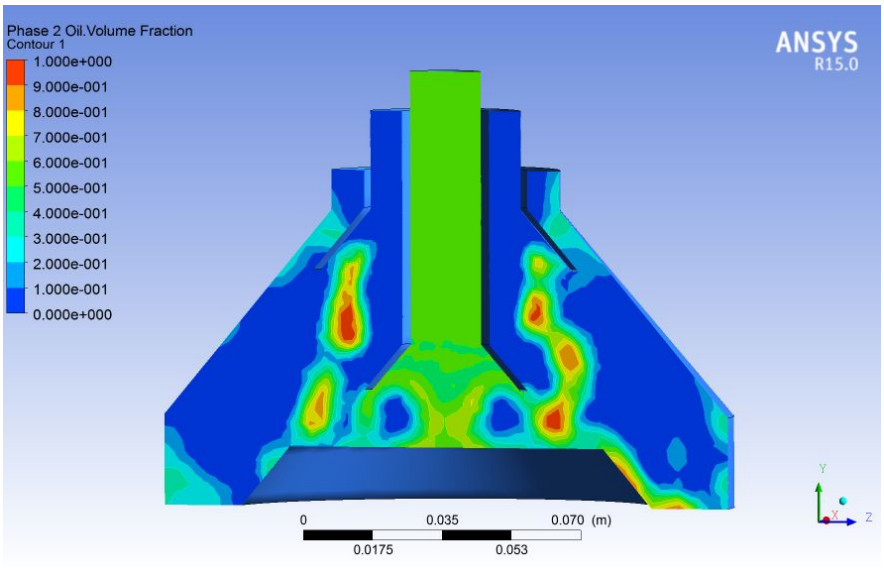

Figure 4.14: Oil volume fraction after 1000 iterations($\omega = 102.8 rads^{-1}$)

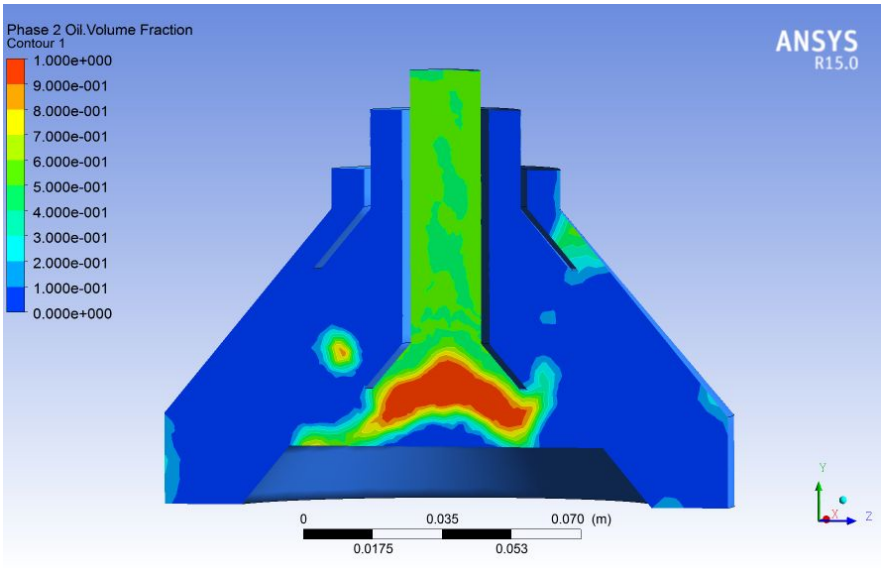

Figure 4.15: Oil volume fraction after 4000 iterations($\omega = 102.8 rads^{-1}$)

By observing the simulation results as depicts in the above figure, it can be identified that the separation of the two liquids is insufficient for a mixture of 50% oil and water. Further, when the area of the mid plane takes in to account, higher fraction of it filled with water and lesser with oil. But, the boundary of separation is intensive and the boundary of the two liquids is clear enough. Therefore it has been decided to use the results after 4000 iterations for the transient stage.

The transient flow simulation inside the centrifuge has also been continued with one tenth($102.8 rads^{-1}$) of the desired speed of rotation. Further, the rotation was carried out for 4 seconds and the corresponding simulation results of oil volume fraction contour at the mid plane after 1 second and 4 seconds are represented by figure 4.16 and 4.17 respectively.

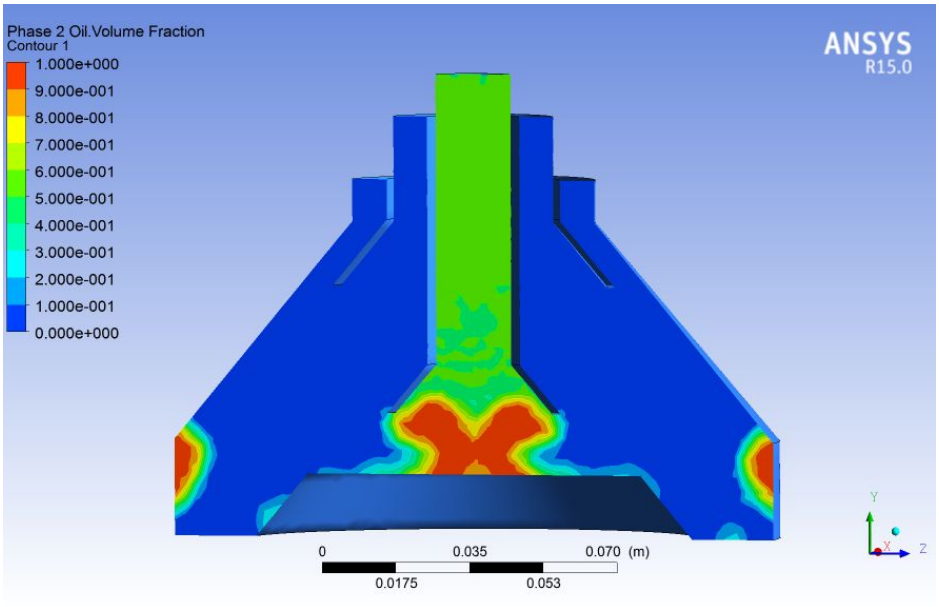

Figure 4.16: Oil volume fraction after 1s($\omega = 102.8 rads^{-1}$)

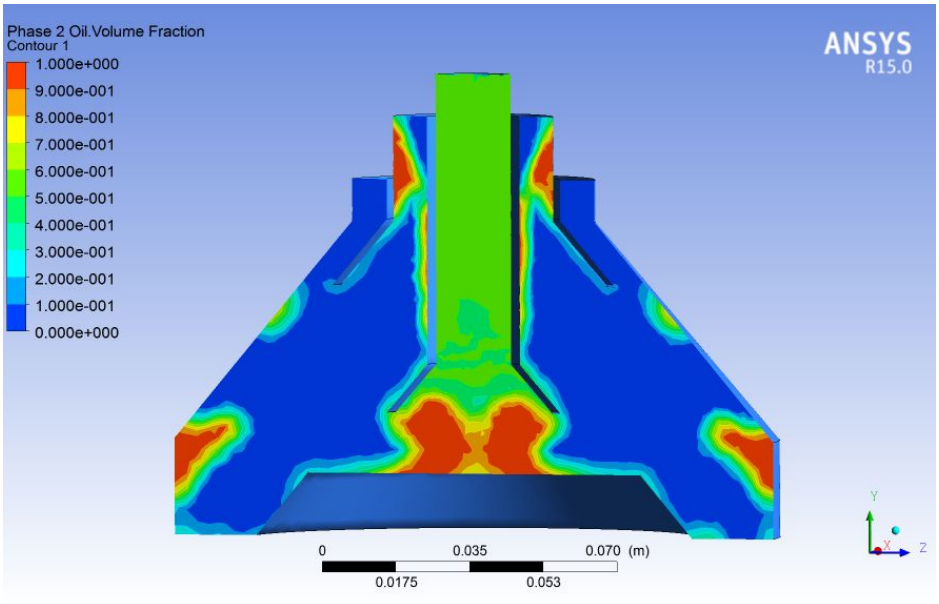

Figure 4.17: Oil volume fraction after 4s($\omega = 102.8 rads^{-1}$)

Even though it cannot observe a drastic difference between 4.16 and 4.17 figures, after 4 seconds of time, a considerable amount of oil volume fraction can be observed in outlet 1 which is for the low density oil out flow. Moreover, according to equation 2.3 and 2.4, the low density liquid should gather around the axis of rotation whereas high dense liquid is pushed towards the wall. However, in comparison with the figures 4.14 and 4.15 of steady flow simulation, it can be observed two symmetric oil patches near the wall region. As highlighted in section 2.1, the gravitational force plays its role over the centrifugal force at low speeds of rotation.

The simulation continues for another three sub stages before achieve the actual rotational speed of $1028 rads^{-1}$. Each and every sub stage operates with the end simulation results of the previous sub stage. In addition, 0.3,0.5 and 0.7 fractions of the desired rotational speed have been taken in to account and the corresponding rotational speeds of these sub stages are as $308.4 rads^{-1}$,$514 rads^{-1}$ and $719.6 rads^{-1}$ respectively. However, the simulation of each of these sub stage has been proceeded for four seconds and the resulting oil volume fraction contours at the beginning and at the end of the each sub stage are represented by figure 4.18 - 4.23 .

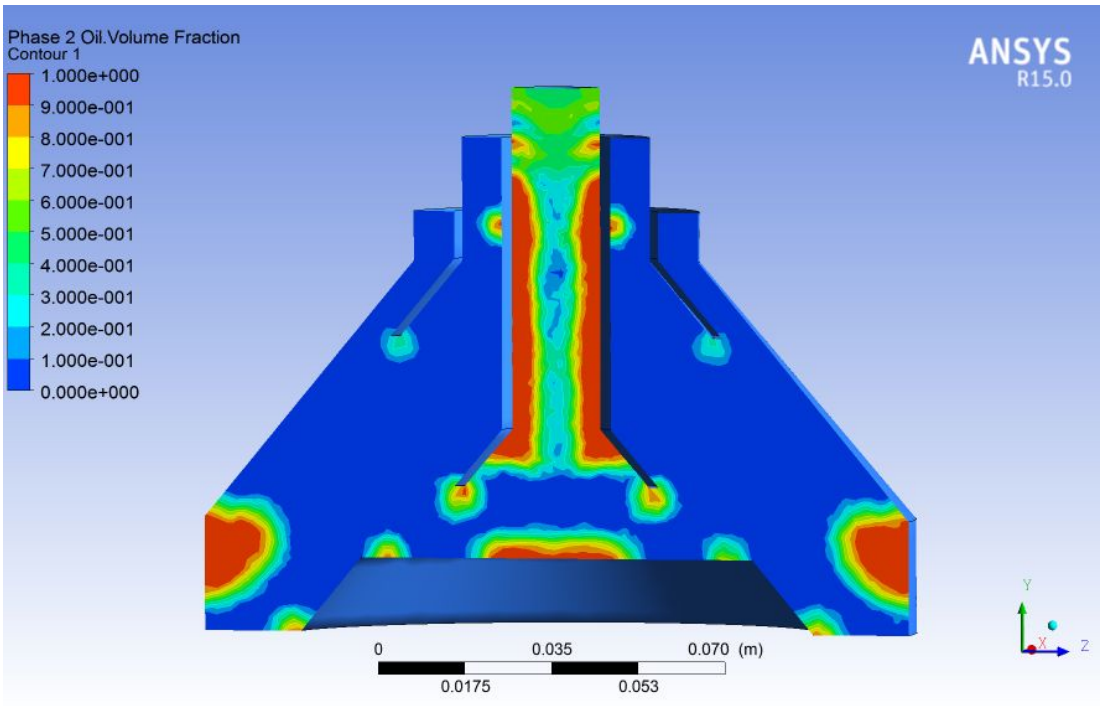

Figure 4.18: Oil volume fraction after 5s($\omega = 308.4 rads^{-1}$)

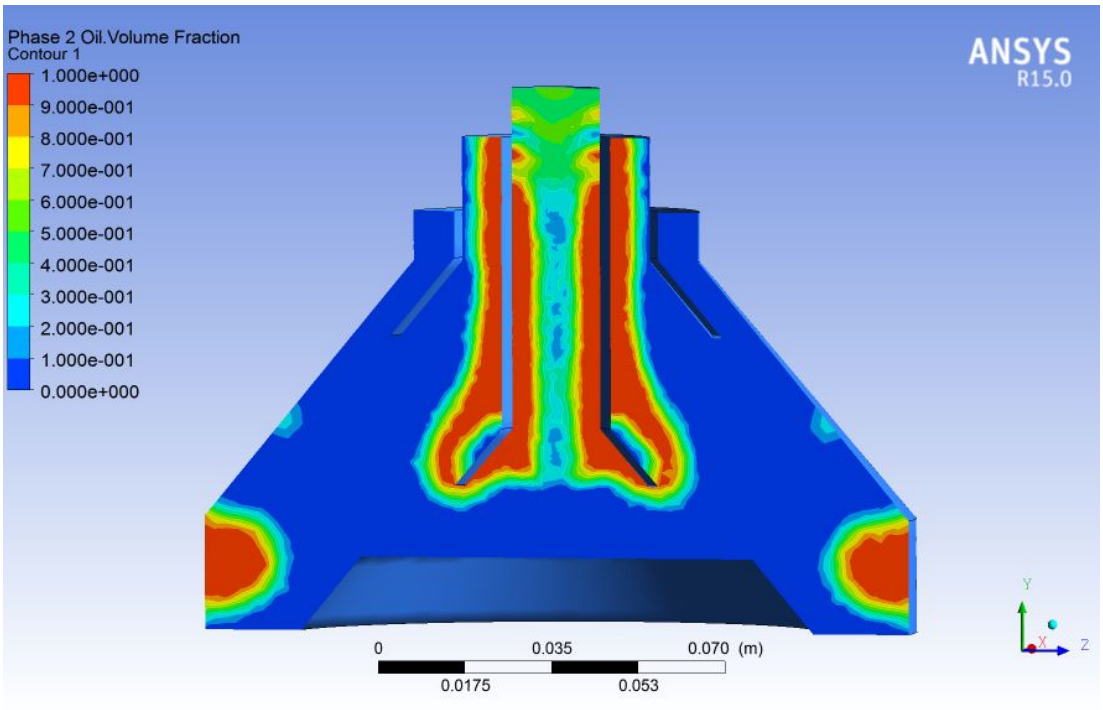

Figure 4.19: Oil volume fraction after 8s($\omega = 308.4 rads^{-1}$)

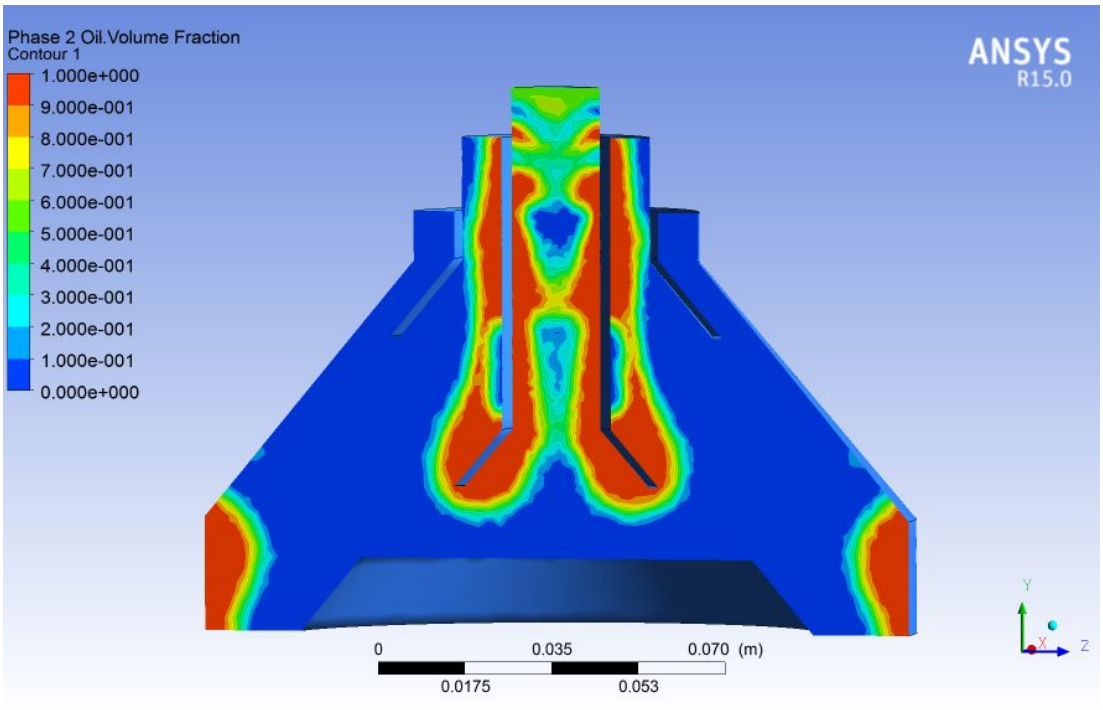

Figure 4.20: Oil volume fraction after 9s($\omega = 514 rads^{-1}$)

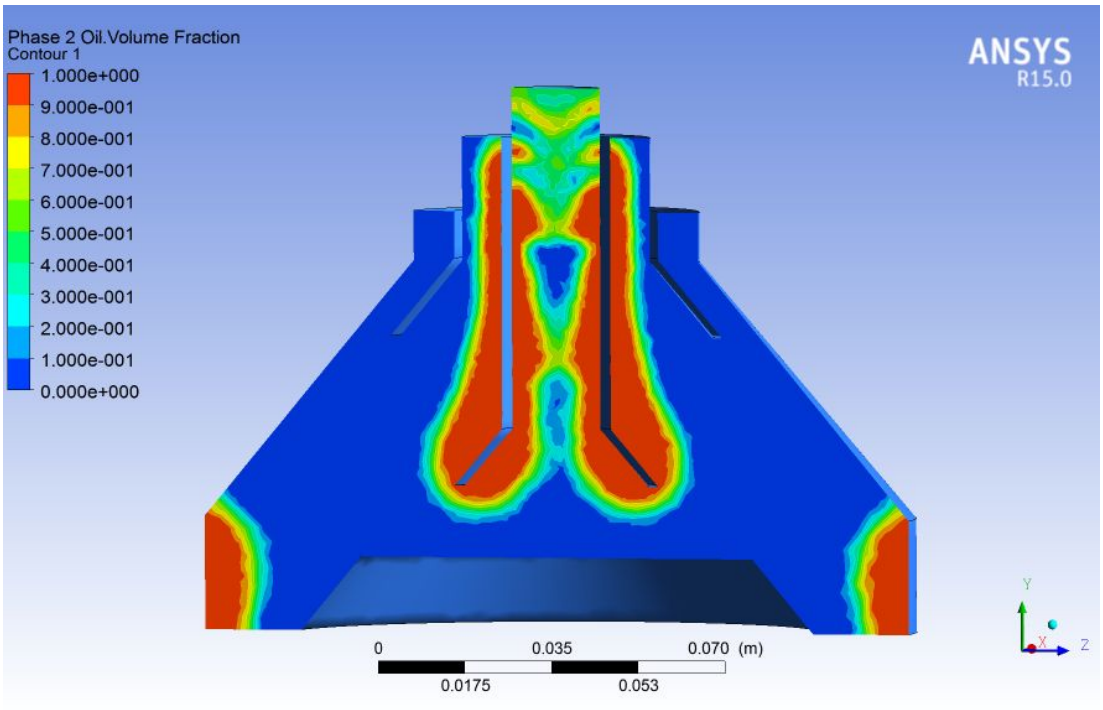

Figure 4.21: Oil volume fraction after 12s($\omega = 514 rads^{-1}$)

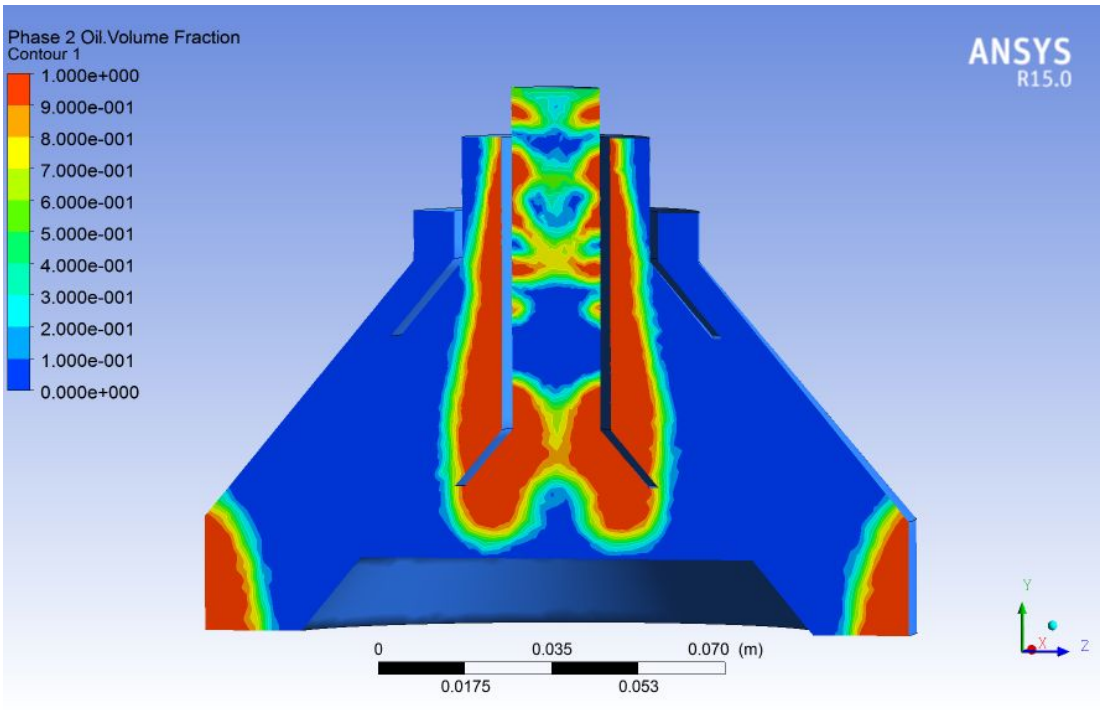

Figure 4.22: Oil volume fraction after 13s($\omega = 719.6 rads^{-1}$)

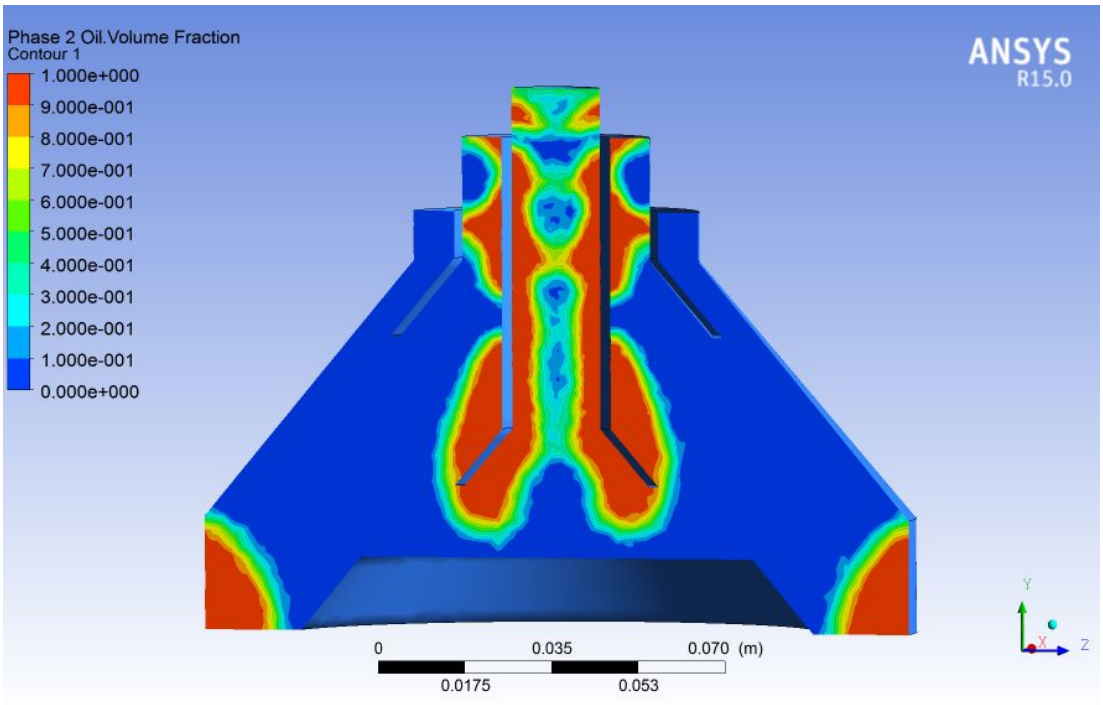

Figure 4.23: Oil volume fraction after 16s($\omega = 719.6 rads^{-1}$)

By observing above series of figures, it can be discovered that, at the end of each sub stage, the area in the mid plane that has covered by the oil volume fraction has gradually increased in the passage of outlet 1. Yet, the two symmetric oil patches near the wall region remains the same, but with different shapes and sizes and has moved more towards the bottom of the centrifuge. However, the outlet 2, which is for the high density water out flow contains only water, even though the oil stream contaminate with little amount of water. After 16 seconds, the centrifuge is provided with it's desired speed of rotation($1028 rads^{-1}$) and then on wards the simulation results of oil volume fraction saved for each and every second.

The simulation results of first four seconds after achieving the inherent rotational speed of the Westfalia centrifugal separator are presented in figure 4.24 - 4.27.

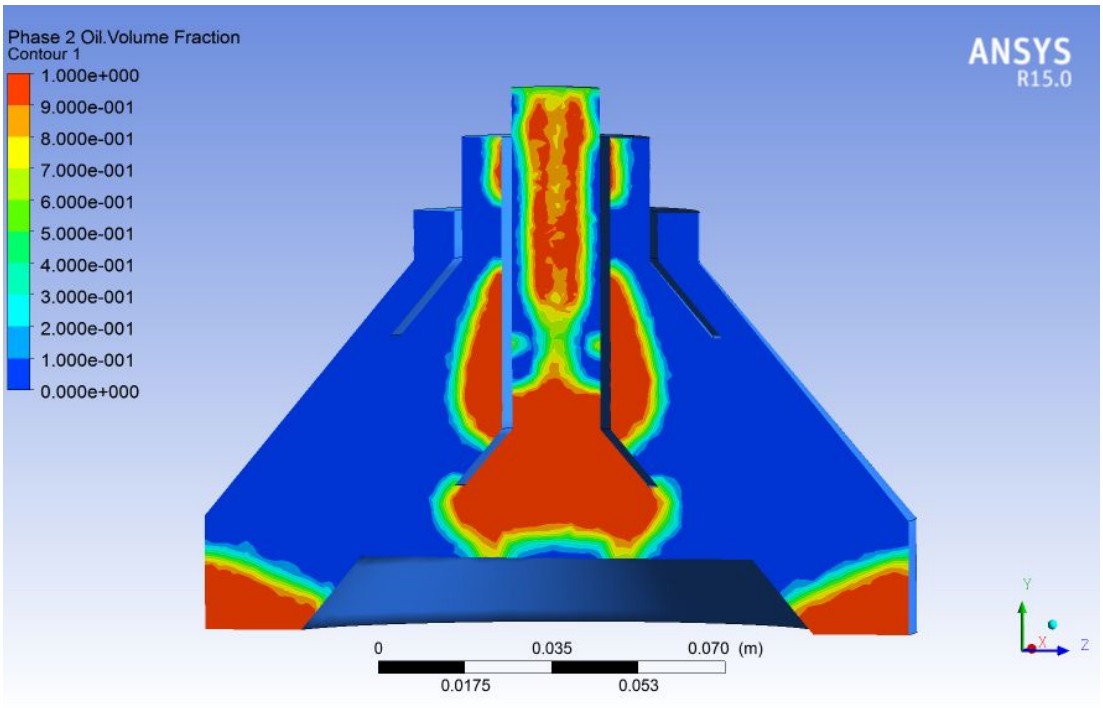

Figure 4.24: Oil volume fraction after 17s($\omega = 1028 rads^{-1}$)

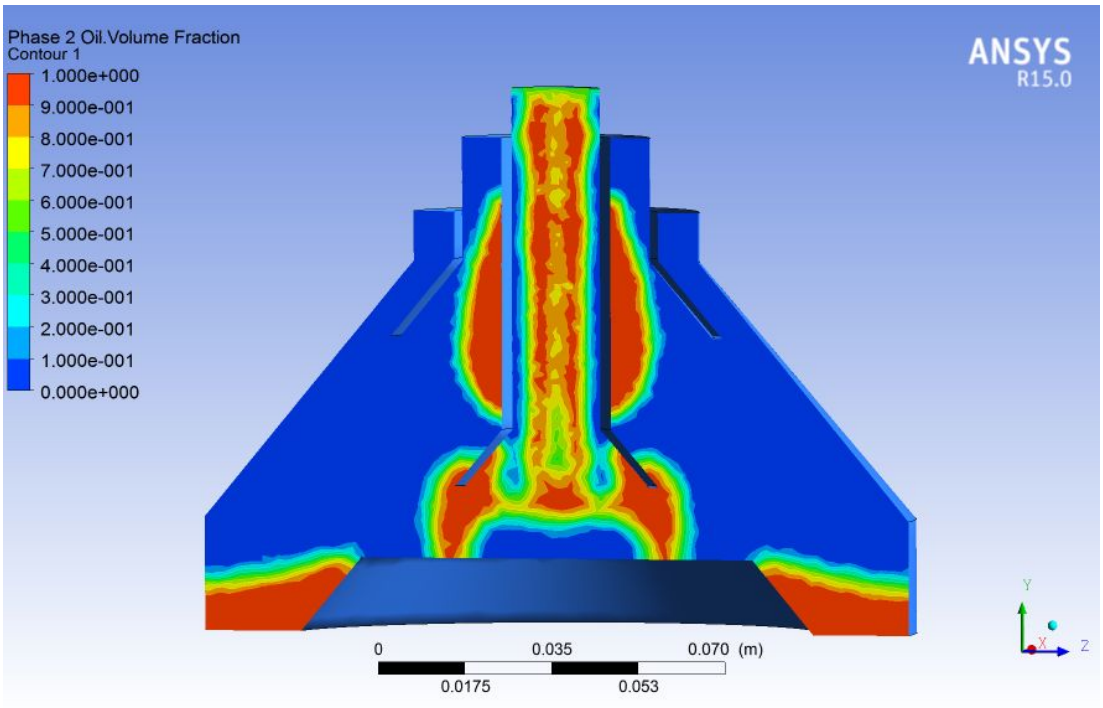

Figure 4.25: Oil volume fraction after 18s($\omega = 1028 rads^{-1}$)

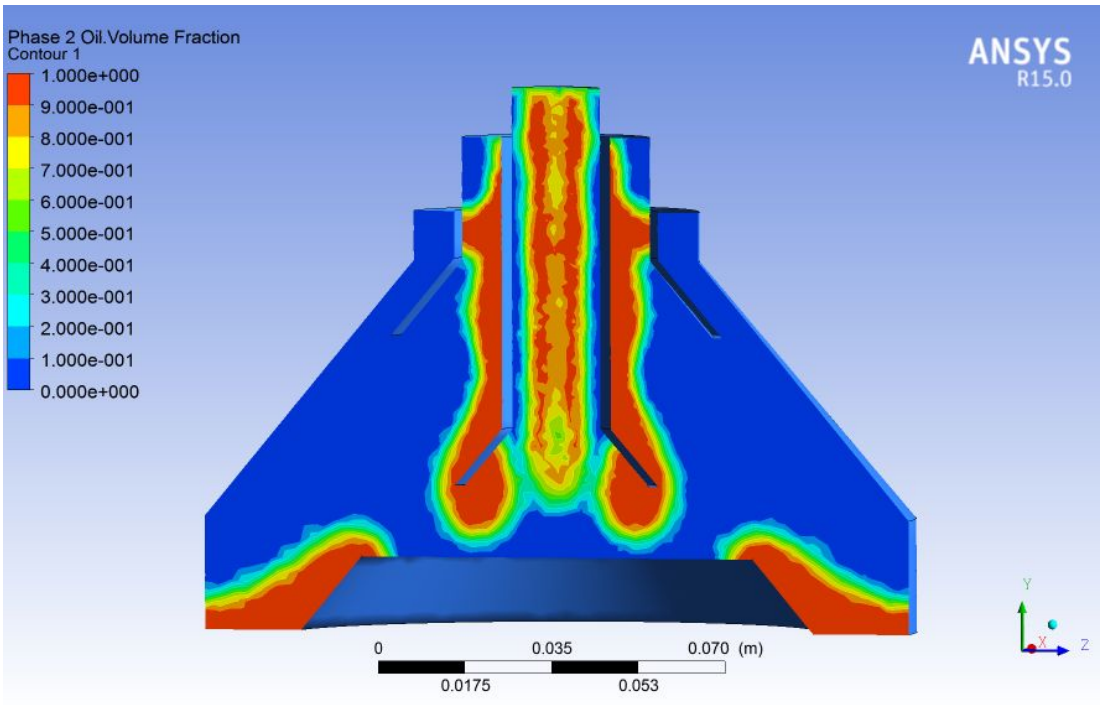

Figure 4.26: Oil volume fraction after 19s($\omega = 1028 rads^{-1}$)

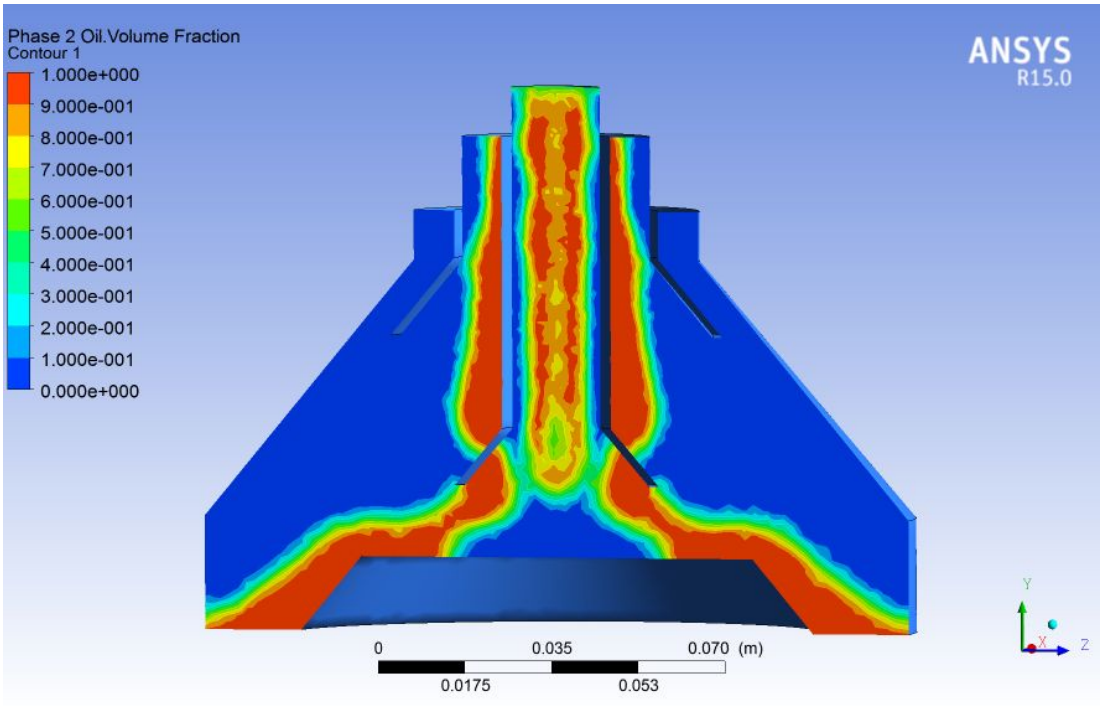

Figure 4.27: Oil volume fraction after 20s($\omega = 1028 rads^{-1}$)

According to above figures, with time the two oil patches near the wall region has biased more towards the centrifuge bottom and after 20 seconds, it has merged with

the main flow inside the passage of the outlet 1. On the other hand, the oil content inside the passage of outlet 1 has significantly increased in compared to figure series of 4.18 - 4.23. Therefore, it can be figured out that gradual increase of rotational speed and time, has intensified and structured the oil-water separation. Moreover, at the default rotational speed of the Westfalia centrifuge, the centrifugal force has overcome the gravitational effect and wiped out the oil accumulation inside the bottom bowl. The compressive scheme which has been used to model volume fraction provided a considerably sharp interface between oil and water as recommended in literature and represented in figure 2.4b. In order to avoid unnecessary repetition and overlong representation, the simulation results after 21s, 24s, 27s and 30s have been chosen to analyze and discuss as depicts in figures 4.28-4.31.

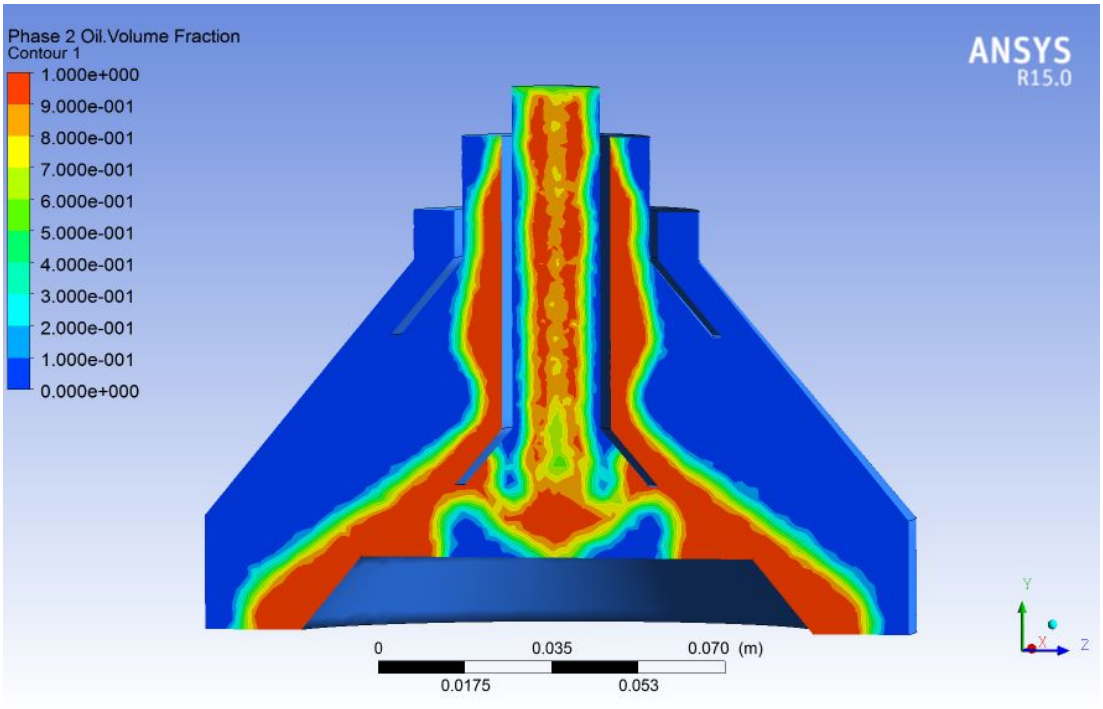

Figure 4.28: Oil volume fraction after 21s($\omega = 1028 rads^{-1}$)

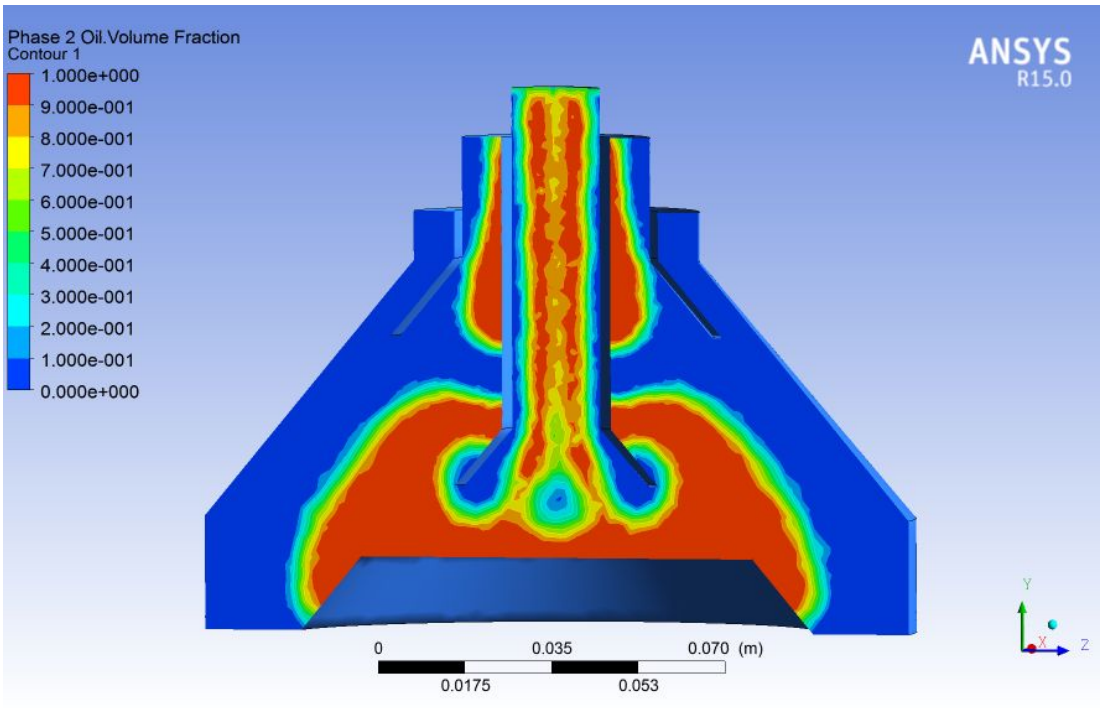

Figure 4.29: Oil volume fraction after 24s($\omega = 1028 rads^{-1}$)

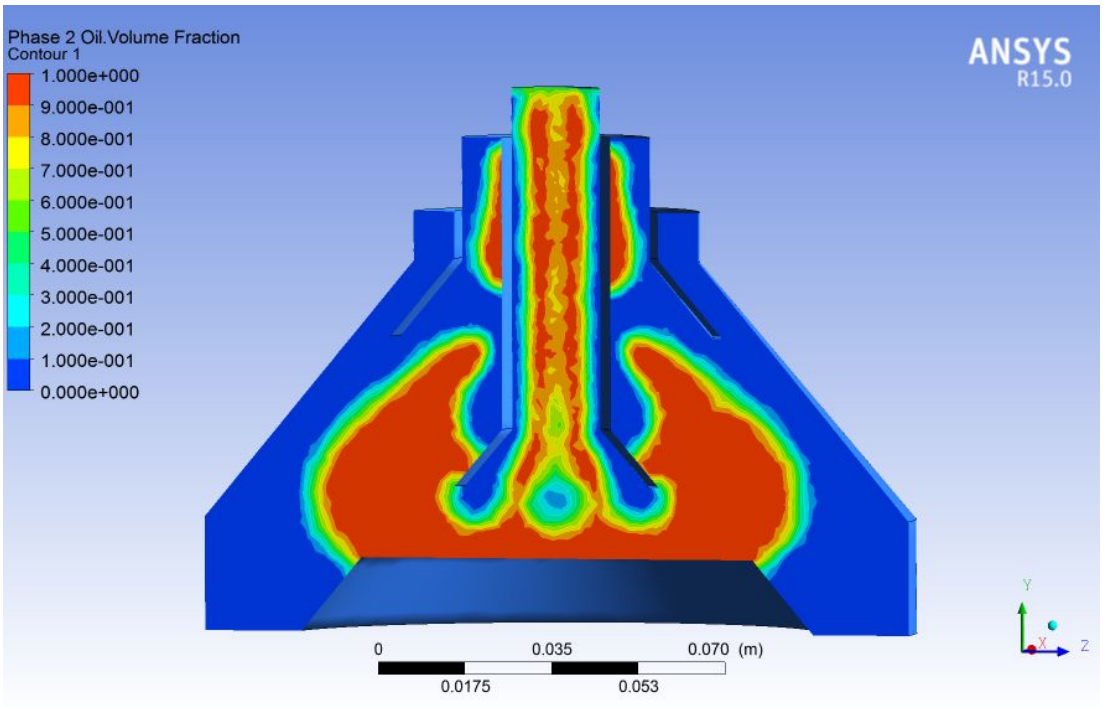

Figure 4.30: Oil volume fraction after 27s($\omega = 1028 rads^{-1}$)

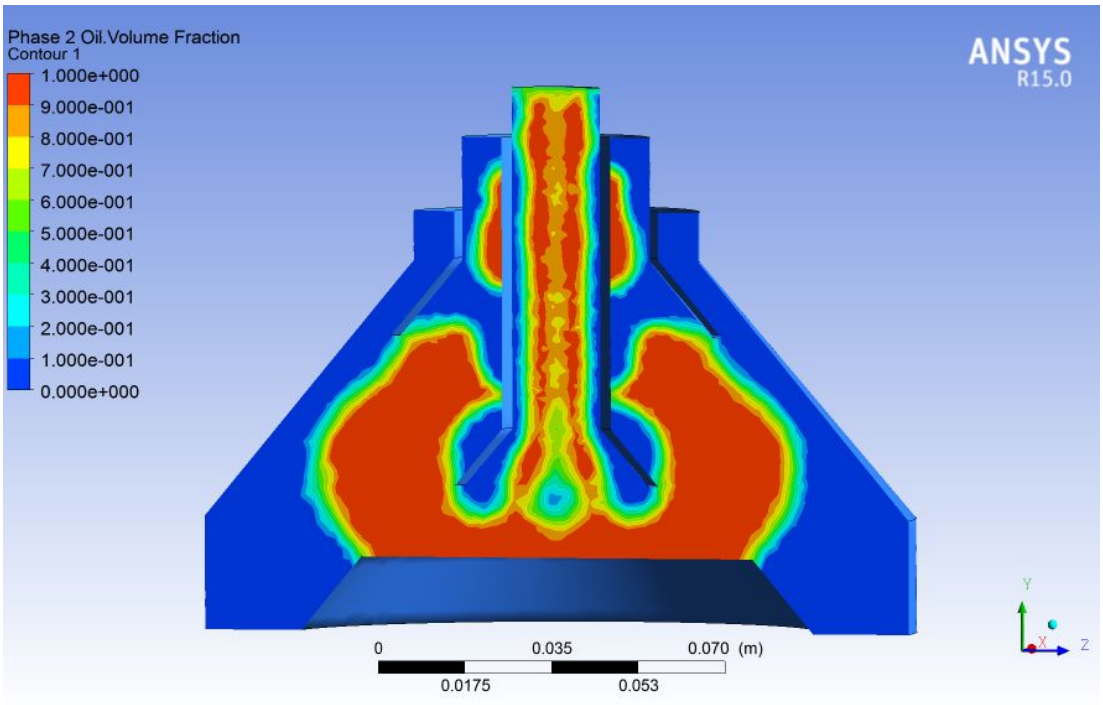

Figure 4.31: Oil volume fraction after 30s($\omega = 1028 rads^{-1}$)

Overlooking the above figures, it can be identified that the simulation results after 21s (figure 4.28), has followed the same trend in flow, even though there's a patch of water just around the axis of rotation in bottom bowl. However, after 24s(figure 4.29) the water patch has further expanded and in contrary with the previous results, the oil flow has separated to two oil plugs inside the oil flow passage of outlet 1. Yet, it can be assumed that this 'plug effect'is due to the unstructured mesh around the sharp bottom edge of the inlet passage and narrowing nature of inlet and outlet 1 passages.

Additionally, when the geometry has been re-drawn with rounded, smooth edges as in actual Westfalia centrifugal separator, the number of mesh nodes and elements has grown three times higher than the considered sharp edged centrifuge and ultimately incompatible with the available computer hardware facility.

However, just after 32 seconds (figure 4.32) the 'plug type flow'has vanished and the passage of outlet 1 has entirely filled with oil, except the sharp corer edge near outlet 1. Therefore in order to closely figure out the nature of the oil flow, the results from 32s-33s has considered and results in each 0.25s of this critical second is represented by figures 4.32 - 4.36.

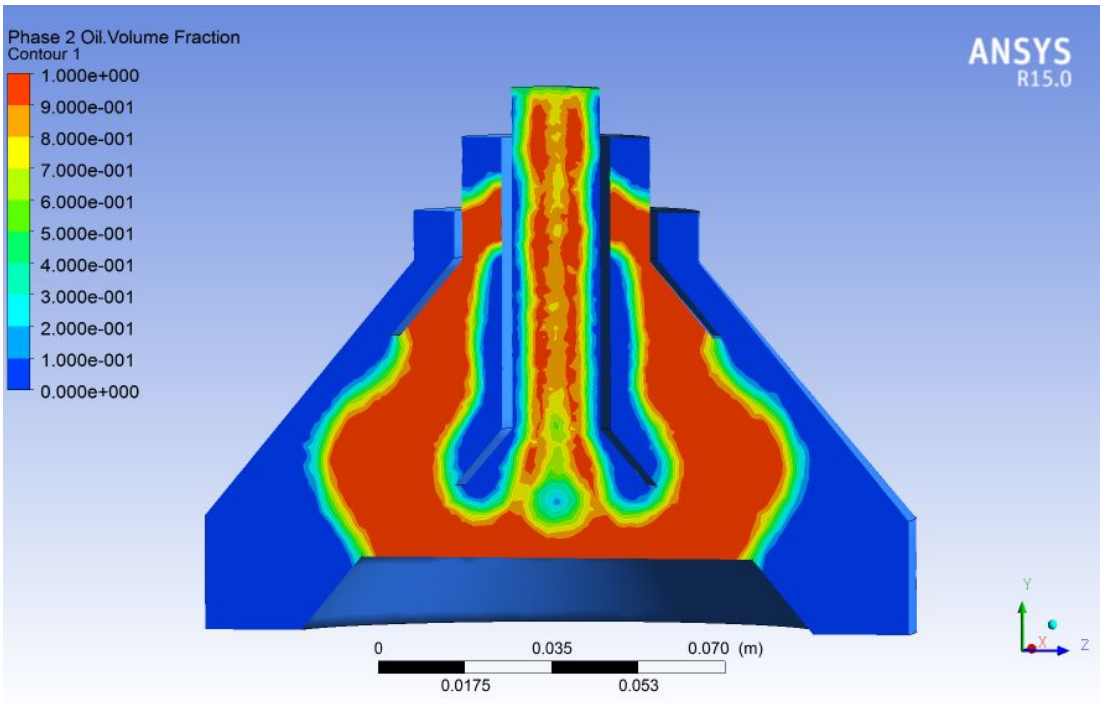

Figure 4.32: Oil volume fraction after 32s($\omega = 1028 rads^{-1}$)

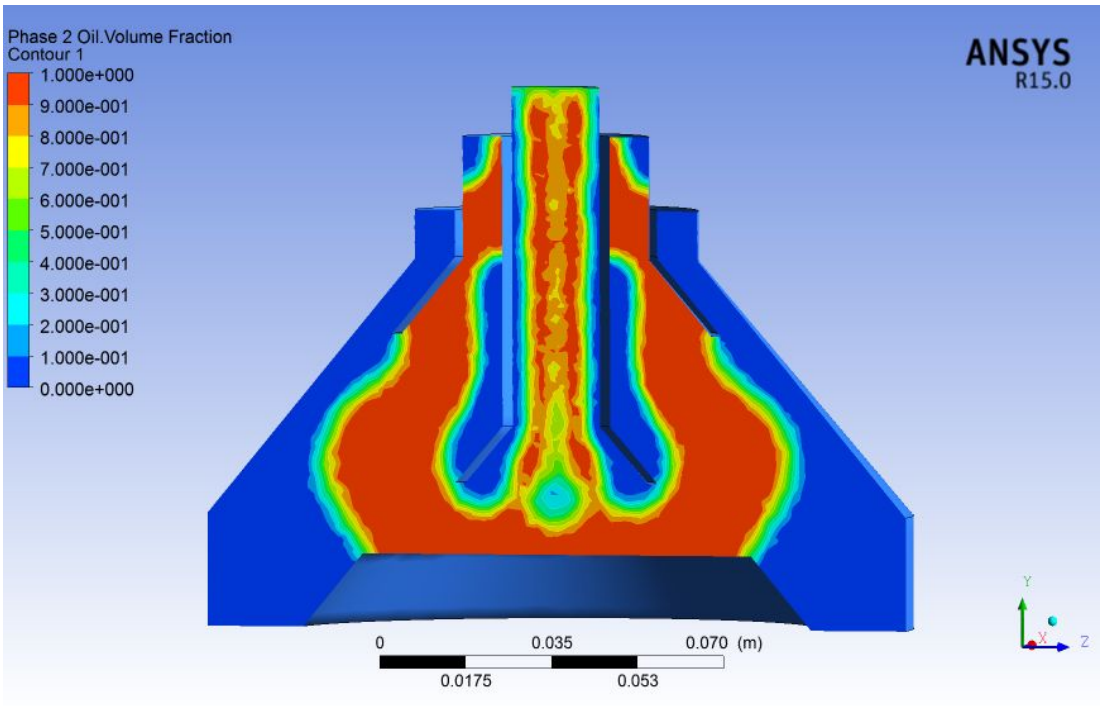

Figure 4.33: Oil volume fraction after 32.25s($\omega = 1028 rads^{-1}$)

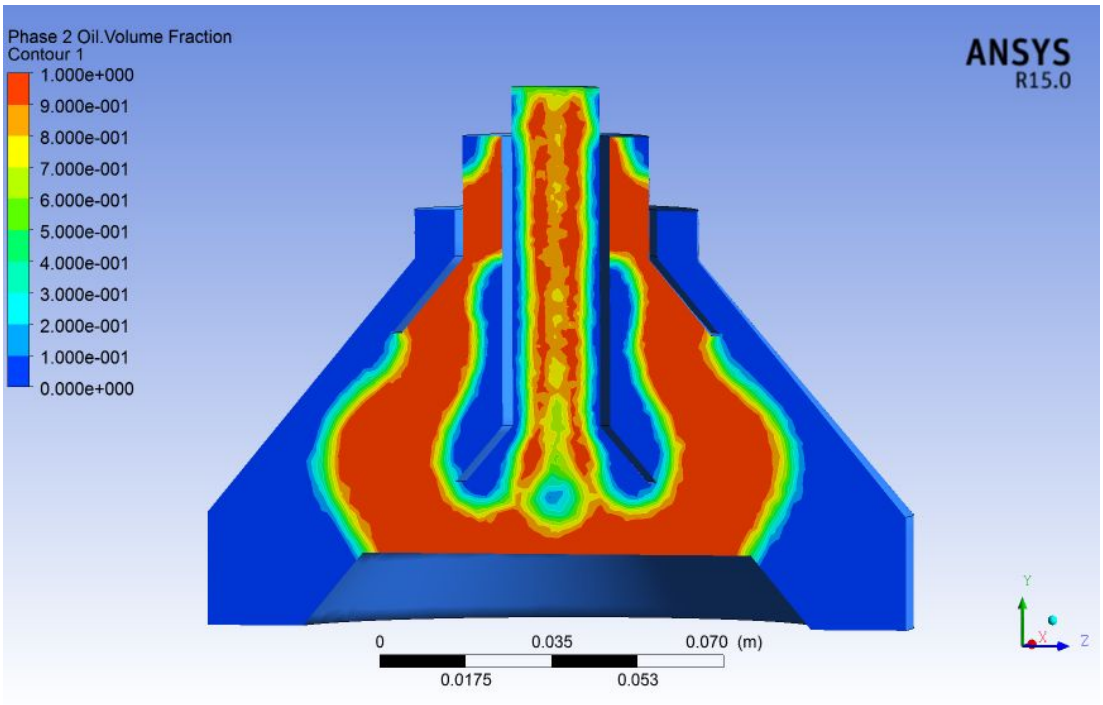

Figure 4.34: Oil volume fraction after 32.5s($\omega = 1028 rads^{-1}$)

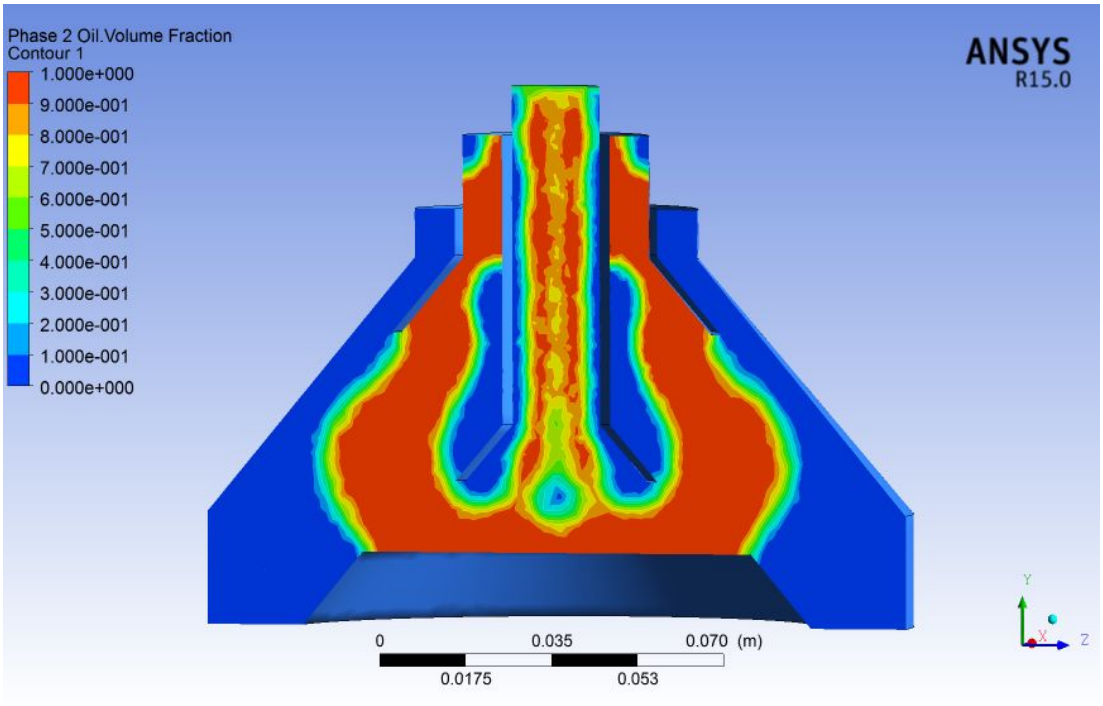

Figure 4.35: Oil volume fraction after 32.75s($\omega = 1028 rads^{-1}$)

By observing the above figure series of 4.32 - 4.36, it can be seen that the low dense oil volume fraction in the mid plane is highly concentrated towards the passage

of outlet 1 whereas the high dense water flow towards the outlet 2. However, contradictory to the theory discussed in section 2.1, there can be seen a blue colored water patch of constant size and shape at the passage and as highlighted before at the sharp edged end of outlet 1. However, it can be assumed that these conflicting water patches at undesirable locations can be avoided with high quality mesh, reduced time step size and maximize the number of iterations per time step.

The simulation results of the next two seconds are also depicted in figure series of 4.36-4.43 for better comparison with figure series of 4.28-4.31.

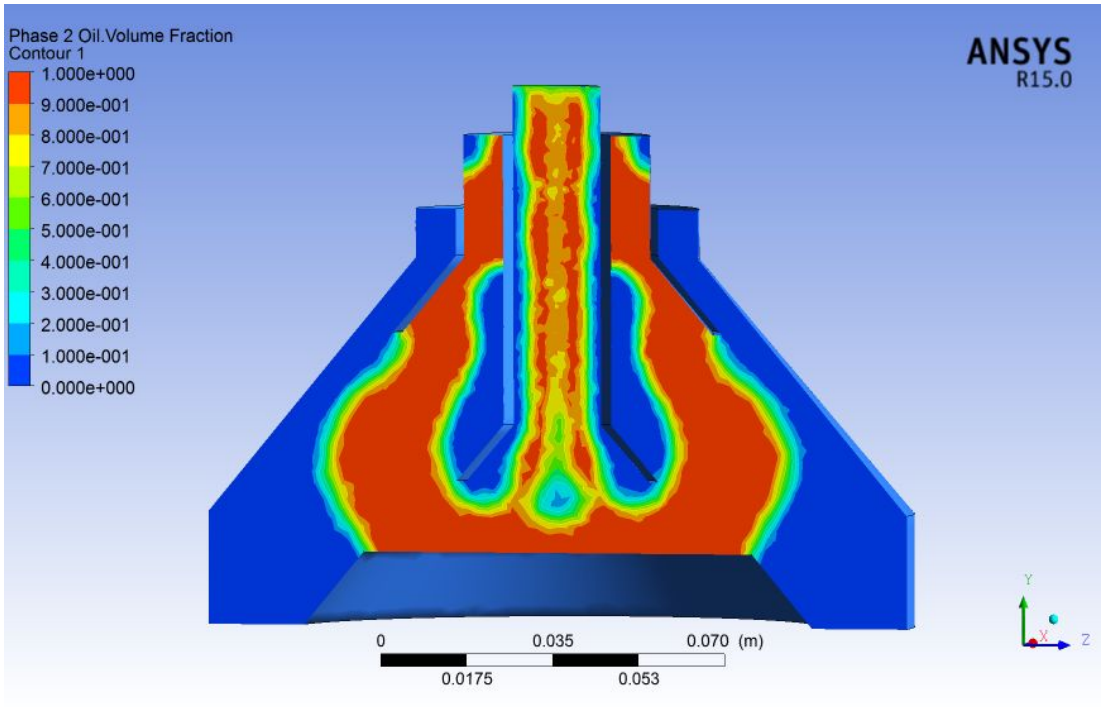

Figure 4.36: Oil volume fraction after 33s($\omega = 1028 rads^{-1}$)

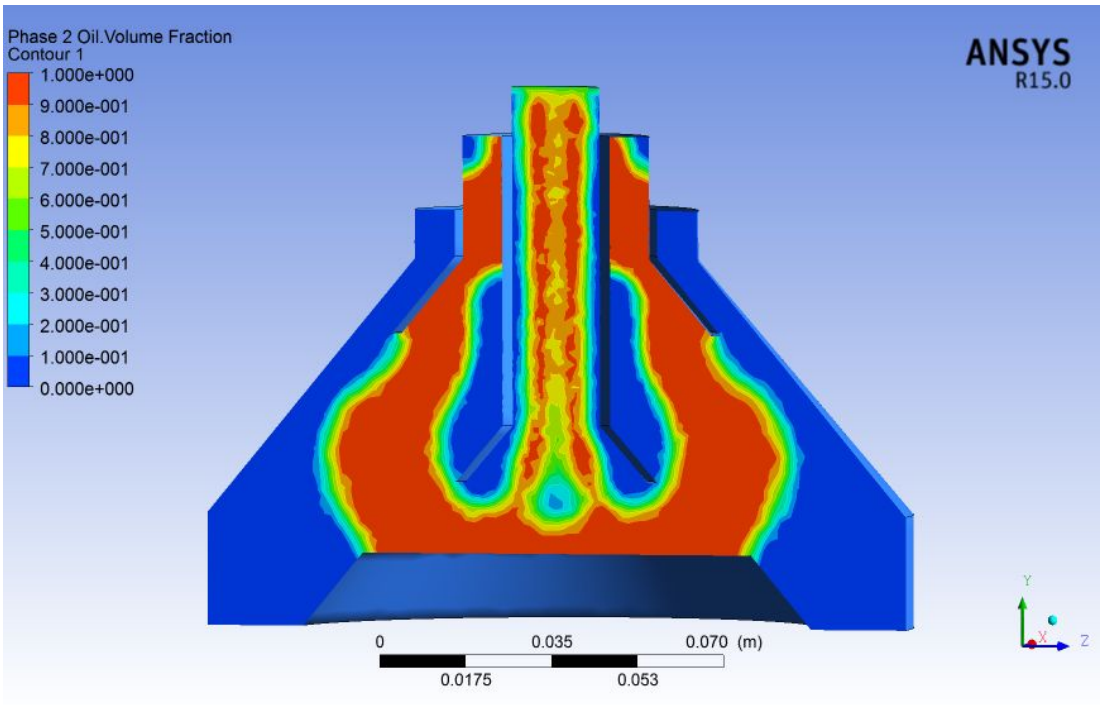

Figure 4.37: Oil volume fraction after 33.25s($\omega = 1028 rads^{-1}$)

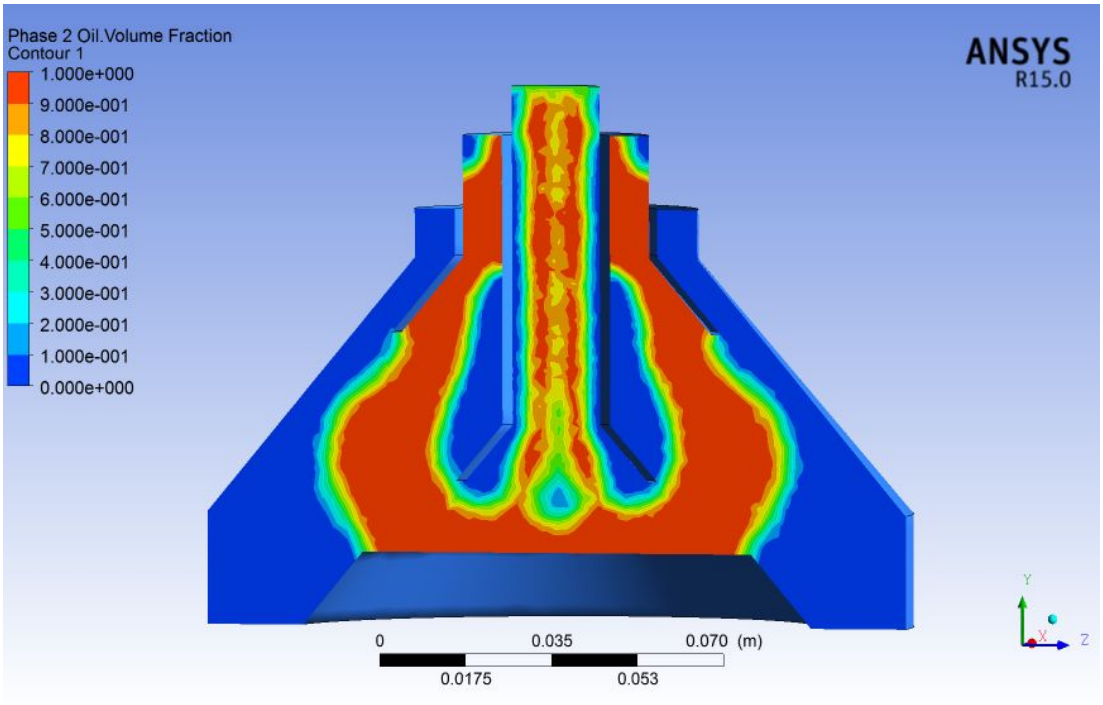

Figure 4.38: Oil volume fraction after 33.5s($\omega = 1028 rads^{-1}$)

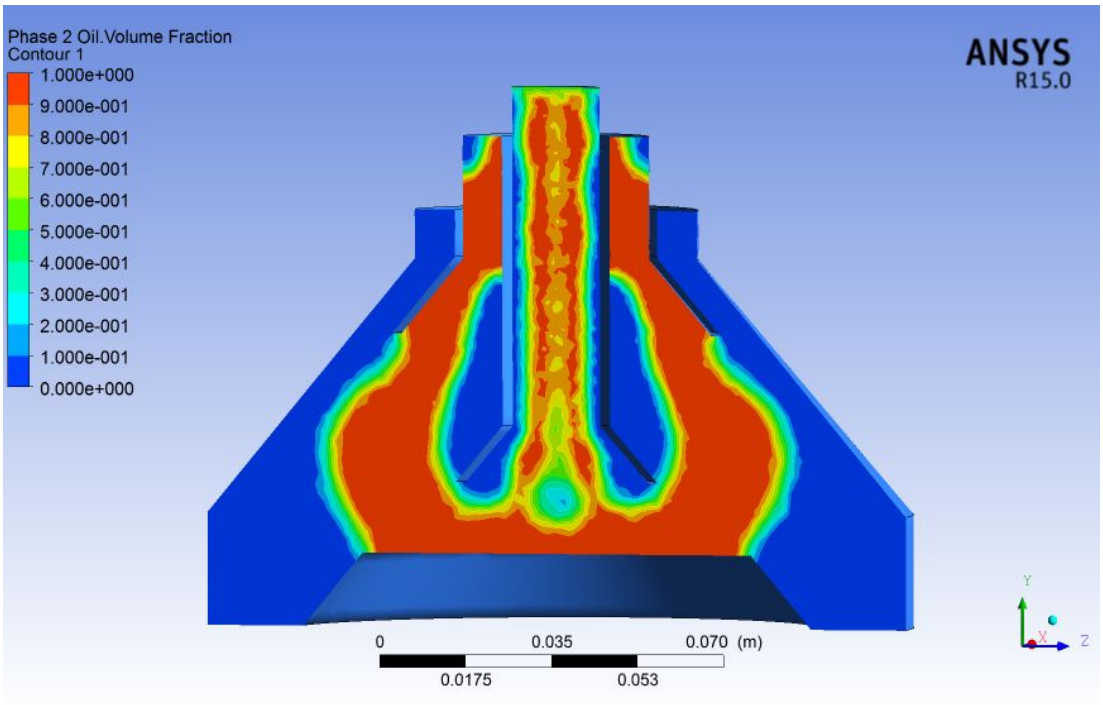

Figure 4.39: Oil volume fraction after 33.75s($\omega = 1028 rads^{-1}$)

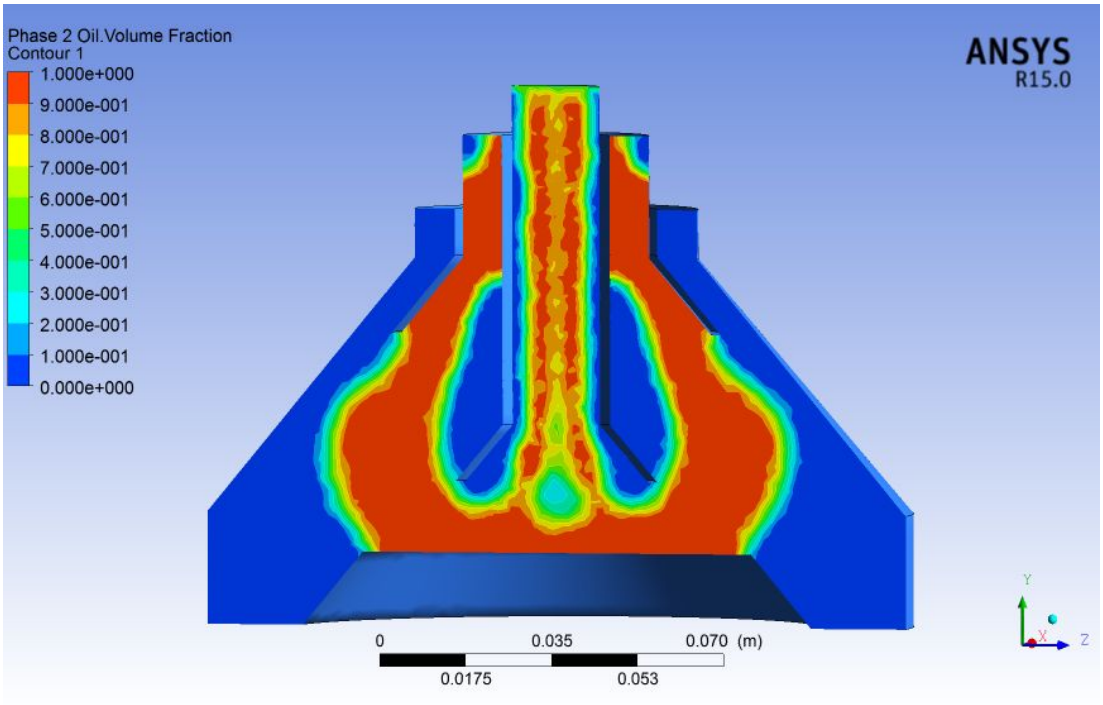

Figure 4.40: Oil volume fraction after 34s($\omega = 1028 rads^{-1}$)

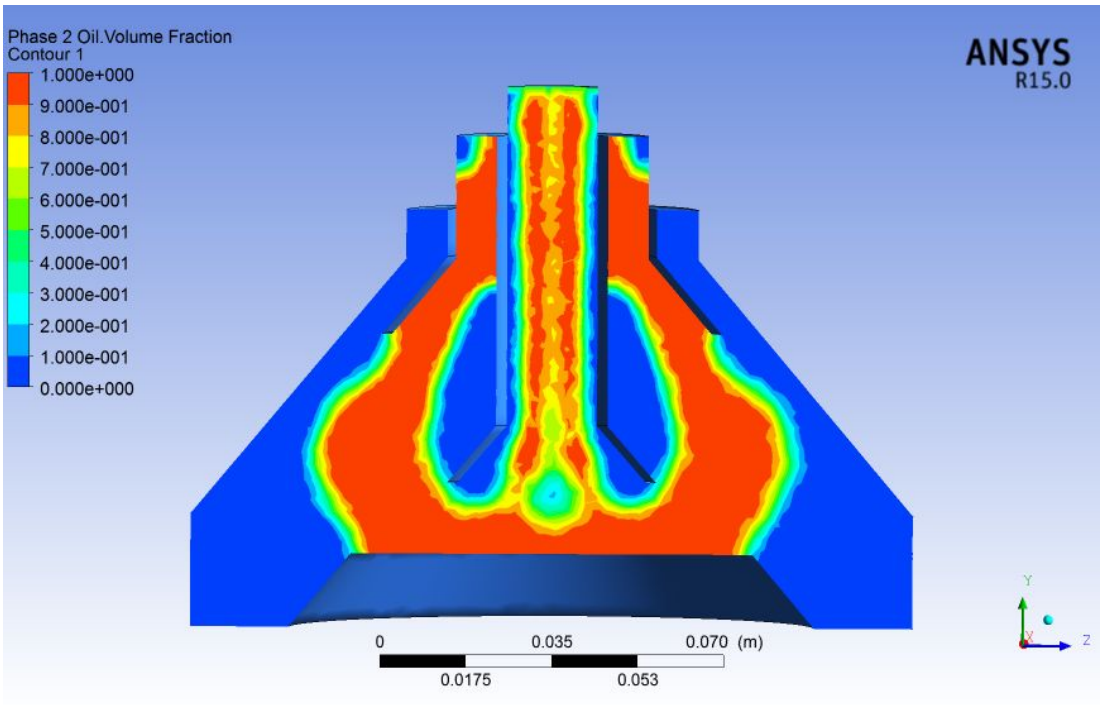

Figure 4.41: Oil volume fraction after 34.25s($\omega = 1028 rads^{-1}$)

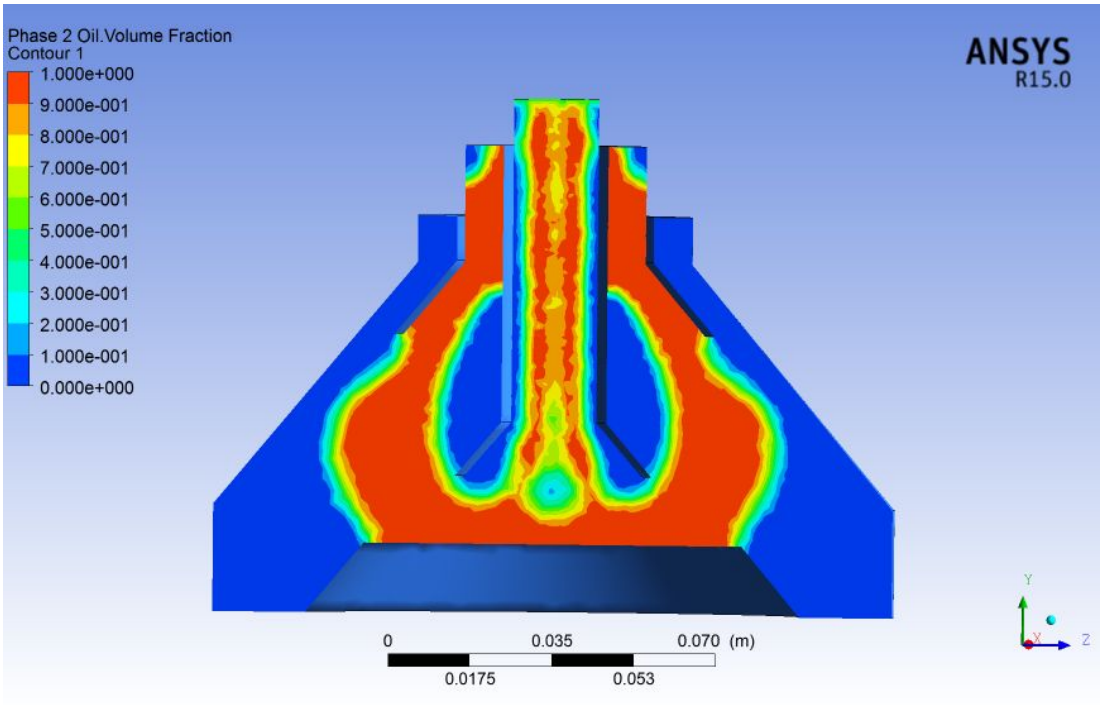

Figure 4.42: Oil volume fraction after 34.5s($\omega = 1028 rads^{-1}$)

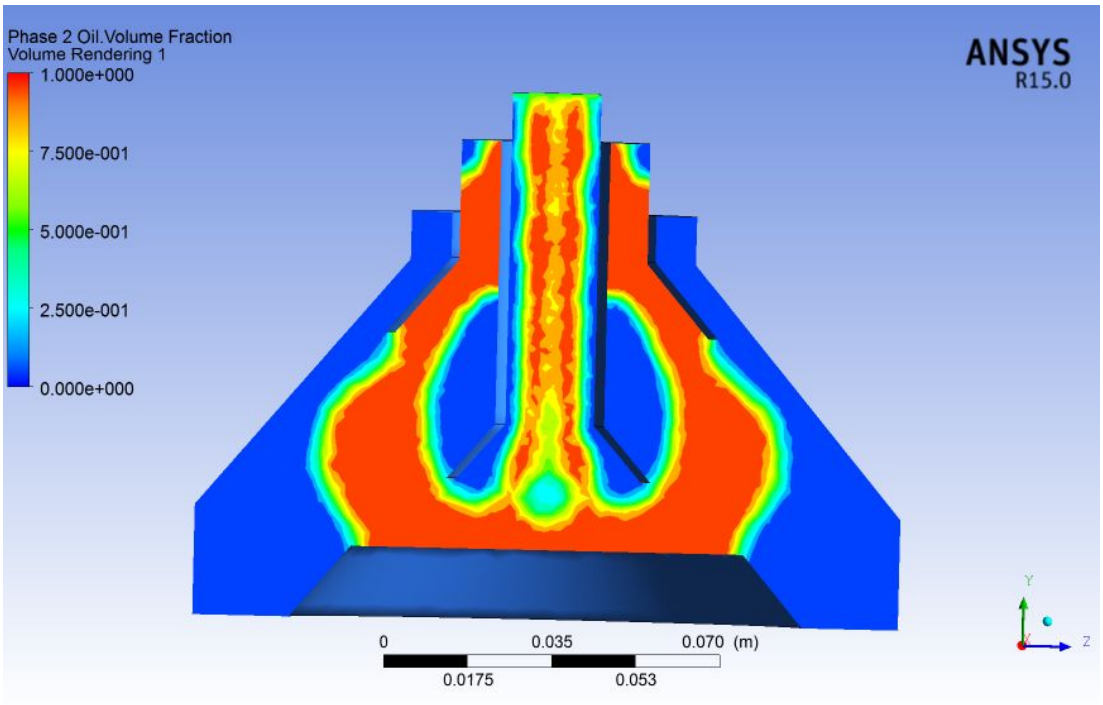

Figure 4.43: Oil volume fraction after 34.75s($\omega = 1028 rads^{-1}$)

By observing figures of 32^{nd} , 33^{rd} and 34^{th} seconds, it can be stated that the flow has obtained a repetitive and arranged pattern and the simulation results are more stable. However, the noticeable feature is the water patch at the passage of outlet 1 has remained almost the same in size and shape. Therefore the model has been run for another two seconds and ended up after 36 seconds.

The figures 4.44 and 4.45 represent the simulation results of the oil volume fraction at the mid plane after 35s and 36s respectively.

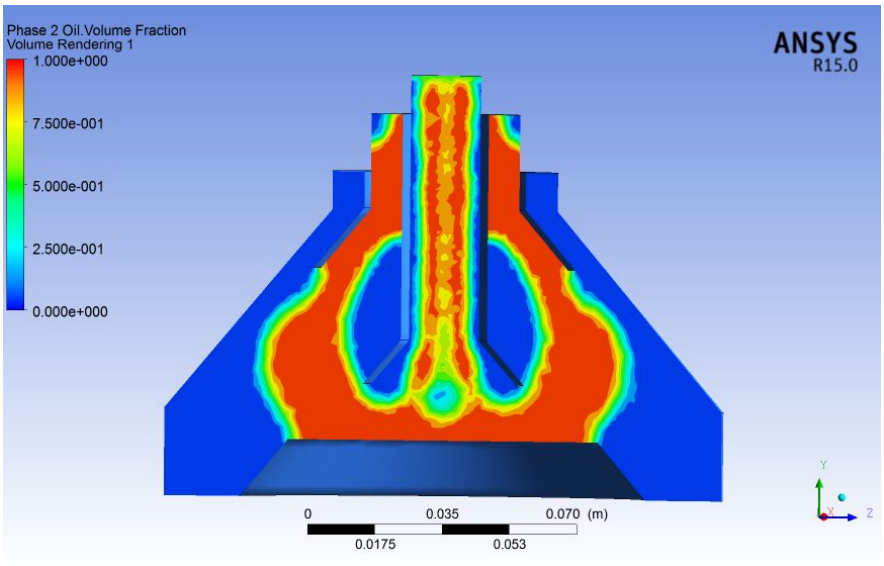

Figure 4.44: Oil volume fraction after 35s($\omega = 1028 rads^{-1}$)

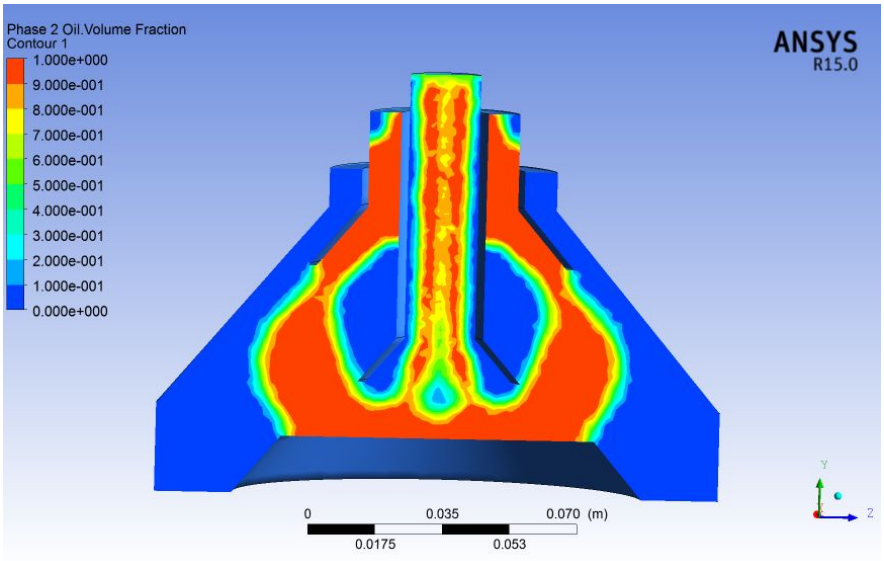

Figure 4.45: Oil volume fraction after 36s($\omega = 1028 rads^{-1}$)

4.2 Experiment Procedure, Results and Discussion

In order to validate the developed model, three trial experiments were carried out using the Westfalia centrifugal separator. The 20 discs which improves the efficiency of liquid separation were removed since the intended centrifuge geometry which used for modeling also didn't contain them as mentioned in section 3.1.3. Therefore, the model

geometry and the real time equipment were compatible in dimensions and all other parts even with the separating disc, except these 20 discs.

4.2.1 Procedure

A 50% coconut oil-water mixture was prepared by mixing $1l$ of each, inside the inlet drum as depicts in figure 4.46. The two components were thoroughly mixed using a stirrer and soon after, switched on the motor of the centrifuge, time was started to measure using a stop watch. The centrifuge was allowed to operate until the $2l$ mixture finished and the respective out flows were collected from the two outlets. Moreover, the liquid mixture flow to inlet passage from the inlet drum was carefully controlled by setting the inlet valve at a controlled position in order to reduce turbulence at the inlet as much as possible. Finally, the amounts of two outlet liquids were measured. Since the resulting liquid of outlet 1 contained some water during the experiment, the mixture was kept inside a separating funnel for 3 days and the respective water and oil volumes were separated out and measured.

Figure 4.46: Inlet coconut oil-water mixture inside the inlet drum

Additionally, the inlet mixture volumetric flow rate was measured by collecting volume of the flowing liquid mixture within one minute time and repeated the procedure for three times and obtained the average of it. Then, dividing it by the inlet area, the inlet mixture velocity was calculated to set as the inlet boundary condition in the model.

4.2.2 Results and Discussion

In all three trial experiments there was no liquid over flow present due to the controlled inlet flow and unavailability of discs. However, the experiment results of three trials have been summarized in table 4.1.

Table 4.1: Experiment results without discs

Trial	Volume of inlet mixture	Volume of outlet 1	Volume of outlet 2	Volume loss
1	2000ml	660ml	655ml	685ml
2	2000ml	1030ml	860ml	110ml
3	2000ml	1040ml	860ml	100ml

The figure 4.47 depicts the liquid out flows after trial 3 with emptied overflow bucket.

Figure 4.47: Liquid out flows after trial 3

By looking at the volume loss column, it can be observed that the maximum volume loss has recorded in the first trial whereas the volume loss in next two trials are almost the same. Further, when the centrifuge runs for the first time with emptied inside, at the end of the trial run a certain volume has trapped it's inside. Moreover, by comparing volume losses in trial 2 and 3, it can be noted that an average volume loss of 105ml occurred in operation of the centrifuge even though the centrifuge inside has filled with

the liquid mixture after the first trial. Therefore 580ml of liquid mixture has trapped inside the centrifuge which should be equal to centrifuge volume.

During all three trials, the outlet 2 has only produced water and the collected water volume of trial 3 is represented by figure 4.48. Even though, the inlet mixture contains 1000ml of water, by referring to 'volume of outlet 2' column of table 4.1, it can be noticed a 140ml of water reduction . However, it can be assumed that this reduced volume should be trapped inside, as highlighted before.Moreover, the figure 4.49 depicts the water volume fraction of the outlet 2 which is for the high density water out flow and the water volume fraction in the mid plane of the centrifuge. By referring to simulation results in figure 4.49 and experiment results in table 4.1, it can be stated that the simulation results are exactly comply the experimental findings of outlet 2, since there's no single drop of oil presents in outlet 2 in both experimental and simulation scenarios.

Figure 4.48: Outlet 2 liquid (water) of Trial 3

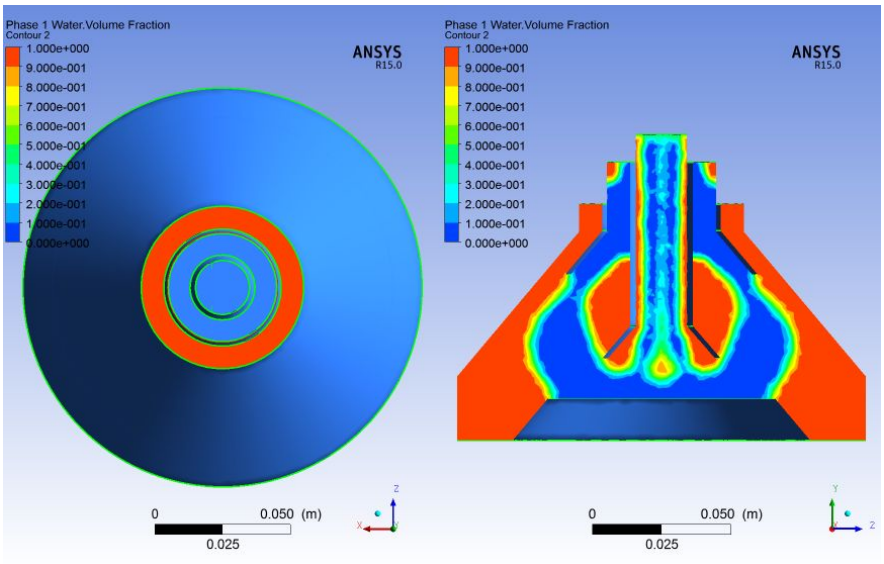

Figure 4.49: Water volume fraction in outlet 2 and the mid plane

The outlet 1 which is for the low density oil out flow has produced more than 1l volume which was even higher than the inlet volume of oil. Therefore, the collected out flow of outlet 1 has filled in to a separating funnel and allowed the gravity separation for three days. The figure 4.50 represents the separated oil and water components of trial 1,2 and 3 inside the separating funnel.

(a) Trial 1 (b) Trial 2 (c) Trial 3

Figure 4.50: Oil - water separation in side the separating funnel

After 3 days, the separated liquids were carefully taken out from the separating funnel and the corresponding volumes were measured and the results has shown in table 4.2.

Table 4.2: Experiment results of outlet 1

Trial	Oil Volume (%)	Water Volume (%)
1	580ml (87.87%)	80ml (12.13%)
2	960ml (93.8%)	70ml(6.2%)
3	968ml (93.09%)	70ml(6.9%)

According to the experiment results depicted in table 4.2, it can be figured out that oil volume fraction of the outlet 1 varies from 0.85-0.95.

The simulation results of oil volume fraction of a plane just below 0.8cm of the outlet 1 and parallel to it, is depicted in figure 4.51.

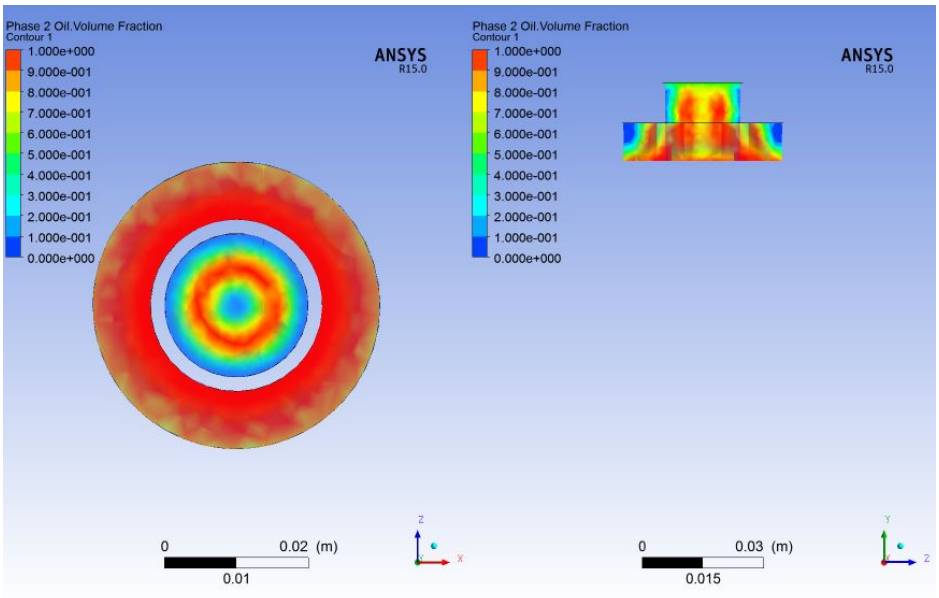

Figure 4.51: Oil volume fraction of a plane below 0.8cm of outlet 1

By referring to the above figure, it can be noticed that the oil volume fraction of the plane below 0.8cm of the outlet 1, varies in the range of 0.8-1, since the area of it covered with orange and red colored patches. However as the right hand side sub figure of figure 4.51 depicts, the oil flow path inside the outlet 1 gets narrower near the face of outlet 1 due to the reasons highlighted and discussed in subsection 4.1.4. However, it is very much clear that these simulation results represents in figure 4.51 are considerably compatible with the three trial experiment results.

CHAPTER 5 : CONCLUSIONS AND RECOMMENDATIONS

The first two section of the final 5^{th} chapter of this thesis summarizes the conclusions that can be made with simulation and experiment results according to the detailed comparison and analysis which has been emphasized on previous chapter. In addition, the next 5.3 section includes a brief outline on suitability of centrifugation as an water removal method from oil water mixtures. Further, the chapter concludes, recommending some modifications and the improvements for the model and the equipment in the view point of the researcher.

5.1 CFD Simulation Results

- The 3D, CFD model of the centrifuge was initially run under frame motion, with SIMPLE algorithm along with steady state for 4000 iterations and the results of it has been used for the mesh motion under PISO algorithm with transient motion with gradually incrementing rotational speeds. Therefore, it can be stated that this technique which has been used to run the three dimensional model leads the results of better accuracy.

- As highlighted in subsection 4.1.3, the two out lets have recorded high turbulent intensities which are ultimately wastage of energy and even the inlet has a medium level of turbulence.

- Since the simulation results of the flow parameters discussed in 4^{th} chapter are considerably inline with the theoretical results, it can be stated that ANSYS Fluent, 3D flow simulation results are accurate enough for theoretical validation of the model.

- The simulation results revealed the behavior of the phase separation which cannot be observed or experienced by any other practical method inside the Westfalia separator with a significant level of accuracy.

5.2 Experiment Results

- The removal of discs which improve the efficiency of separation, avoid the overflowing of the liquid mixture and also the real time trial equipment perfectly matched with the geometry selected for the modeling.

- The experiment results can only be used to compare the phase separation of coconut oil and water and since the results of the three trial experiments are compatible with the phase separation of the model, it can be stated that the model is validated by empirical results.

5.3 Centrifugation as a water removal method from oil-water mixtures

As highlighted in section 1.1 and 1.3 in chapter 1, disc stack centrifuges are applied for oil processing, in order to remove undesirable water content and separate out the required product stream of oil. However, by considering the simulation results and experimental findings it can be declared that centrifugation is a quite effective and efficient method to remove water from a mixture of water and coconut oil. Even though, the out flow of outlet 1(oil outlet) has contaminated with little amount of water, the separation is above 80% whereas the outlet 2 outflows 100% water without even a slight contamination with oil. However, the significant fact of these results is that the Westfalia disc stack centrifuge performs quite good even without the discs which intensify the efficiency of separation.

5.4 Recommendations

- This research work is an initial attempt to model the westfalia separator without the discs of improving efficiency. Therefore, the modeling of the entire equipment along with advanced computer hardware facility would improve the separation efficiency and accuracy of the simulation results.

- In considering the selected geometry without the discs, it can also be recommended to use much refined mesh with precise advanced size functions, reduced

time step size and increased number of iterations per time step with powerful computer hardware support would avoid contradictions and enhance the accuracy of the results as well. For instance, it can be noted that the water patch at the outlet 1 would not be there with these modifications.

- Reduced turbulence at inlet and outlets of the equipment would result better quality outputs with higher efficiency of separation. Further, in reality the centrifuges are equipped with various inlet and outlet devices to reduce this turbulent inlet-outlet flow behaviors and it can be recommended to fix one of them for the Westfalia separator as well.

APPENDIX A MODIFIED REYNOLDS NUMBER CALCULATION

Calculation of Mass Fractions

The input mixture to the centrifuge contains 0.5 volume fraction of water and liquid phases. Therefore with the use of densities, respective mass fractions can be calculated as follows.

$$
\begin{aligned}
Density\,of\,water\,(\rho_{water}) &= 998.2\,kgm^{-3} \\
Density\,of\,coconutoil\,(\rho_{oil}) &= 924\,kgm^{-3} \\
Mass\,fraction\,of\,water\,(m_{water}) &= \frac{998.2\,kgm^{-3}\times 0.5}{(998.2\,kgm^{-3}\times 0.5)+(924\,kgm^{-3}\times 0.5)} \\
&= 0.51925 \\
Mass\,fraction\,of\,coconutoil,(m_{oil}) &= 1-51925 \\
&= 0.48075
\end{aligned}
$$

Calculation of Kinematic Viscosity of the Mixture

Kinematic viscosity of water and coconut oil is considered as 1.004×10^{-6} [31, p. 1861] and 3×10^{-5} [32] respectively. Therefore, the kinematic viscosity of this feed mixture can be calculated using Gambill method [17]as follows.

$$\nu^{\frac{1}{3}} = x_w\nu_w^{\frac{1}{3}} + x_o\nu_o^{\frac{1}{3}} \tag{A.1}$$

where:

ν is kinematic viscosity of liquid mixture

ν_w is kinematic viscosity of water

ν_o is kinematic viscosity of coconut oil

x_w is mass fraction of water

x_o is mass fraction of coconut oil

Therefore the calculated kinematic viscosity of the liquid mixture is 8.120601×10^{-6}.

Calculation of Modified Reynolds Number

In order to calculate the mean diameter the geometric shape of the centrifuge, (neglecting inlets and outlets) has been assumed to a cylindrical shape and the maximum (13cm) and minimum(6cm) diameters of the conical region has been taken in to account. Therefore, the calculated mean diameter for the conical section with reasonable assumptions is 9.5cm. Taking the rotational speed of the centrifuge as it's operational speed of 9820rpm (163.67rps) the modified Reynolds number for the considered rotating flow is,

$$\begin{aligned} The\, modified\, Reynolds\, Number = \frac{ND^2}{\nu} &= \frac{163.67rps \times (0.095m)^(2)}{8.120601 \times 10^{-6}} \\ &= 1.8189 \times 10^7 \end{aligned}$$

REFERENCE LIST

[1] J. Van Der Lnden, "Liquid-liquid separation in disc stack centrifuge," Master's thesis, Delft University of Technology, February 1987.

[2] *Controlling the separation of liquids and solids*, Alfa Laval Corporate AB, Rudeboksvägen 1, SE-226 55 Lund, Sweden.

[3] *THE FLOTTWEG DISK STACK CENTRIFUGE*, Flottweg SE, Industriestraße 6-8, 84137 Vilsbiburg, Deutschland (Germany).

[4] F. Boysa, W. Ayers, and J. Swithenbank, "Fundamental mathematical modelling approach to cyclonyclone design." *Chem. Eng. Res. Des.*, vol. 60, pp. 222–230, July 1982.

[5] C. Haig, A. Hursthouse, D. Sykes, and S. Mcilwain, "The rapid development of small scale cyclones — numerical modelling versus empirical models," *Applied Mathematical Modelling*, vol. 40, pp. 6082–6104, February 2016.

[6] C. Cortes and A. Gil, "Modeling the gas and particle flow inside cyclone separators," *Progress in energy and combustion Science*, vol. 33, no. 5, pp. 409–452, 2007.

[7] A. Nowakowski, J. Cullivan, R. Williams, and T. Dyakowski, "Application of cfd to modelling of the flow in hydrocyclones. is this a realizable option or still a research challenge?" *Minerals Engineering*, vol. 17, no. 5, pp. 661–669, 2004.

[8] E. Dick, J. Vierendeels, A. Serbrugyns, and J. V. Voorde, "Performance prediction of centrifugal pumps with cfd-tools," *Task quarterly*, vol. 5, pp. 579–594, 2001.

[9] K. E. Wardle, T. R. Allen, and R. Swaney, "Computational fluid dynamics (cfd) study of the flow in an annular centrifugal contactor," *Separation science and technology*, vol. 41, no. 10, pp. 2225–2244, 2006.

[10] K. E. Wardle, "Open-source cfd simulations of liquid–liquid flow in the annular centrifugal contactor," *Separation Science and Technology*, vol. 46, no. 15, pp. 2409–2417, 2011.

[11] B. Yu, "Cfd modeling of two-stage parallel plate sedimentation centrifuge for microalgae dewatering," Master's thesis, Department of Sustainable Process and Energy Faculty of Mechanical, Maritime and Materials Engineering in Delft University of Technology., March 2012.

[12] X. R. Fernández and H. Nirschl, "Cfd simulation of a solid bowl centrifuge used for waste managent," in *A Numerical And Experimental Study*, 2000.

[13] M. V. C. Alves, J. R. Barbosa, and A. T. Prata, "Analytical and cfd modeling of the fluid flow in an eccentric-tube centrifugal oil pump for hermetic compressors," *International Journal of Refrigeration*, vol. 36, no. 7, pp. 1905–1915, 2013.

[14] L. Dong, S. Fu, and H. Yuan, "Numerical simulation on pressure field in a decanter centrifuge," *Chem. Ind. Eng. Pro*, vol. 33, no. 2, pp. 309–313, 2014.

[15] J. Richardson, J. Harker, and J. Backhurst, *Coulson and Richardson's CHEMICAL ENGINEERING*, 5th ed. Linacre House, Jordan Hill, Oxford OX2 8DP 225 Wildwood Avenue, Woburn, MA 01801-20: Bath Press, Bath, 2002, vol. 2.

[16] *ANSYS Fluent Theory Guide*, ANSYS, Inc., 275 Technology Drive Canonsburg, PA 15317, November 2013.

[17] W. R. Gambill, "How to estimate mixtures viscosities," *Chemical Engineering*, vol. 66, pp. 151–152, 1959.

[18] H. Versteeg and W. Malalasekara, *An Introduction to Computational Fluid Dynamics,THE FINITE VOLUME METHOD*, 2nd ed. Edinburgh Gate,Harlow,Essex CM20 2JE,England: Pearson Education Limited, 2007.

[19] *FLUENT User's Guide*, November 2001, chapter 10 : Modeling Turbulence.

[20] "Solver settings," Introductory FLUENT Training, December 2006.

[21] "Introduction to cfd methodology,introductionto introduction to ansys fluent," ANSYS Customer Training Material, 2010.

[22] M. Ozen, "Meshing workshop," OZEN ENGINEERING, INC, Tech. Rep., November 2014.

[23] *ANSYS Meshing User's Guide*, ANSYS, Inc., 275 Technology Drive Canonsburg, PA 15317, November 2013.

[24] "The density of some common liquids," November 2015.

[25] F. Yeaple, *Fluid Power Design Handbook*, 3rd ed. CRC Press, October 1995.

[26] M. Keating, "Accelerating cfd solutions, several recent enhancements in ansys fluent solver capabilities accelerate convergence and reduce solution time," in *ANSYS Advantage*, 1st ed., 2011, vol. Volume V, pp. 49–50.

[27] D. Sofialidis, "Using moving reference frames and sliding meshes," Introductory Training in ANSYS Fluent, University of Ljubljana, Faculty of Mechanical Engineering, Ljubljana, Slovenia, September 2013.

[28] *The FLUENT User's Guide*, Fluent Inc., November 2001, volume 2,Chapter 9,Modeling Flows in Moving Zones.

[29] F. Russo and N. T. Basse, "Scaling of turbulence intensity for low-speed flow in smooth pipes," *Flow Measurement and Instrumentation*, vol. 52, pp. 101–114, 2016.

[30] J. Jaramillo, C. Pérez-Segarra, I. Rodriguez, and A. Olivia, "Numerical study of plane and round impinging jets using rans models," *Numerical Heat Transfer, Part B: Fundamentals*, vol. 54, pp. 213–237, 2008.

[31] J. C. Crittenden, R. R. Trussell, D. W. Hand, K. J. Howe, and G. Tchobanoglous, *MWH's Water Treatment: Principles and Design, Third Edition,*, 3rd ed. Hoboken, New Jersey: John Wiley and Sons, March 2012.

[32] E. Oberg, F. Jones, H. Horton, H. Ryffel, and C. McCauley, *Machinery's Handbook*, 30th ed., March 2016.